DEVELOPMENT OF A VIBRATION-BASED HEALTH MONITORING STRATEGY FOR ONSHORE AND OFFSHORE PIPELINES

by

Pejman Razi

Submitted in partial fulfilment of the requirements
for the degree of Doctor of Philosophy

at

Dalhousie University
Halifax, Nova Scotia
November 2013

I dedicate this dissertation to my parents, Ali and Mehri
who taught me the meaning of unconditional love,
and my brother, Pooyan.

Table of Contents

LIST OF TABLES

LIST OF FIGURES

ABSTRACT

Aging mechanical, civil, aerospace, marine and offshore structures require continuous and accurate assessment on their integrity to avoid potentially hazardous failures. To further facilitate this crucial demand, a new technical terminology, generally referred to as structural health monitoring (SHM) has been coined in three past decades. SHM involves deployment of a sensory network on such structures in order to gather useful data, such that processing and interpreting the data through specific algorithms would enable one to detect defects and anomalies within the structures.

This dissertation presents the results of a series of efforts expended towards the refinement and enhancement of a vibration-based SHM technique, which was originated within our research group. In the adopted damage detection scheme, vibration data are gathered from structures via piezoelectric sensors. Data are processed by a robust signal processing approach, known as the empirical mode decomposition (EMD) in order to establish energy-based damage indices (EMD_EDIs). Interpretation of the damage indices enables detection of onset, location and advancement of defects within structures.

A series of adjustments and modifications were devised and implemented to the application of the originally developed methodology, such that, besides increasing the methodology's robustness and accuracy, they also facilitate a remote vibration-based SHM targeting onshore and offshore pipelines.

The integrity of the method in detection of bolt-loosening in a bolted flange joint of a full-scale pipeline was verified through numerical simulations and experimental investigations. The source of a significant inconsistency reported in the previous trials was identified and resolved. Also, for the first time, the remote application of the technique was facilitated by incorporating an advanced wireless data acquisition system. Moreover, the application of the methodology was extended to detection of cracks in girth-welds of offshore pipelines. In this regard, a comprehensive discussion is first provided, which identifies the role of parameters that influence the accuracy of numerical modeling of the dynamic response of submerged structures. The experimental and numerical investigation following the aforementioned modeling efforts presents encouraging results in detection of an advancing notch in the girth-weld of a submerged pipe. The use of a piezoelectric-based excitation technique, incorporated for the first time in the application of the methodology would evidence the enhanced practicality and robustness of the approach. The study concludes with a successful detection of a real-life sharp propagating crack in a beam due to cyclic loadings.

LIST OF ABERAVIATIONS AND SYMBOLS USED

a	Scale parameter, and Crack length
$a(t)$	Instantaneous amplitude
A	Cross section
ANSI	American National Society Institute
ASTM	American Society for Testing and Materials International
AUT	Automated Ultrasonic Testing
b	Translation parameter, and Width
c_1	The first IMF
c_i	IMFs
c_n	nth IMF derived from sifting process
$\tilde{c}$	Damping matrix
C	Damping matrix
c	Speed of sound in the medium
CLT	Classical Laminate Theory
CWT	Continuous Wavelet transform
$D\left(\frac{C}{m^2}\right)$	Electrical displacement
DAQ	Data Acquisition System
DC	Damage Case
DFT	Discrete Fourier Transform
DWT	Discrete Wavelet transform
D_{ij}	Bending stiffness elements
$d\left(\frac{C}{N}\right)$	Matrix of piezoelectric strain coefficients
d_{bolt}	Bolt diameter
E	Modulus of elasticity
E_{ij}	Elastic moduli

$E_{Damaged}$	EMD energy of an IMF at damaged state of the structure
$E_{Healthy}$	EMD energy of an IMF at healthy state of the structure
EI	Bending rigidity
EMD	Empirical Mode Decomposition
EMD_E	EMD energy of an IMF
EMD_EDI	EMD energy damage index
EWL	Effective Water Level
f	Frequency
f_o	Instantaneous frequency (Hz)
F	Force
$\boldsymbol{F}$	Force vector
$F(t)$	Force as a function of time
$F(\omega)$	Force as a function of frequency
FC	Fatigue Crack
FE	Finite Element
FEM	Finite Element Method
FFT	Fast Fourier Transform
FLD	First Line of Defence
FRP	Fiber Reinforced Polymer
FSI	Fluid Structure Interaction
FT	Fourier Transform
$\boldsymbol{g}$	Acceleration due to gravity
G_{ij}	Shear moduli
$\boldsymbol{h}$	Height of fluid
H	Stiffness matrix for fluid
H	Height of the beam
h_1	Difference between the signal $x(t)$ and mean m_1 in the first sifting
h_{1k}	Difference between the signal h_{1k} and the mean m_{1k} in the kth sifting

HHT	Hilbert-Huang Transform
HT	Hilbert Transform
I	Moment of inertia
IMF	Intrinsic Mode Function
IO	Index of Orthogonality
k	Nut factor
K	Stiffness per unit length
K	Stress intensity factor
$\boldsymbol{K}$	Stiffness Matrix
LDV	Laser Doppler Vibrometer
LEFM	Linear Elastic Fracture Mechanics
LVDT	Linear Variable Differential Transformer
m_1	Mean of the upper and lower envelopes in the first sifting
m_{1k}	Mean of the upper and lower envelopes in the kth sifting process
m, n	Parameters for power-of-two logarithmic discretization of a, b
M	Mass per unit length
$\boldsymbol{M}$	Mass matrix
MOIH	Manually Operated Instrumented Hammer
n	Time sample index in DFT
NDE	Non-Destructive Evaluation
NDT	Non-Destructive Testing
$\boldsymbol{n}$	Unit normal vector
$\boldsymbol{N}_u$	Shape functions for displacement
$\boldsymbol{N}_p$	Shape functions for acoustic pressure
OD	Outer Diameter
p	Dynamic/acoustic pressure
$\tilde{\boldsymbol{P}}$	Acoustic pressure vector
p_s	Static pressure

PLC	Programmable logic Controller
PZT	Lead Zirconate Titanate
$\boldsymbol{Q}$	Coupling matrix
$\boldsymbol{r}$	radius
r_1	Residue after extraction of first IMF
r_n	n^{th} residue derived after extraction of n^{th} IMF
ROV	Remote Operating Vehicle
RT	Radiography Testing
SAE	Society of Automotive Engineers
SD	Standard Deviation
SDC	Specific Damping Capacity
SEM	Spectral Element Method
SHM	Structural Health Monitoring
SNR	Signal to Noise Ratio
SOV	Space Operation Vehicle
$S_E\left(\frac{m^2}{N}\right)$	Matrix of mechanical compliance coefficients
t	Time, and pipe's wall thickness
$T(a,b)$	Wavelet transform of the time signal $x(t)$
$T\left(\frac{N}{m^2}\right)$	Stress tensor
TPS	Thermal Protection System
U	Velocity in lateral direction
$\tilde{\boldsymbol{\iota}}$	Nodal displacement vector
$\boldsymbol{u}$	Displacement vector
UNC	Unified National Coarse
V	Velocity
VBDD	Vibration-Based Damage Detection
VB-SHM	Vibration-Based Structural Health Monitoring
WT	Wavelet Transform
WDAQ	Wireless Data Acquisitions System

$x(t)$	Continuous time signal, and displacement as a function of time
$\{\boldsymbol{X}\}$	Eigenmodes
$X(f)$	Fourier transform of the signal $x(t)$
$x(n)$	Time signal sampled at uniform steps
X	Displacement in x-direction
$X(k)$	Discrete Fourier Transform of sampled time signal $x(n)$
$X(\tau, f)$	Short Term Fourier Transform of the signal $x(t)$
$x_m(t)$	Approximation of the signal $x(t)$ derived from wavelet analysis
$y(t)$	Hilbert transform of $x(t)$
Y_i^E	Short-circuit elastic modulus in piezoelectric materials
$z(t)$	Analytic signal defined by the Hilbert Transform
$\theta(t)$	Instantaneous phase
$\alpha(\omega)$	Receptance
ω	Angular instantaneous frequency
ν	Poisson's ratio
ν_{ij}	Poisson's ratio
λ_i	Boundary-dependent constants
ρ	Mass density
ρ_f	Fluid density
σ	Bending stress
$\varepsilon^T\left(\frac{F}{m}\right)$	Matrix of dielectric permittivity
$\psi(t)$	Mother wavelet function
Ω_f	Fluid domain
Γ_i	Boundary domain
ϕ	Velocity potential
τ	Torque

ACKNOWLEDGEMENT

I would like to express my deepest gratitude to Professor Farid Taheri for his continuous support, encouragement, and professional attitude, which enabled me to complete this dissertation.

I wish to extend my appreciation to all of my committee members; Prof. Abraham Q. Wang, Dr. Neil Pegg and Dr. Serguei Iakovlev for their helpful technical comments on my thesis.

I am very thankful to the skillful technicians of our department, Mr. Brian Kennedy, Mr. Mr. Blair Nickerson and Mr. Jesse Keane for their assistance and technical support throughout my experimental works.

The financial support of the Natural Sciences and Engineering Council of Canada (NSERC) and the Petroleum Research Atlantic Canada (PRAC) are gratefully acknowledged.

CHAPTER 1 INTRODUCTION

1.1 STRUCTURAL HEALTH MONITORING

Maintenance of operational systems is a routine task that assures safe performance of mechanical, aerospace, and civil infrastructures. The integrity (hence the safe operations of such systems) become susceptible to wear and damage under long-term operational/environmental conditions. As an example, pipelines buried in deep oceans conveying oil and gas are prone to severe corrosion, and become subject to fluctuating loads as a result of vortex-induced vibrations, as an example. Aircraft also exemplify such circumstances; enormous dynamics loads during landing and take-off events and aerodynamic fatigue loads exasperated by turbulence threaten safe flights. Consequently, failure to detect and quantify such potential damage would lead to catastrophic disasters. For instance, the 2010 Gulf of Mexico oil spill disaster claimed 11 lives and had huge environmental impact. As a result, the integrity assessment of such structures is a vital task, which is usually performed in a periodic fashion.

Several Non-Destructive Evaluation (NDE) methods have been established for integrity assessment of various structures. For instance, bolted flange joints are consistently monitored by various techniques following a set of guidelines [1]. Detection of corrosion, the most common cause of bolted flange joint failure, is carried out by means of a guided wave technique or visual inspections, depending on the in-situ conditions. Fatigue of the bolts caused by cyclic or vibrational loads is interrogated via ultrasonic techniques such as phased array [1]. Offshore pipelines, on the other hand, are monitored by divers or remotely operated vehicles (ROVs) equipped with NDE equipment [2]. Automated Ultrasonic Testing (AUT) is the most updated tool for monitoring girth welds of both offshore and onshore pipelines; fatigue cracks, and various types of weld defects are detected and quantified by this approach [3]. Some of the above-mentioned NDE approaches have been proven to provide a detailed scan of a system's sub-structures. However, nearly all of the NDE methods share common disadvantages that would impede an effective integrity assessment. Examples of such impeding factors are:

- Requirement for skilled operators

- Access to the zone to be monitored
- Operational cost
- Shut-down of the entire system as it is the case for Radiography Testing (RT)

To address the above issues, a new field of NDE, namely Structural Health Monitoring (SHM), has recently been evolved. SHM involves incorporation of smart materials into structures in order to monitor the integrity of the system. The gathered data from the sensors are processed within a set of algorithms and the output are used as the basis for assessing the structure's integrity. This process could be accomplished in both active (online) and passive (offline) fashions [4]. Basic elements of SHM are shown in Figure 1-1.

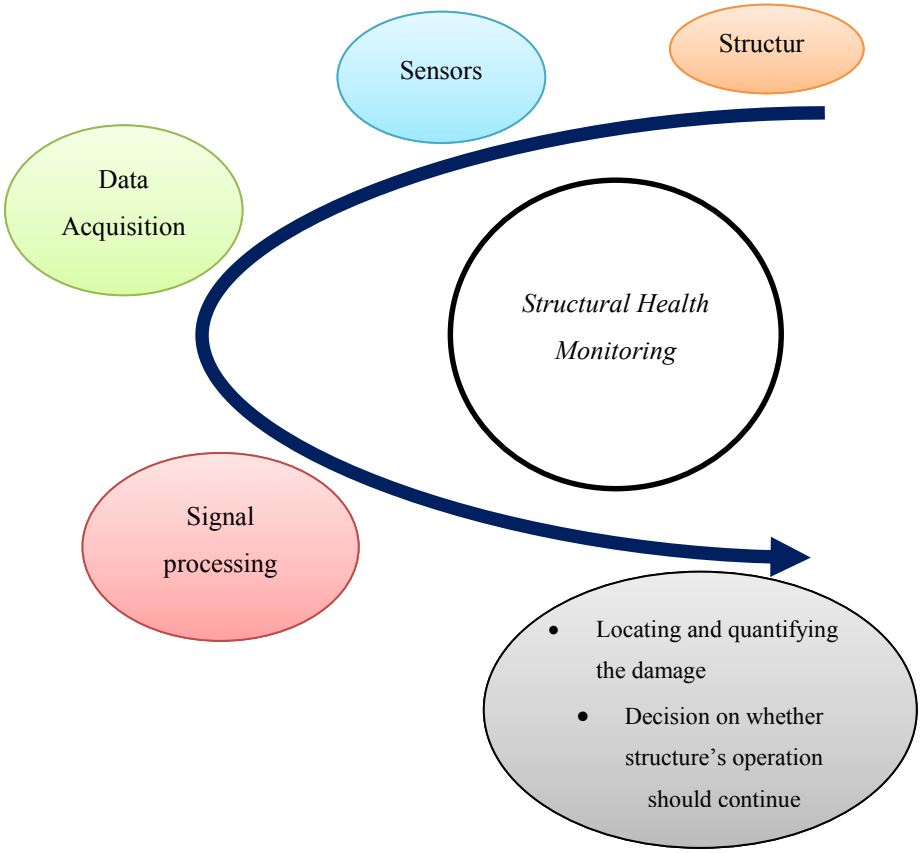

Figure 1-1: Basic elements of SHM

As such, SHM is expected to alleviate the drawbacks of the traditional NDE techniques. Of the various SHM approaches, one can mention vibration-based, impedance-based and fiber optic methods. These techniques are mainly categorized based on the type of sensors they incorporate. Regardless of SHM approaches, SHM in general aims to include the following tasks [4]:

(i) Detecting the damage

(ii) Localization of damage

(iii) Quantify the extent of damage

(iv) Estimate the remaining life

In most approaches, the first two tasks are successfully accomplished. However, it usually demands incorporation of large numbers of sensors if the potential damage is to be explored within the whole structure. The quantification of damage by various approaches has also been evaluated. It is likely to have a better estimation of damage size in the early stage of damage growth rather than at the critical levels of damage [5, 6]. Consequently, the predication of remaining life of a structure is a challenging task, specifically for complex structures. SHM of large complex structures requires a scan of the entire system with numerous sensors and a robust signal processing technique that could reasonably quantify the extent of damage.

The present thesis aims at further development and enhancement of a vibration-based SHM (VB-SHM) approach. Therefore, elements and application of a VB-SHM are briefly explained in the following subsection. The motivation and objectives for the present work will be described in the next section. This chapter ends with an outline of the organization of the thesis.

1.1.1 Vibration-based Structural Health Monitoring (VB-SHM)

In a typical VB-SHM, as elucidated in Figure 1-2, the structure is excited via an instrumented manual or automated hammer. The induced vibration signals are then gathered in an analogue format by appropriate contact/non-contact sensors (e.g., accelerometers, piezoelectrics, or a laser doppler vibrometer). The individual sensor's signal include important information about both the local and global mechanical/modal properties of the system. Since the initiation of damage would alter the mechanical properties of structures (e.g., stiffness, mass, damping) to different extents, the vibration signals could potentially sense the existence and track the progression of defects, so long as they are deciphered appropriately.

The analogue signals need to be converted into a digital format in order for the vibration data to be recorded, processed and interpreted by an appropriate algorithm within a

computer. For this, one requires a Data Acquisition (DAQ) system. The last part of the VB-SHM is the data processing. The digital data from the sensors are fed into an appropriate damage detection algorithm. Such an algorithm extracts and compares damage sensitive features embedded within the signals (e.g., natural frequencies, mode shapes, and time/frequency-domain representations of the signals). The outcome of the processing unit would dictate the continuation/shut down of the operation of the monitored system.

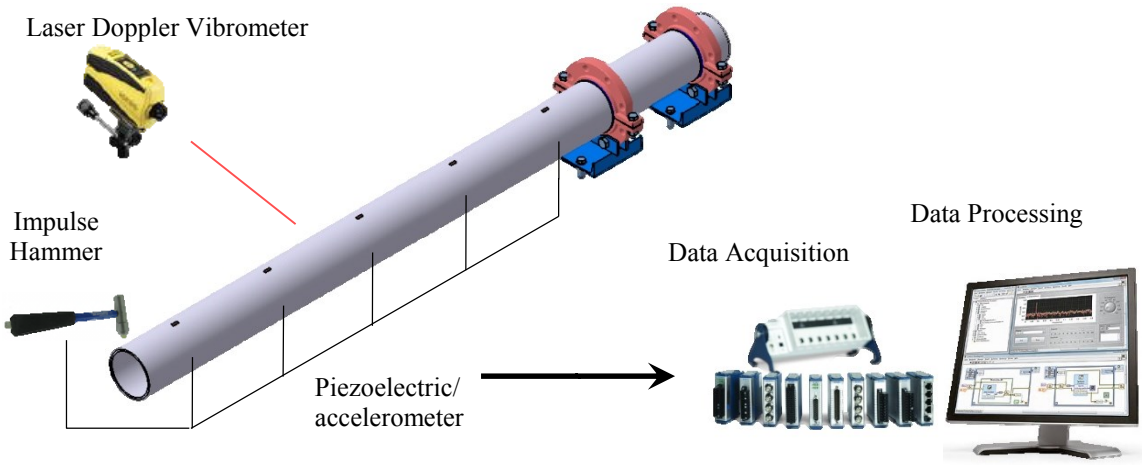

Figure 1-2: Various elements of VB-SHM

1.2 MOTIVATION AND OBJECTIVES

The present study is a continuation toward the enhancement and extension of the application of a novel VB-SHM developed earlier in our research group [7]. This methodology was invented by Cheraghi and Taheri in 2007 [7]. It took its name eventually as Empirical Mode Decomposition_ Energy Damage Index (EMD_EDI). Its application was verified experimentally and numerically mainly on pipelines, by Rezaei and Taheri [8-10]. This VB-SHM has been applied for monitoring common types of damage, including corrosions, loosening of bolted flange joints, and cracks in girth-weld of pipelines.

The methods yielded encouraging results on the above-mentioned defects evidenced by the published works, albeit, some inconsistencies were reported [8-11]. Also, recommendations proposed by the main researchers suggested the use of a wireless sensing unit as opposed to the cumbersome wire-based system in order to increase the versatility

and utility of the approach. All the case-studies in the past works were devoted to health monitoring of onshore pipelines. Owing to their vital importance, especially for offshore applications, adjustments and subsequent verifications of the developed methodology were amongst the main motivations of the present work. It was also of interest to extend the application of current health monitoring strategy (EMD_EDI) into examination of real-life damage scenarios as opposed to their simulated counterparts.

To address the above-mentioned demands, the objectives of the present work can be summarized as follows:

- Resolving the inconsistency observed in detection of bolt-loosening in bolted flange joints of pipelines reported in [11].
- Integrity assessment of the developed methods for a wireless/remote data acquisition.
- Development and adjustment of the EMD_EDI for health monitoring of offshore pipelines.
- Exploring the capability of the EMD_EDI in detection real-life damage scenarios (e.g., detection of fatigue cracks as opposed to typical investigations for notch)

1.3 THESIS LAYOUT

This dissertation has been divided into seven chapters including the present chapter, which offers an introduction to the subject of the research, and clarifies the motivation and objectives pursued throughout the thesis.

Chapter 2 begins with a review of various vibration-based techniques. Advantages and disadvantages of each method are briefly described. This chapter also includes a comprehensive review of related past works. Literature surveys on detection of bolt-loosening in joints, and fatigue cracks/notches in structures are presented. A review on the VB-SHM of offshore pipelines is preceded by an introduction to challenges of applications, modeling techniques of submerged structures.

The rest of the thesis presents the results of both experimental and numerical studies that is believed to fulfill the demands and recommendations mentioned in the previous section. Accordingly, chapter three to six are individual studies compiled into journal paper format that are either published or under review for publication.

As stated before, the early works in our research group reported some inconsistency in application of EMD_EDI, mainly in detection of bolt loosening in bolted flange joints of pipelines [11]. The inconsistency routed in the reproducibility of the processed signals, which, in turn blurred the accuracy of the EMD_EDI in tracking the advancement of damage. Chapter 3 is exclusively devoted to addressing and resolving the reported inconsistency, and verification of a wireless sensing unit as a viable DAQ system. For this purpose, experimental and numerical frameworks were designed for health monitoring of a bolted flange joint of a full-scale pipeline. The source of the inconsistency was mainly attributed to reconstruction of the signals being converted from analogue to digital format. Also, reproducibility of the impacts was significantly improved by employing an electrical hammer. Hence, more accurate collection and recording of the sensors' signals, besides the repeatable excitation, considerably improved the consistency of the signal processing protocol. These modifications enabled the EMD_EDI to substantially increase its resolution in tracking the damage progression. The wireless DAQ executed the conversion of signals from analogue to digital format as accurate and to be as reliable as the wire-based DAQ employed in our previous trials. As such, it will render the future utility of EMD_EDI viable for remote applications.

Chapters 4 is an explanatory section that guides the readers through the theoretical and numerical modeling aspects of two commonly used approaches for assessing the dynamic response of submerged bodies. It discusses the influences of various parameters affecting the integrity of VB-SHM trials when applied to submerged structures and the associated challenges. The eigenvalue and transient analyses reported in the chapter uncover some of the most important key factors that must be considered in order to conduct successful structural health monitoring. For instance, it highlights the importance of use of an appropriate dynamic modeling approach for the numerical simulation of the VB-SHM. Therefore, the performance of two widely-used modeling approaches, namely the "added mass" and "coupled acoustic-structural" approaches in analyzing the vibration response of a submerged pipe, were assessed and compared. The second approach was demonstrated to be more suitable for use in association with the vibration-based damage detection strategies, as it more accurately represented the dynamics of the submerged pipe. Moreover, the influence of operational variability on the accuracy of VB-SHM of

submerged structures was studied. Abrupt reductions/increases in the internal and external pressures that could be experienced by a submerged pipe were considered as the operational variability. It was determined that the change in the vibration response of the submerged pipe (hence, the accuracy of pipe's VB-SHM), depends on pipe's stiffness and the level of the imposed operational variability. To further explore the influence of the parameters, three different pipes (i.e., with different stiffness) were considered. The vibration response of the submerged steel pipe considered in the study (i.e., the pipe with highest stiffness) remained almost unaffected in the presence of the considered operational variability. Therefore, VB-SHM of the submerged steel pipe could be reliably accomplished in practice. On the other hand, the vibration response of the less stiff pipes (the E-glass/epoxy and carbon/epoxy pipes) showed notable sensitivity to the same operational variability. Therefore, it is recommended that the VB-SHM of such composite pipes be conducted with outmost diligence.

Chapter 5 presents the results of extensive experimental and numerical studies on VB-SHM of a submerged pipe. They focused on detection and tracking of a propagating notch in the girth-weld of a submerged aluminum pipe. The numerical simulations were conducted on ABAQUS platform, and the following experimental verifications were carried out in our laboratory tank. Piezoelectric-based actuation/sensing units were successfully modeled in the ABAQUS. To initiate the vibration into the submerged pipe, two means were designed and fabricated, and their performances were compared. One was a waterproofed pneumatic hammer, fabricated to impart typical impulsive force routinely used in VB- SHMs. The other involved the assessment of feasibility of excitation through one of the piezopolymers. The latter means was proven to offer a simpler, more reliable, and less expensive excitation method. It should be noted that the aforementioned piezoelectric-based actuation unit was adopted into our methodology for the first time. The study concluded that only two piezoelectric transducer would be required for a successful health monitoring of girth-welds within the submerged pipe.

Moreover, consideration of a notch (slot) as a replacement for a fatigue crack has been commonly used by VB-SHM researchers [5]. This simplifying assumption could approximate the dynamic properties of the structure hosting real-life fatigue cracks. However, great care must be taken, since it has been explicitly shown that the dynamic

characteristics of a structure could variably change as a function of width and depth ratio of the notch [12]. It is, therefore, believed a damage detection strategy could not be deemed reliable in detecting real-life fatigue cracks, unless it is tested for actual sharp cracks.

In consideration of the above-mentioned fact, chapter 6 demonstrates the capability of EMD_EDI in detection of fatigue cracks in structures, thus paving the way for a more advanced VB-SHM of pipelines' girth-welds. For that, fatigue cracks of various dimensions were introduced into an aluminum beam. Two low-cost piezoelectric sensors monitored the beam vibration as it was excited by a manual modal hammer. Performance of EMD_EDI in detecting the fatigue cracks was compared against some other VB-SHM approaches including the natural frequency and damping analyses. It is concluded that the EMD_EDI could identify both the initiation and progression of sharp cracks in the same order of resolution as reported in the encouraging study of notches reported by other researchers [9]. Also, EMD_EDI is proved to outperform the prediction obtained through the natural frequency and damping analyses, especially if a local inspection of a structure is pursued (e.g. girth-weld of a pipeline).

Chapter 7 closes the thesis by providing overall conclusions and recommendations for pursuing the development of current VB-SHM strategy.

It should be mentioned that some of the materials presented in the thesis may be repeated as the thesis is presented in a paper publication format.

1.4 SUMMARY OF THE CONTRIBUTIONS

The following main contributions towards the improvements and further refinements of a vibration-based damage detection methodology, which was originated and developed within our research group, were achieved through the works conducted within the auspices of the thesis.

(i) The root of the significant inconsistency observed in detection of bolt-loosening in bolted flange joints of pipelines reported in the previous trials [11] was successfully identified and resolved.

(ii) Wireless/remote application of the methodology was successfully accomplished. This significantly enhances the utility of the method in comparison to the previously-tried wire-based applications.

(iii) The application of the method was extended to health monitoring of submerged pipes.

(iv) An autonomous piezoelectric-based sensing/actuation unit was incorporated for the first time into the application of the method. This enhancement improved the robustness of the technique.

(v) Capability of the method in detection of real-life damage scenarios was examined (e.g., detection of real sharp fatigue crack as opposed to typically considered notches).

1.5 REFERENCES

1. *Guidelines for the management of the integrity of bolted joints for pressurized systems*. 2007, Energy Institue: London.
2. Na, W.-B. and T. Kundu, *Underwater pipeline inspection using guided waves.* Transactions-American Society of Mechanical Engineers Journal of Pressure Vessel Technology, 2002. **124**(2): p. 196-200.
3. *Application notes*. 2012 [cited 2012 February]; Available from: http://www.olympus-ims.com/.
4. Balageas, D.F., C. P.; G¨uemes, A., *Structural health monitoring*. 2006, Newport Beach, CA: ISTE.
5. Razi, P., R.A. Esmaeel, and F. Taheri, *Application of a robust vibration-based non-destructive method for detection of fatigue cracks in structures.* Smart Materials and Structures, 2011. **20**(11): p. 115017.
6. Afshari, M., T. Marquié, and D.J. Inman. *Automated structural health monitoring of bolted joints in railroad switches*. in *Proceedings of ASME 2009 Rail Transportation Division Fall Conference*. 2009.
7. Cheraghi, N. and F. Taheri, *A damage index for structural health monitoring based on the empirical mode decomposition.* Mechanics of Materials and Structures, 2007. **2**(1): p. 43-62.
8. Rezaei, D. and F. Taheri, *Experimental validation of a novel structural damage detection method based on empirical mode decomposition.* Smart Materials and Structures, 2009. **18**(4): p. 045004.
9. Rezaei, D. and F. Taheri, *Damage identification in beams using empirical mode decomposition.* Structural Health Monitoring, 2011. **10**(3): p. 261-274.
10. Rezaei, D. and F. Taheri, *Health monitoring of pipeline girth weld using empirical mode decomposition.* Smart Materials and Structures, 2010. **19**(5): p. 055016.
11. Esmaeel, R.A., J. Briand, and F. Taheri, *Computational simulation and experimental verification of a new vibration-based structural health monitoring approach using piezoelectric sensors.* Structural Health Monitoring, 2011. **11**(2): p. 237-250.

CHAPTER 2 BACKGROUND AND LITERATURE REVIEW

This chapter presents a review of VB SHM's principals and its various approaches, including the basis for the developed strategy utilized in this thesis. The insight into our developed damage detection algorithm (EMD_EDI), as well as modifications made in its hardware/software will be presented in the next chapters. This chapter also provides exclusive review of literature for individual health monitoring practices completed in the thesis.

2.1 VIBRATION-BASED STRAUCTURAL HEALTH MONITORING (VB-SHM): BASIS AND APPROACHES

Consider the following equation describing the motion of a continuous system (e.g. the pipe shown in Figure 1-2) in modal space:

$$\boldsymbol{M}\ddot{\boldsymbol{x}}(t) + \boldsymbol{C}\dot{\boldsymbol{x}}(t) + \boldsymbol{K}\boldsymbol{x}(t) = \boldsymbol{F}(t) \qquad 2\text{-}1$$

where, $\boldsymbol{M}$, $\boldsymbol{C}$, and $\boldsymbol{K}$ are the matrices representing the mass, damping, and stiffness matrices of the system, respectively. $\boldsymbol{F}(t)$ is the external force function applied to the structure, and $\boldsymbol{x}(t)$ is the time-dependent displacement response of the system. The above equation can be rearranged to solve for its eigenvalues, $\boldsymbol{\omega}$, and eigenmodes, $\{\boldsymbol{x}\}$:

$$(\boldsymbol{M}\boldsymbol{\omega}^2 + \boldsymbol{C}\boldsymbol{\omega} + \boldsymbol{K})\{\boldsymbol{x}\} = 0 \qquad 2\text{-}2$$

Note that the free vibration of the system (no external force) and a harmonic response, $\boldsymbol{X}(t) = \{\boldsymbol{X}\}e^{i\omega t}$, have been assumed.

In an experimental procedure, one can deploy appropriate sensors on a structure (see Figure 1-2) to obtain its eigensolution. This process is facilitated by feeding the sensors' signals into appropriate software that applies modal analysis technique [1].

Initiation of damage would alter the physical properties of a system (e.g., stiffness, mass, and damping), hence changing the eigensolution/dynamic response of the system. Any attempt to identify the damage from the system's eigensolution or its dynamic response in time/frequency domains is referred to as VB-SHM. Various VB-SHM techniques have

been developed, which can fall under two main streams as described in the next subsections.

2.1.1 Modal-Based Approach

In this approach, the modal properties (e.g., natural frequencies and mode shapes) of structures at lower modes are interrogated periodically (as stated before, these parameters can be measured by incorporating appropriate sensors onto the system). Deviations in the measured natural frequencies and the mode shapes could warn the onset and propagation of damage. Natural frequencies of a system can be reasonably easily determined by incorporating usually one sensor, thus promoting the application of this approach. However, these are considered as the global properties of the system. Therefore, identification of damage location is almost impossible, except for some simple structural geometries (e.g., beam-type structures) [2]. Also, the existence of damage can reliably be detected only when the defect is relatively severe [3].

On the other hand, mode shapes of structures provide both global and local information on a structures' dynamic response. Monitoring the deviations in the mode shapes can, therefore, be a suitable candidate for identifying the location of damage. However, the measurement of mode shapes is a cumbersome task, which requires deployment of a large number of sensors on a structure [4].

Applications of modal-based VB-SHM into various systems have been presented in section 2.2.

2.1.2 Time/Frequency-domain Signal Processing Approach

Upon introduction of defects, dynamic response of a system deviates from its healthy condition. This change is a consequence of alteration in eigensolution of damaged structure. The variation could manifest itself in the time-history or frequency spectrum of the vibration signals gathered via sensors bonded onto structures. Damage might also alter the signals' maximum amplitude, energy, or signal's general pattern. For instance, the beating phenomenon observed in the vibration of structures hosting fatigue cracks has been reported in literature [5]. This phenomenon enables one to monitor the integrity of structures by examination of its vibration signal's time-history. Likewise, frequency

spectrums transferred from the vibration signals' time-histories contain discernible features, facilitating the process of health monitoring [6].

Identification of damage through time/frequency domain of signals is considered a local inspection. Usually, a wave is propagated in the inspection area via piezoelectric actuators or the random vibrations induced by system's surrounding environment. Then, the receiver sensors record the vibration signals, which are fed into a processing unit for establishing damage indices. In contrast to modal-based approaches, it is possible to interrogate higher frequencies (e.g., ultrasonic range- more than 20 kHz). This would, however, limit the inspection area because of a high rate of damping for this range of frequencies.

Various signal processing techniques can also be adopted to unveil damage-sensitive features within the time/frequency domain representation of signals. The most important signal processing techniques that have been used in damage detection practices are discussed in the next subsections.

2.1.2.1 Fast Fourier Transform (FFT)

The well-known Fourier analysis expresses any periodic or non-periodic function by a series of sine and cosine terms with individual amplitude, frequency, and phases. It serves as a means to construct the frequency domain of a time-signal. The Fourier Transform (FT) of a continuous signal can be obtained by calculating the following integral:

$$X(f) = \int_{-\infty}^{+\infty} x(t) e^{-i2\pi ft} dt \qquad 2\text{-}3$$

Where t and f represent the time and frequency, respectively. $X(f)$ is the FT of the signal, $x(t)$. In practical applications, a non-continuous (discrete) form of a signal would be in hand. It is because the analogue (continuous) data from the sensors is digitized (non-continues), in order to enable a computer to read the data. Once the N number of discrete samples from a function, $x(n)$, are available, the FT of $x(n)$ takes the following form, which is called the Discrete Fourier Transform (DFT):

$$X(k) = \sum_{n=0}^{N-1} x(n) e^{-j(\frac{2\pi}{N})kn} \quad for\ k = 0,1,2,...,N-1 \qquad 2\text{-}4$$

where $(n = 0,1,2,...,N-1)$ is the time-sample index. DFT transforms a series of time-domain samples to frequency-domain samples. The number of arithmetic operations

required for DFT is of order $O(N^2)$. The Fast Fourier Transform (FFT) is a DFT that applies algorithms to reduce the number of multiplications to order of $O(N \log_2 N)$.

FFT has served in VB-SHM as a means to extract damage sensitive features and establish damage indices. Cheraghi *et al.* [6] conducted a numerical study for detection of corrosion in pipelines via piezoelectric sensors. They introduced the energy of the frequency spectrums of the sensors' signals as a damage sensitive feature. Damage indices were established by comparing those energies calculated for healthy and damaged pipe. Location of damage was successfully estimated as the neighbor sensors produced noticeably larger damage indices compared to the rest of the sensors. The damage intensity was also determined by observing an increased rate of damage indices produced by the sensors close to the defect.

As discussed, FFT reveals the frequency component of a time-signal. In case of stationary signals (the frequency content of signals does not change over the time), therefore, FFT could provide complete information about the signal. However, many phenomena are known as non-stationary, that is their frequency content changes as the time elapses. In such cases, FFT falls short of providing time-modulated frequency information. As such, other signal processing techniques have been developed to address this issue.

2.1.2.2 Wavelet Transform (WT)

The Wavelet Transform (WT) evolved during 1990s to address the shortfalls of the FFT, mainly in dealing with the non-stationary signals. WT employs a "wavelike" window function that can move along the time axis. The window can also dilate/compress itself as it sweeps the time axis. This wavelike window is called a "wavelet". Multiplying the time/scale-adjustable wavelet by the signal would provide a time-modulated frequency spectrum of the signal.

Different wavelets have been adopted in dealing with various signals. The Mexican hat, Guassian, Haar, and Morlet are the most commonly used wavelets. Figure 2-1(a) shows the Mexican Hat wavelet defined by the following function:

$$\psi(t) = \left(1 - t^2\right) e^{-\frac{t^2}{2}} \qquad 2\text{-}5$$

Figure 2-1 (b) and (c) elucidate the wavelet translation along the time axis and its dilation/compression, respectively. The WT of a continuous time-signal can be established by the following integral:

$$T(a,b) = \frac{1}{\sqrt{a}} \int_{-\infty}^{+\infty} x(t)\psi^* \left(\frac{t-b}{a} \right) dt \qquad 2\text{-}6$$

Since the transformation is conducted over a continuous signal, it's called a Continuous Wavelet Transform (CWT). $T(a,b)$ represents the WT of the signal, $x(t)$. b is the translation parameter and is responsible for the movement of the wavelet along the time axis. a is the scale parameter that controls the dilation and compression of the wavelet. Multiplying the wavelet at its dilated shape (i.e., larger values of a) with the signal produces relatively large coefficients (i.e., $T(a,b)$) for the portion of the signal with longer period (low frequencies). Conversely, it produces large coefficients for the portion of the signal with shorter period (high frequencies) at its compressed shape. Figure 2-2 clarifies the wavelet action on the signal as it moves step-wise along a typical time-signal with various dilation rates. When $a = 1$, the wavelet tends to capture/match the longer period of the signal, hence, the integral defined in Equation 2-6 would yield large coefficients for this specific value of scale parameter. Likewise, as $a = 1/3$ the wavelet pairs with smaller period (higher frequency) of the signal. As such, a plot of wavelet coefficients, $T(a,b)$, would provide meaningful information on the time-modulated frequency spectrum of time-signals.

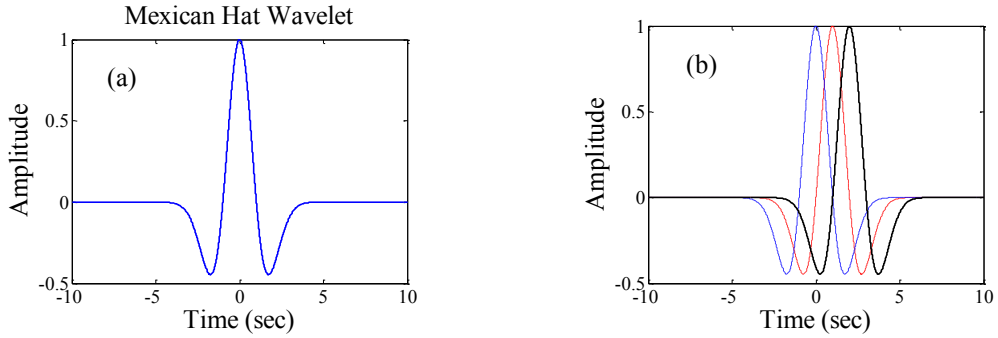

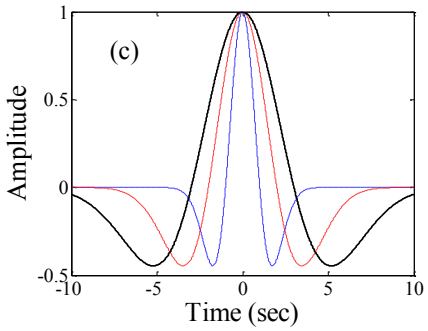

Figure 2-1: (a) The Mexican Hat Wavelet (b) time translation and (c) dilation/compression of the wavelet.

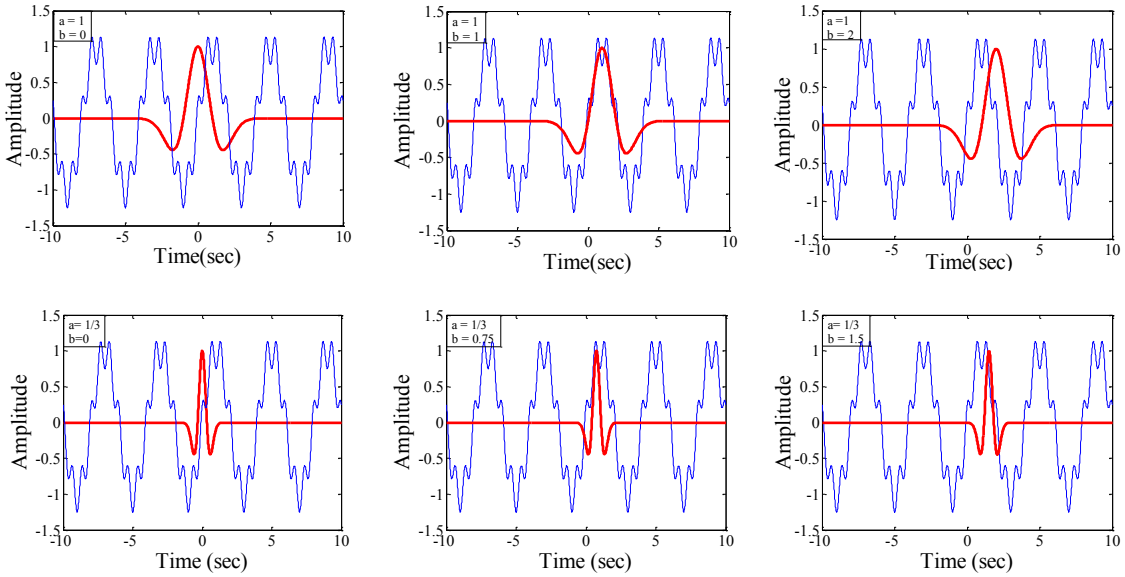

Figure 2-2: A signal being scanned by the Mexican Hat wavelet with various dilation rates, a, and translation parameters, b.

In CWT, Equation 2-6 is executed by smoothly shifting a scalable wavelet for both the time and frequency domains over the whole signal. This would be a computationally expensive process. Often times, faster speeds may be required. Discrete Wavelet Transform (DWT) offers significant reduction in the computational time by calculating the same integral with discrete wavelets (i.e., wavelets with discrete scale and translation steps). One of the commonly used ways of discretizing the scale and translation parameters is to adopt the power-of-two logarithmic basis as given below:

$$a = 2^m \qquad b = n \times 2^m \tag{2-7}$$

Subsequently, the DWT can be expressed by:

$$T_{m,n} = \int_{-\infty}^{+\infty} x(t) \frac{1}{\sqrt{2^m}} \psi\left(2^{-m} t - n\right) dt \qquad 2\text{-}8$$

Researchers have been adopting different versions of the WT in VB-SHM of various structures. Peng *et al.* [7] employed the Wavelet Packet Transform (WPT) for health monitoring of subsea pipelines. The vibration signals of the implemented sensors excited by the ambient wave force were fed into the damage detection algorithm. An energy-based damage index was introduced for identification of free-span locations and their severities. The numerical and the experimental studies on the scaled pipe verified the effectiveness of their methodology. Melhem and Kim [8] utilized the CWT for damage detection of typical concrete highway structures. Fatigue loadings were applied to the structure. Acceleration measurements due to impact tests were gathered in specified cycles of the fatigue loading. Comparison of the two dimensional (time-frequency contours) plots of the CWT revealed clear indications on the presence and the progression of damage. Cheraghi *et al.* [6] compared the performance of WT and WPT for degradation assessment of a pipe. Their numerical study concluded that the two energy-based approaches were successful in detection of simulated corrosion within the pipe. Albeit, the WT slightly outperformed the WPT.

The WT is known to provide a multi-resolution time-frequency representation of a time-signal. The plot of WT values gives a good time resolution and poor frequency resolution at high frequencies, and good frequency resolution, but poor time resolution at lower frequencies. Also, selection of an appropriate mother wavelet is usually essential in achieving the best time-frequency representations of specific signals. Likewise, the FFT is more suited to linear systems; it gives meaningful representation of the signals having "interwave" frequency modulation (gradual frequency change). However, it is not able to accommodate non-linear systems, as their signals contain "intrawave" frequency modulation (abruptly change in frequency) [9]. Therefore, a signal processing method described below was subsequently developed in an effort to resolve the above-mentioned issues.

2.1.2.3 Hilbert-Huang Transform (HHT)

In 1998, Huang *et al.* [9] introduced a revolutionary signal processing technique, which was named the Empirical Mode Decomposition (EMD). It can be accompanied by the Hilbert Transform (HT) scheme to yield the time-modulated frequency content of a signal. The decomposition and the subsequent HT is referred to as Hilbert-Huang Transform (HHT). This method outperforms the WT in terms of resolution, adaptability, and the capability of analyzing non-linear signals.

EMD decomposes a signal into a set of oscillatory functions which are called the Intrinsic Mode Functions (IMFs). IMFs are independent of one another and contain certain frequency component(s) of the signal. The decomposition is achieved via an empirical process called "sifting". The algorithm starts with fitting two cubic splines through the local maxima and minima of a time-signal, x(t), constructing the upper and lower envelopes (see Figure 2-3). The average of the envelopes (m_1) is subtracted from the original signal. The results would be the first component, h_1.

$$h_1 = x(t) - m_1 \tag{2-9}$$

Ideally, h_1 should be the first IMF. However, a multiple sifting process is usually needed to achieve the IMFs that would be well-suited for the HHT [9]. That is because if the IMF signal has a non-zero mean greater than unity (asymmetric signal), then both the phase function and the instantaneous frequency obtained from the subsequent HT would be negative values, thus yielding meaningless results. Therefore, h_1 is treated as a new signal and the same procedure is repeated onto it, as if it was the original signal. The second component, h_{11}, would be given by:

$$h_{11} = h_1 - m_{11} \tag{2-10}$$

where m_{11} is the mean of the cubic splines constructed from the local maxima and minima of h_1. The sifting process continues until a stopping criterion, SD, as proposed by Huang *et al.* is met [9]:

$$SD = \sum_{t=0}^{T} \left[\frac{\left| h_{1(k-1)}(t) - h_{1k}(t) \right|^2}{h_{1(k-1)}^2(t)} \right] \leq 0.2 \qquad 2\text{-}11$$

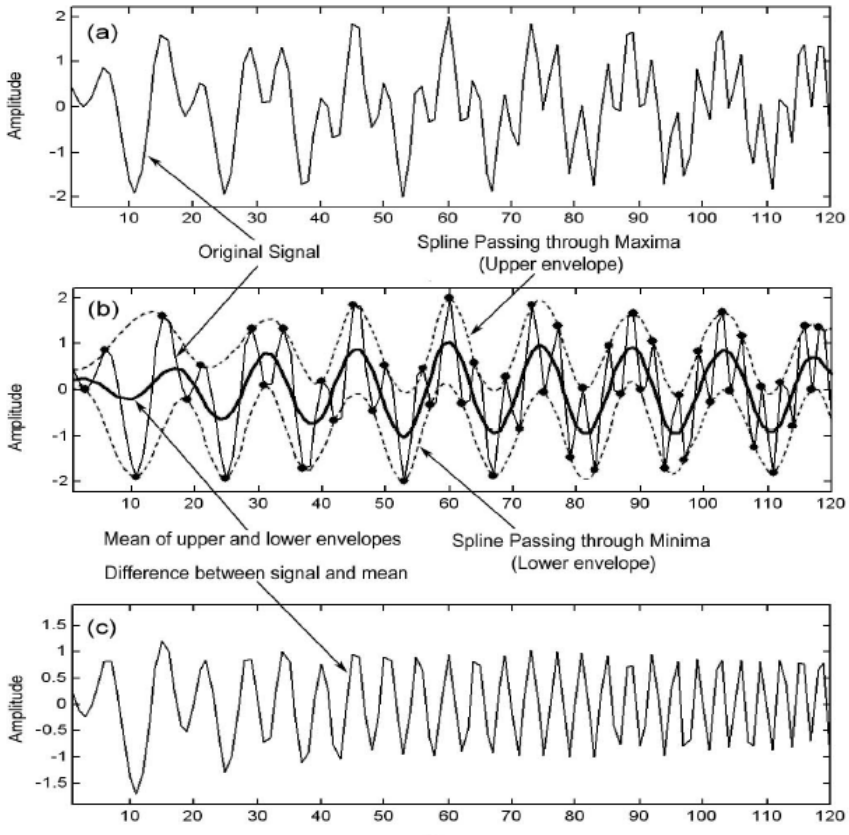

Figure 2-3: A schematic representation of the sifting process. (a) The original signal; (b) the signal in a thin solid line, the upper and lower envelopes in dashed lines; the mean in a thick solid line and (c) the difference between the signal and the mean [9].

Figure 2-4 shows the results after the first and ninth sifting processes. As can be noted, the signal shown in Figure 2-4(b) meets the essential requirement (symmetry) for an acceptable IMF. At this point, the resultant signal is called the first IMF of the signal, c_1.

$$c_1 = h_{1k} \qquad 2\text{-}12$$

The first IMF usually contains the finest oscillation or period of the signal; the sifting process separates the finest oscillatory component or equivalently the highest frequency of the signal.

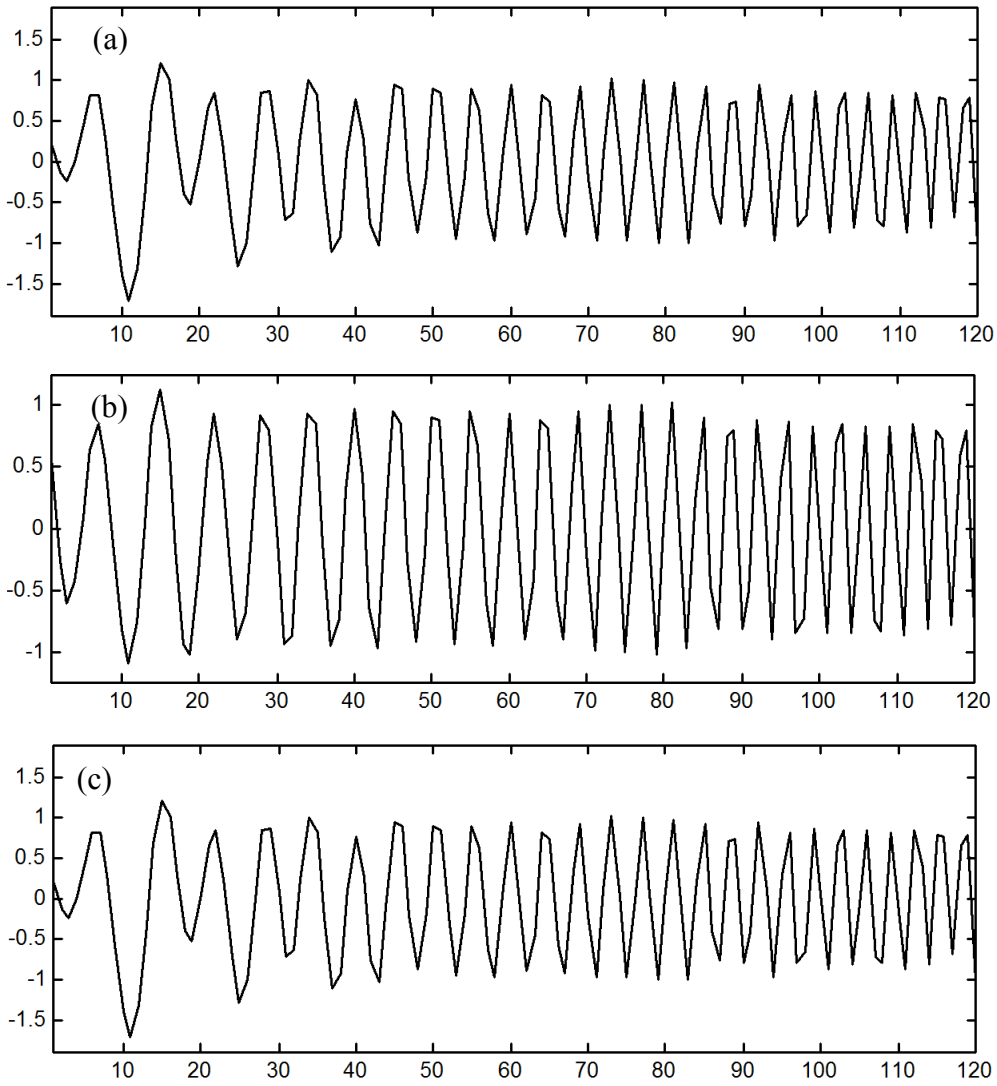

Figure 2-4: Effect of repeated sifting process. (a) After 2nd sifting of the result in Figure 2-3(c), the resulting signal is improved in terms of its symmetry, but still requires more sifting to eliminate the asymmetry. (b) After 9th sifting of the signal in Figure 2-3(c), the result show a very good symmetry, thus it can be considered as an IMF [9].

To extract the other IMFs, the first IMF, c_1, is subtracted from the original signal, $x(t)$:

$$r_1 = x(t) - c_1 \qquad 2\text{-}13$$

The sifting process is then repeated for the residue, r_1, until reaching the second IMF. Extracting the IMFs of a signal continues until the following criteria are met [9]:

i. The nth IMF, c_n, or residue r_n becomes less than a pre-assumed value, or

ii. The n^{th} residue becomes a monotonic signal, such that no further IMF can be extracted from it.

The driven IMFs are well-suited for HHT and assure a high resolution representation of the signal in time-frequency domains. EMD is a complete decomposition and as mentioned earlier, the extracted IMFs are orthogonal or independent of each other. The completeness of the decomposition is assured as one can reconstruct the original signal from the following identity:

$$x(t) = \sum_{i=1}^{n} c_i + r_n \qquad 2\text{-}14$$

The orthogonality has been verified numerically by Huang *et al* [9]. They included the residue as an additional element such that the Equation 2-14 takes the following form:

$$x(t) = \sum_{j=1}^{n+1} c_j(t) \qquad 2\text{-}15$$

Taking the square of the signal:

$$x^2(t) = \sum_{j=1}^{n+1} c_j^2(t) + 2\sum_{j=1}^{n+1}\sum_{k=1}^{n1} c_j(t)c_k(t) \qquad 2\text{-}16$$

Orthogonality of the signal necessitate the sum of cross terms given in the right hand side of the Equation 2-16 to be zero. An overall index of orthogonality is therefore defined as follows [9]:

$$IO = \sum_{t=0}^{T}\left(\sum_{j=1}^{n+1}\sum_{k=1}^{n+1} c_j(t)c_k(t)x^2(t)\right) \qquad 2\text{-}17$$

For wind data examined by Huang *et al.* [9], the IO value was determined to be only 0.0067 (therefore, proving the orthogonality of the signals) . So far, one can decompose a signal into its IMFs, each of which contains specific oscillatory component(s) of the signal. The time-frequency modulated representation of the signal can be consequently graphed by passing the IMFs through the so called HT. As the IMFs are time-signals, one can compute the HT of the IMFs by considering the following convolution integral:

$$H\left[x(t)\right] = y(t) = \frac{1}{\pi} P\int_{-\infty}^{+\infty} \frac{x(\tau)}{t-\tau} d\tau \qquad 2\text{-}18$$

Where $x(t)$ is replaced with individual IMFs. The term P dictates the Cauchy principal value that prevents the integral from having singularities. $y(t)$ is the best local fit of a trigonometric function. The term, $1/t$ bolds the local properties. An analytical signal can then be constructed by the complex conjugate of $x(t)$ and its Hilbert transform, $y(t)$ [9]:

$$z(t) = x(t) + iy(t) \tag{2-19}$$

Or in polar coordinate:

$$z(t) = a(t)e^{i\theta(t)}$$
$$a(t) = \sqrt{x^2(t) + y^2(t)} \qquad \theta(t) = a\tan\left(\frac{\mathrm{y}(t)}{x(t)}\right) \tag{2-20}$$

A term called "instantaneous frequency", ω, can be defined as follows:

$$\omega = 2\pi f_0 = \frac{d\theta(\mathrm{t})}{dt} \tag{2-21}$$

This time-modulated frequency, ω, enables one to analyze the non-stationary signals. Owing to its simplicity, adaptability (data-driven), and capability in analyzing non-linear signals, HHT became recently popular in VB-SHM. Loutridis [10] showed that the instantaneous frequency and the energy of the IMFs are good candidates for damage detection. He examined identification of cracking and tooth loss in a gear system. The aforementioned features extracted from the vibration signal of the gear system resulted in a successful damage detection. Cheraghi and Taheri [11] suggested the energy of the vibration signal's first IMF as an effective damage detection indicator. In a numerical study, they deployed piezoelectric sensors onto a cantilever pipe for monitoring purposes. Damage scenarios included various reductions in wall thickness of the pipe at different locations as a means to simulate corrosion. Location and intensity of corrosion could be identified successfully. Bao *et al* [12] introduced the energy of the HHT spectrum of the vibration signals as a damage indicator. They were able to locate and quantify the simulated corrosion in a pipeline by monitoring its vibration under ambient excitation.

As a closing remark for this section, Table 2-1 compares various signal processing techniques described above. In Table 2-1, being "adaptable" means the signal processing method is data-based. The basis for the FFT is a series of cosine and sine terms. The wavelet is the basis for the WT. Once a wavelet is selected, the whole data has to be

analyzed with that specific wavelet. Hence, FFT and WT are not considered “adaptive” or data-based (in here, data-based signal processing is a processing tool which does not need any predefined operator (such as wavelets or trigonometric functions) for decomposition of a signal).While, in HHT, the signal is decomposed by an empirical method, which is completely data-based. Adaptability makes the signal processing highly robust and sound, especially in dealing with non-linear systems [9].

Table 2-1: Comparison of various signal processing techniques.

	FFT	**WT**	**HHT**
Adaptability	×	×	✓
Linear Systems	✓	✓	✓
Non-Linear Systems	×	×	✓
Stationary Signals	✓	✓	✓
Non-Stationary Signals	×	✓	✓

2.2 REVIEW OF THE SELECTED VIBRATION-BASED DAMAGE DETECTION PRACTICES

VB-SHM methods have been applied for detection of various types of damage within different structures being served in wide range of applications including aerospace, mechanical and civil infrastructures [13]. This section focuses on the review of the past works conducted on the damage detection practices attempted in the present thesis. It briefly discusses the successes, deficiencies of the previous VB-SHM trials. It also provides an insight into practical challenges, and the key parameters that could influence the integrity of the VB-SHM practices.

2.2.1 VB-SHM of Bolted Joints

Bolted joints are used in various engineering applications. Some examples are mating of pipelines conveying oil and gas, railroad switches, aerospace structural components, bridges, and many other applications. Bolted joints are susceptible to defects such as corrosion, and self-loosening, which is usually initiated by vibration or severe cyclic

thermal loads [14]. These defects, upon being undetected, could cause leakage or complete failure of the joints. Therefore, routine inspections must be organized to prevent potentially catastrophic failures. As such, preload on the bolts are regularly checked by torque wrenches. The other types of bolt failure (e.g., due to corrosion) are examined by various non-destructive techniques including visual inspection, ultrasonic and radiography techniques [14]. Reduction in labor cost, inspection time, and providing possibility of assessment in harsh conditions (e.g., buried structures, and inaccessible components) have encouraged researchers to apply SHM techniques for effective detection of defects within such joints. Impedance and vibration-based techniques have therefore been adopted for this practice.

Loosening of bolted joints would reduce the overall stiffness of the structure hosting the joints. It would also change the local pattern of energy dissipation, hence modifying the local damping. Therefore, as discussed in section 2.1, detection of bolt loosening is feasible through VB-SHM methods. Researchers have been applying the two approaches described earlier (i.e., the modal and time/frequency domain signal processing techniques) for detection of bolt loosening and track its severity.

It is noteworthy that VB-SHM approaches have shown variable sensitivity in detecting loosening of bolts. Ideally, determination of torque levels on each bolt is desirable. This practice would eliminate failures of bolted joints. However, such a practice in most realistic cases is not feasible, and often times only the fully tightened/untightened states of the bolts may be distinguished. As such, in the review of the past works special attention is paid to this perspective.

He and Zhu [15, 16] developed a numerical model, which could accurately predict the dynamic behavior of a full-scale pipeline mated with bolted joints. The model enabled detection of bolt loosening via an optimization algorithm. The deviances between the experimentally measured and numerically calculated natural frequencies of the pipe were used as objective functions. The conducted case studies revealed that the loosening of bolts could only be identified when all the bolts were fully untightened. Moreover, the study did not explore whether the in-between tightening torque levels could be determined (e.g., when whole set of bolts are loosened to 50% of their fully tightened level). The outcome of that study reached the same conclusion as was reported in the previous works; that is,

examination of natural frequencies is a reliable damage detection tool when a structure has a severe level of damage [3].

On the other hand, time/frequency domain signal processing approaches have been proven to be more successful in providing details on bolt loosening. Milanese *et al.* [17] employed fiber optic strain sensing system on a composite /metal lap bolted joint for observing joint's integrity when excited by a random force. Two statistical parameters from the frequency and time domain measurements of strains were adopted as damage sensitive features. Examination of these two features revealed that the fully-tight and finger-tight states of the bolts could be well-determined. However, the ability of the method in discerning the in-between loosening states was not addressed.

Mickens *et al* [18] proposed a damage index for health monitoring of aircraft joints based on the deviation in the frequency spectrum of the time-signals received by the sensors. Piezoelectric sensors/actuators were strategically deployed on an aircraft wing to monitor the loosening of rivets (using screws in their work). The suggested index was successful in warning for loosened screws and tracking progression of loosening when the loose screw was located in-between the actuator and sensing units. The neighboring sensors were able to identify the existence of the loosened screw, but failed to accurately predicting its progression.

Amerini and Meo [19] used the acoustic/ultrasonic waves for monitoring the health states of the bolts in an aluminum bolted single lap joint. Three damage indices were constructed from the time and frequency domain of the sensors' signals. All the developed damage indices were capable of identifying various degrees of torque levels on the bolts, especially in discerning fully tightened and finger tight states of the bolts. However, the damage indices became saturated at high torque levels, thus providing relatively low resolution in detecting the onset of bolt loosening.

Yang and Chang [20, 21] deployed smart piezoelectric washers on the thermal protection system (TPS) of a space operation vehicle (SOV) for health monitoring of the system's bolted joints. One of the embedded piezoelectric sensors/actuators was assigned to generate ultrasonic waves that traveled into the joint region, while the others acted as listeners. It was theoretically shown that the torque level on each joint can be identified upon extracting the energy and specific damping capacity (SDC) from the sensory

network's signals. The hypothesis was experimentally verified under a simulated acoustic environment.

Lack of studies and the inefficiency of the modal methods in addressing the health monitoring of bolted flange joints of pipelines motivated our research group to consider this problem.

Esmaeel *et al* [22] applied an energy-based approach, developed in our research group, for detection and quantifying the bolt loosening in bolted flange joints of a full-scale pipeline. The pipe was excited at a specified location near the joint via an instrumented hammer. The piezoelectric sensors bonded on the pipe and the flange monitored the vibrations. The energy of the first IMF of sensors' signals, obtained via the Empirical Mode Decomposition (EMD), was used as a damage sensitive feature. A damage index based on the comparison of energies was constructed for evaluation of the bolted flanged joint's integrity. The numerical study resulted in encouraging results in identifying the onset of bolt loosening, and its progression. Experimental verification of the approach verified the integrity of the method in detection of bolt loosening. However, major discrepancies were noted in tracking damage progression. Inconsistency in the impact loads was claimed to be responsible for the discrepancies.

As a result, chapter 3 details the development of a reliable VB-SHM for detection, localization, and quantification of loosening of bolts in mechanically fastened joints in pipelines. Major sources of the inconsistency noted in past trials [22] were successfully identified and resolved. The utility of the developed approach has been increased by incorporating a wireless sensing unit, which enables remote data collection. The effect of uncertainties (e.g., changes in the boundary conditions) was also studied; this is believed to be a crucial consideration should one adopt the method for in-situ applications.

2.2.2 VB-SHM of Offshore Pipelines

Health monitoring of offshore pipelines is a challenging task. The monitoring is currently done by employing divers or remotely operated vehicles (ROVs) equipped with various NDT apparatus [23]. Pipelines are primarily examined for initiation of corrosion in various locations, and defects in their girth-welds. VB-SHM can potentially offer a simpler and more cost-effective alternative, practically serving as an initial alarm before having to

conduct the costly NDTs. As a result, the feasibility of VB-SHM algorithms for damage detection of submerged structures has started being examined in very recent years. This section introduces the key factors involved in appropriate modeling of submerged structures. It introduces the challenges in relation to damage detection of offshore structures. The available techniques for analytical/numerical modeling of submerged structures are also introduced, which will be further explained in the next chapters. The section continues with the review of the works carried out for vibration-based damage detection of submerged structures.

2.2.2.1 Modeling the Dynamic Response of Submerged Structures: Key Factors and Challenges

Submergence of structures introduces new challenges for application of vibration-based approaches. Pipelines experience variable internal pressure during operation. This oscillating pressure, which may be caused by the internal fluid, can affect the pipeline's stiffness, and hence dynamic response of the pipe. This poses a serious obstacle in implementation of any VB-SHM techniques; so does the external pressure, which varies linearly at different depths of water. Zou *et al* [24] reported a negligible decrease in the bending eigenvalues of a submerged composite pipeline as the internal pressure was increased. Ross *et al.* [25] studied the effect of external pressure on the vibration of a prolate dome made of urethane plastic. They noticed a drastic reduction in some of the eigenvalues in response to a stepwise increase in the external pressure.

Also, care must be taken in selecting an appropriate numerical modeling approach for proper representation of fluid-structure interaction. Two available techniques, namely the "added mass" and "coupled acoustic-structural" have been customarily used in modeling the situation. The "added mass" approach assumes a set of simplifying assumptions, and thus is less computationally intensive [26]. It may, however, lead to erroneous results if the assumptions are violated (examples of these assumptions include 1. Incompressibility of the fluid 2. Ideal fluid (inviscid fluid) 3. The velocity potential must be known). On the other hand, the "coupled acoustic-structural" approach provide a more general representation of the fluid-structure interaction, but at a higher computation cost. Zeinoddini *et al* [27] studied the free-spanning submerged pipeline with the two

approaches. They concluded that the "added mass" approach provided a conservative prediction on dynamic response of the pipe. The differences between the predictions was confined to 15% under earthquake excitation, while it reached 60% when the pipe was subjected to a harmonic excitation. These two modeling approaches have been further explained in the following chapters.

Zhu *et al.* [28] proposed a VB-SHM approach for offshore pipelines. Eigenvalues of a pipeline resting on seabed were numerically evaluated via the two modeling techniques. It was found that the difference between the considered natural frequencies remained below 3%. Therefore, they opted for the less time-consuming method (i.e., the "added mass").

Kramer *et al.* [29] compared the eigenvalues of the submerged composite plates obtained via an analytical approach and the "coupled acoustic-structural" technique executed on the ABAQUS platform. The analytical approach adapted the "added mass" and the strip theory for derivation of the differential equations. The model neglected the shear effect, warping effects, and assumes the chord-wise bending was not likely to happen (i.e., beam, or strip assumption). The numerical and analytical approaches were in close agreement when the aspect ratio of the plate (i.e., thickness to chord ratio) remained relatively high (i.e., close to a beam-type structure). However, for the plate-like configuration with low aspect ratio, there were deviations in predicted eigenvalues extracted from the two approaches. Albeit, the general trend of the variation in natural frequencies could be captured for a submerged composite plate having different fiber angles. Therefore, the analytical method was recommended for the early stages of design, since it offered a much faster analysis compared to the latter approach (a few seconds vs. a few hours computing with 17 CPU nodes).

Therefore, chapter 4 provide detailed discussions on the above-mentioned challenges that one may encounter in development of a reliable VB-SHM strategy for offshore structures. Composite structures are also considered as they are anisotropic and have generally lower density than metals, which could affect the fluid-structure interaction (FSI) [30].

2.2.2.2 VB-SHM of Submerged Structures: Review

Vibration-based techniques have been proposed for specific offshore structures such as platforms, towers, and pipelines [22, 31-34]. However, there have been few studies

addressing the VB-SHM of offshore structures considering FSI. Nearly all of them were conducted in recent years (since 2008). The other damage detection approaches, similar to VB-SHM of offshore structures, can be categorized into two main streams described in section 2.1 (i.e., the modal, and time/frequency domain signal processing approaches).

Zhu *et al.* [28] adopted a statistical finite element model updating for health monitoring of a submerged pipe. The natural frequencies and mode shapes of the pipe were considered as the updating parameters. In their experimental study, the vibration data obtained through waterproofed accelerometers were processed to extract the modal parameters. Free-spanning of the pipe and corrosion constituted the damage scenarios. They were respectively simulated by reducing the support's stiffness and reductions in the stiffness of the pipe at various locations. Numerical and experimental verifications proved the robustness of the method in localizing the damage. Albeit, there were some inconsistencies reported in estimation of the damage size. That was mainly due to noise and modeling errors, which were purposefully simulated in their analysis to account for the real-life scenarios. The "added mass" approach was adopted for modeling the surrounding water. Measurement of the mode shapes, (a fairly significant and onerous effort, which is mandatory for the model updating), and the ability to assess only relatively large damage cases are believed to be the downsides of this approach.

Na and Kundu [23] examined the application of guided waves for identification of mechanical defects in a scaled aluminum pipe submerged in water. The investigated defects included a gouge, removed metal, and a dent. The monitoring system consisted of a transmitter and receiver. Ultrasonic waves, in forms of frequency sweeps, were generated by the transducer and propagated along the pipe. The time histories of the signals were recorded through the receiver unit. The variation of the average signal amplitude against the frequencies were used as the damage indicator. Only 500 mm of the pipe could be scanned by this approach, which is considered a relatively large distance having employed only two transducers. Adjustment of the transducer angle (for wave propagation) to achieve the finest sensitivity for damage detection can be deemed as the drawback of the method.

Rizzo *et al.* [35] adapted a non-contact actuation/sensing apparatus for damage detection of a submerged plate. A pulsed laser generated stress waves on the plate, while two immersion transducers, made of piezoelectric materials, captured the reflected waves. They

introduced a notch and a small circle into the plate to simulate damage. The plate was scanned along its length by a pulse/sensing unit at step-wise locations. The Continuous Wavelet Transform (CWT) was used to process the time-signals. A damage sensitive parameter, was extracted from the joint time-frequency representation of the signals received at specified locations. The method could identify the location of damage by producing large damage indices as the sensing probes passed across the damages. Dependency of the approach's sensitivity to several parameters, including the angle of pulse laser, selected frequency range, water temperature, and the laser-plate distance, were deemed as the downsides of the method. Also, the method produced large damage indices only when the sensors were passing across the damages.

Peng *et al.* [7] introduced an energy-based damage index for locating the free span along pipelines. The feasibility of the hypothesis was assessed by a numerical study. A submerged pipe, modeled by the "added mass" approach, was vibrated by a simulated ambient excitation source, and the acceleration data was recorded through the sensors mounted along the pipe. The signals were passed through the wavelet packet transform in order to establish the energy-based indices. The numerical study showed that the free spanning of the pipeline can be confidently predicted with the exception for short lengths of free span (e.g., 5 % of the whole length in the studied case). The experimental study supported the findings on the free-spanning detection. In both studies, the locations of the free-spanning were correctly identified through observing larger damage indices for the sensors within the free-span regions. However, it was determined that the magnitude of produced damage indices were not proportional to damage severity. Therefore, the damage could not be quantified precisely.

Bao *et al.* [36] presented a numerical study (applying the "added mass" approach), followed by an experimental validation on vibration-based health monitoring of offshore pipelines. The ambient vibration was simulated by a wave generator in the experiment. Then, the acceleration data gathered from the pipe was taken into a time-series signal processing algorithm. Damage indices were established by comparing time-series of the intact and damaged states of the pipeline. The applied approach was proved to be reliable in identifying free-spanning damage. However, it failed to effectively predict the loss in

pipe's stiffness, or reduction in its thickness which simulate the effect of corrosion in real-life.

Chen *et al.* [37] proposed a method to detect the damage in a plate submerged into a shallow depth of water with an array of water-proofed piezoelectric sensors, acting as transmitters/receivers. Their study involved numerical simulations as well as experimental validation. They incorporated the conventional eight-node acoustic element offered in ABAQUS to model the surrounding water in their numerical study (i.e., the "coupled acoustic-structural" approach). The damage identification approach was an energy-based method; anti-symmetric lamb waves were generated by piezoelectric patches and the energy of the signals received by adjacent piezoelectric sensors were processed by a probability-based diagnostic imaging approach. Identification of a through-thickness hole and chemical corrosion in the submerged plate was attempted. The method could precisely locate those damages. However, the ability of their method in estimating the severity of the damage was not studied.

Our research group presented the results of a study on health monitoring of a pipelines' girth-welds [31]. Piezoelectric sensors were bonded circumferentially on either sides of the girth-weld. Our developed VB-SHM scheme (i.e., EMD_EDI) was employed to detect growing notches introduced next to the girth-weld. The numerical and experimental studies corroborated the integrity of the method in estimating the location and severity of damage scenarios. The encouraging results obtained for the full-scale pipe tested in air motivated us to reconsider the damage type within a submerged pipe. Therefore, chapters 5 presents details of the corresponding experiments and computer simulations. A series of modifications were also made to the instrumentation in order to improve the reliability of the actuation/sensing units in submerged environments. The modifications in the actuation unit enables autonomous application of this approach, in that, no external source of excitation (e.g., impact hammer) would be needed. The numerical model is also adjusted accordingly, thus providing a powerful tool for conducting parametric studies on the modified platform.

2.2.3 VB-SHM of Structures Hosting Fatigue Cracks

Fatigue cracks on structures may develop as a result of cyclic loading. Various VB-SHM techniques have been developed with the aim of detecting such defects, which has been demonstrated to be a very challenging SHM task. Most of the investigators, however, have considered detection of notch/slot instead of real-life sharp fatigue cracks. Interaction of cracks' surfaces would alter the local stiffness of structures, hence it introduces non-linearity [38]. Specifically, during a vibration event, the stiffness alternate in a periodic fashion due to the harmonic percussion of crack's surfaces. The utilization of the conventional signal processing techniques (e.g., FFT, and WT) would not then be appropriate choices in dealing with non-linear systems/signals. It should also be noted that the linear elastic fracture mechanics (LEFM) constituted the basis for the development of the available numerical models in those studies. The main reason for consideration of notch/slot is believed to be due to the inefficiency of the adopted numerical and conventional signal processing techniques in the past studies.

Cawley and Ray [39] compared the reduction in natural frequencies of a beam hosting a slot with those of a cracked beam. They concluded that the rate of reductions in the beam's eigenvalues became almost similar as the width of the slot reached to that of sharp cracks. In other words, as the width of the notch deviates from that of a fatigue crack, the notch reduced the eigenvalues at a faster rate than did the fatigue crack.

Rizos *et al* [40] modeled a notch with a rotational spring, whose stiffness was a function of the crack size. Location and size of the notch in a beam were identified by experimental measurement of one of the beam's mode shapes. It should be noted that measurement of the mode shapes is a challenging task. In addition, analytical modeling of the problem would only be feasible for simple structures (e.g. beams).

Lele and Maiti [41] adopted this approach for detection of a notch in a thick beam. Instead of measuring a mode shape, few natural frequencies were used for identification of the notch. This modification makes the process more applicable, as natural frequencies are easier to obtain than the measurement of the mode shape.

Kim and Stubbs [2] employed the modal sensitivity concept into an algorithm designed for crack identification. The algorithm takes few natural frequencies of the structure as the inputs, and outputs the crack location and its size. They used the experimental data reported

by [42] on the natural frequencies of free-free beams hosting different sizes of notches at various locations. Encouraging results were reported, specifically in identifying notches' locations.

Qian *et al* [43] proposed a numerical model for a cracked beam. A new stiffness matrix was established for an element of a beam hosting a crack. LEFM was used to derive the damaged beam's stiffness matrix. Subsequently, eigenvalues of the cracked beam were evaluated and compared with those of the intact beam. In an inverse approach, Nahvi and Jabbari [44] adopted the model and measured the first two eigenvalues and eigenmodes of a cantilever beam hosting a notch to estimate the location and depth of the notch in the beam.

Rezaei and Taheri [45] investigated the sensitivity of their energy-based damage index in detection of a notch in a beam. Piezoelectric sensors were bonded adjacent to the notch. The beam was impacted by hammer and the vibration signals were gathered by the sensors. The signals were processed through EMD for the establishment of the damage indices. The indices compared the IMF energy of the healthy and damaged states of the beam. The results revealed that the adapted strategy could determine the existence of the notch and track its progression (i.e., the increase in the notch size) with a high level of sensitivity. This method, however, could be applied for local inspections. They extended the application of their method into health monitoring of pipeline girth-welds [31]. A progressing surface-breaking notch could be successfully identified by the EMD-based approach. Piezoelectrics sensors bonded on the circumference of the pipe showed various degrees of sensitivity to the growing notch. Sensors closer to the damage produced higher damage indices. Nonetheless, nearly all the sensors were able to detect the presence of damage and quantify its progression. Numerical simulations of this case study were also presented using the ABAQUS platform.

There are few studies that have considered the dynamic behavior of structures hosting fatigue cracks. Modena [46] examined the modal properties of precast hollow concrete floor panels, before and after the presence of a crack. They found that the natural frequencies were insensitive to the presence of the crack. However, the damping ratio showed a higher level of sensitivity. Andreaus and Baragatti [47] reported the same

findings as they examined the fundamental frequency and damping ratio of a cracked aluminum bar.

Zhang and Testa [48] studied the effect of a crack's surface closure on the vibration of a T-beam. The beam was impacted with variable impact loads and the obtained frequencies were plotted against the variable loads. The first frequency of the cracked beam experienced a considerable decrease once the impact load caused the complete separation of the crack's surfaces; damping of the beam showed a similar behavior.

Rezaee and Hassannejad [5] developed an analytical model for a beam hosting a fatigue crack. Damping and non-linear local stiffness terms were developed. Their experimental studies verified the reliability of the proposed model.

The above reviewed works on detection of fatigue cracks attests to the insensitivity of the modal methods to the presence and progression of real-life sharp cracks.

In our investigations, encouraging results were also observed when detecting and quantifying a notch in girth-weld of a submerged pipe as presented in chapters six and seven. It would be desirable, however, to reconsider this case study by considering a real-life sharp fatigue crack. The data-driven nature of our EMD-based approach makes it independent of numerical models. Also, as stated earlier, EMD is a robust signal processing tool, which can accommodate non-linear systems/signals (see Table 2-1). These two features suggest that the EMD-based approach is a proper candidate for SHM of structures hosting sharp cracks. Visual monitoring of surface-breaking fatigue cracks on a pipe is a challenging task, requiring special instrumentation. Quantifying such sharp cracks on a beam would, however, be possible by the use of a magnifying camera. This fact therefore motivated us to first consider the problem of sharp crack for a beam geometry before proceeding to health monitoring of a pipeline's girth-weld. Therefore, chapter 6 presents the results of the efforts expended on detection and quantification of a sharp fatigue crack in an aluminum beam by the EMD-based approach.

2.3 REFERENCES

1. Ewins, D.J., *Theoretical basis, modal testing: theory, practice and application*. 2nd ed. 2000, Philadelphia: PA: Research Studies Press Ltd.
2. Kim, J.T. and N. Stubbs, *Crack detection in beam-type structures using frequency data.* Journal of Sound and Vibration, 2003. **259**(1): p. 145-160.

3. Farrar, C.R. and S.W. Doebling, *Damage detection II: field applications to large structures*, in *Modal analysis and testing (NATO science series)*, J.M.M. Silva and N.M.M. Maia, Editors. 1999, Kluwer Academic Publishers: Dordrecht. p. 1-29.
4. Chandrashekhar, M. and R. Ganguli, *Structural damage detection using modal curvature and fuzzy logic.* Structural Health Monitoring, 2009. **8**(4): p. 267-282.
5. Rezaee, M. and R. Hassannejad, *Damped free vibration analysis of a beam with a fatigue crack using energy balance method.* Physical Science, 2010. **5**(6): p. 793-803.
6. Cheraghi, N., G.P. Zou, and F. Taheri, *Piezoelectric-based degradation assessment of a pipe using Fourier and Wavelet analyses.* Computer-Aided Civil and Infrastructure Engineering, 2005. **20**(5): p. 369-382.
7. Peng, X.-L., H. Hao, and Z.-X. Li, *Application of wavelet packet transform in subsea pipeline bedding condition assessment.* Engineering Structures, 2012. **39**: p. 50-65.
8. Melhem, H. and H. Kim, *Damage detection in concrete by Fourier and Wavelet analyses.* Journal of Engineering Mechanics, 2003. **129**(5): p. 571-577.
9. Huang, N.E., et al., *The empirical mode decomposition and the Hilbert spectrum for nonlinear and non-stationary time series analysis.* Proceedings of the Royal Society of London. Series A: Mathematical, Physical and Engineering Sciences, 1998. **454**(1971): p. 903-995.
10. Loutridis, S., *Damage detection in gear systems using empirical mode decomposition.* Engineering Structures, 2004. **26**(12): p. 1833-1841.
11. Cheraghi, N. and F. Taheri, *A damage index for structural health monitoring based on the empirical mode decomposition.* Mechanics of Materials and Structures, 2007. **2**(1): p. 43-62.
12. Bao, C.X., H. Hao, and Z.X. Li, *Vibration-based damage detection of pipeline system by HHT method.* Applied Mechanics and Materials, 2011. **99**: p. 1067-1072.
13. Doebling, S.W., C.R. Farrar, and M.B. Prime, *A summary review of vibration-based damage identification methods.* Shock and vibration digest, 1998. **30**(2): p. 91-105.
14. *Guidelines for the management of the integrity of bolted joints for pressurized systems*. 2007, Energy Institue: London.
15. He, K. and W.D. Zhu, *A vibration-based structural damage detection method and its applications to engineering structures.* International Journal of Smart and Nano Materials, 2011. **2**(3): p. 194-218.
16. He, K. and W.D. Zhu, *Structural damage detection using changes in natural frequencies: theory and applications.* Journal of Physics: Conference Series, 2011. **305**: p. 012054.
17. Milanese, A., et al., *Modeling and Detection of Joint Loosening using Output-Only Broad-Band Vibration Data.* Structural Health Monitoring, 2008. **7**(4): p. 309-328.
18. Mickens, T., et al., *Structural health monitoring of an aircraft joint.* Mechanical Systems and Signal Processing, 2003. **17**(2): p. 285-303.
19. Amerini, F. and M. Meo, *Structural health monitoring of bolted joints using linear and nonlinear acoustic/ultrasound methods.* Structural Health Monitoring, 2011. **10**(6): p. 659-672.

20. Yang, J. and F.-K. Chang, *Detection of bolt loosening in C–C composite thermal protection panels: I. Diagnostic principle.* Smart Materials and Structures, 2006. **15**(2): p. 581-590.
21. Yang, J. and F.-K. Chang, *Detection of bolt loosening in C–C composite thermal protection panels: II. Experimental verification.* Smart Materials and Structures, 2006. **15**(2): p. 591-599.
22. Esmaeel, R.A., J. Briand, and F. Taheri, *Computational simulation and experimental verification of a new vibration-based structural health monitoring approach using piezoelectric sensors.* Structural Health Monitoring, 2011. **11**(2): p. 237-250.
23. Na, W.-B. and T. Kundu, *Underwater pipeline inspection using guided waves.* Transactions-American Society of Mechanical Engineers Journal of Pressure Vessel Technology, 2002. **124**(2): p. 196-200.
24. Zou, G., N. Cheraghi, and F. Taheri, *Fluid-induced vibration of composite natural gas pipelines.* International journal of solids and structures, 2005. **42**(3): p. 1253-1268.
25. Ross, C.T.F., et al., *Vibration of a thin-walled prolate dome under external water pressure.* Ocean Engineering, 2007. **34**(3-4): p. 560-575.
26. Blevins, R.D., *Flow-Induced Vibration*. 2nd ed. 2001, Malabar: Krieger.
27. Zeinoddini, M., G.A.R. Parke, and S.M. Sadrossadat, *Free-spanning submarine pipeline response to severe ground excitations: water-pipeline interactions.* Journal of Pipeline Systems Engineering and Practice, 2012. **3**(4): p. 135-149.
28. Zhu, X., H. Hao, and X. Peng, *Dynamic assessment of underwater pipeline systems using statistical model updating.* International Journal of Structural Stability and Dynamics, 2008. **8**(02): p. 271-297.
29. Kramer, M.R., Z. Liu, and Y.L. Young, *Free vibration of cantilevered composite plates in air and in water.* Composite Structures, 2013. **95**: p. 254-263.
30. Kwon, Y.W., et al., *Transient dynamic response and failure of sandwich composite structures under impact loading with fluid structure interaction.* Applied Composite Materials, 2012. **19**(6): p. 921-940.
31. Rezaei, D. and F. Taheri, *Health monitoring of pipeline girth weld using empirical mode decomposition.* Smart Materials and Structures, 2010. **19**(5): p. 055016.
32. Li, H., S. Wang, and H. Yang. *Modal strain energy decomposition method for damage detection of an offshore structure using modal testing information*. in *Third Chinese-German Joint Symposium on Coastal and Ocean Engineering*. 2006.
33. Nichols, J.M., *Structural health monitoring of offshore structures using ambient excitation.* Applied Ocean Research, 2003. **25**(3): p. 101-114.
34. Mangal, L., V. Idichandy, and C. Ganapathy, *Structural monitoring of offshore platforms using impulse and relaxation response.* Ocean Engineering, 2001. **28**(6): p. 689-705.
35. Rizzo, P., J.-G. Han, and X.-L. Ni, *Structural health monitoring of immersed structures by means of guided ultrasonic waves.* Journal of Intelligent Material Systems and Structures, 2010. **21**(14): p. 1397-1407.
36. Bao, C., H. Hao, and Z. Li, *Vibration-based structural health monitoring of offshore pipelines: numerical and experimental study.* Structural Control and Health Monitoring, 2012.

37. Chen, J., Z. Su, and L. Cheng, *Identification of corrosion damage in submerged structures using fundamental anti-symmetric Lamb waves.* Smart Materials and Structures, 2010. **19**(1): p. 015004.
38. Dimarogonas, A.D., *Vibration of cracked structures: A state of the art review.* Engineering Fracture Mechanics, 1996. **55**(5): p. 831-857.
39. Cawley, P. and R. Ray, *A comparison of the natural frequency changes produced by cracks and slots.* Vibration, Acoustics Stress and Reliability in Design, 1988. **110**(3): p. 366-370.
40. Rizos, P.F., N. Aspragathos, and A.D. Dimarogonas, *Identification of crack location and magnitude in a cantilever beam from the vibration modes.* Journal of Sound and Vibration, 1990. **138**(3): p. 381-388.
41. Lele, S.P. and S.K. Maiti, *Modeling of transverse vibration of short beams for crack detection and measurement of crack extension.* Journal of Sound and Vibration, 2002. **257**(3): p. 559-583.
42. Montalvão E Silva, J.M. and A.J.M. Aráujo Gomes, *Experimental dynamic analysis of cracked free-free beams.* Experimental Mechanics, 1990. **30**(1): p. 20-25.
43. Qian, G.L., S.N. Gu, and J.S. Jiang, *The dynamic behaviour and crack detection of a beam with a crack.* Journal of Sound and Vibration, 1990. **138**(2): p. 233-243.
44. Nahvi, H. and M. Jabbari, *Crack detection in beams using experimental modal data and finite element model.* International Journal of Mechanical Sciences, 2005. **47**(10): p. 1477-1497.
45. Rezaei, D. and F. Taheri, *Damage identification in beams using empirical mode decomposition.* Structural Health Monitoring, 2011. **10**(3): p. 261-274.
46. Modena, C., D. Sonda, and D. Zonta, *Damage localization in reinforced concrete structures by using damping measurements.* Key Engineering Materials, 1999. **167**: p. 132-141.
47. Andreaus, U. and P. Baragatti, *Fatigue crack growth, free vibrations, and breathing crack detection of aluminium alloy and steel beams.* The Journal of Strain Analysis for Engineering Design, 2009. **44**(7): p. 595-608.
48. Zhang, W. and R.B. Testa, *Closure effects on fatigue crack detection.* Engineering Mechanics, 1999. **125**(10): p. 1125-1132.

CHAPTER 3 IMPROVEMENT OF A VIBRATION-BASED DAMAGE DETECTION APPROACH FOR HEALTH MONITORING OF BOLTED FLANGE JOINTS IN PIPELINES

Pejman Razi, Ramadan A Esmaeel and Farid Taheri

Published in the journal of Structural Health Monitoring, 12 (3), 207-224, 2013.

3.1 ABSTRACT

Early detection of bolt loosening is a major concern in the oil and gas industry. In this study, a vibration-based health monitoring strategy has been developed for detecting the loosening of bolts in a pipeline's bolted flange joint. Both numerical and experimental studies are conducted to verify the integrity of our implementation as well as an enhancement developed along with it. Several damage scenarios are simulated by the loosening of the bolts through varying the applied torque on each bolt. An electric impact hammer is used to vibrate (excite) the system in a consistent manner. The induced vibration signals are collected via piezoceramic sensors bonded onto the pipe and flange. These signals are transferred remotely by a wireless data acquisition module and then processed with a code developed in-house in the MATLAB environment. After normalization and filtering of the signals, empirical mode decomposition is applied to establish an effective energy-based damage index. The assessment of the damage indices thus obtained for the various scenarios verifies the integrity of the proposed methodology for identifying the damage and its progression in bolted joints as well as the major enhancements applied onto the methodology.

Keywords: Vibration-based damage detection, bolted joints, bolt loosening, finite element analysis, empirical mode decomposition, remote sensing.

3.2 INTRODUCTION

Bolted joints are widely used in a variety of engineering applications, ranging from aerospace to the oil and gas industries. Self-loosening of bolts, which may be initiated by

vibration or severe cyclic thermal loads is a critical issue in such joints [1]. If the bolt loosening remains undetected, it could potentially cause the joint to leak, followed by complete loosening of the joint and ultimate failure. The outcome could include detrimental effects in applications such as bolted joints used in mating pipelines conveying oil and gas. As a result, accurate and reliable inspection routines need to be conducted frequently in order to ensure the integrity of the system. As such, preloads on the bolts have to be checked frequently by regular torque wrenches. In many cases, however, the joints themselves are buried, submerged, and/or exposed to harsh environmental conditions or located in inaccessible areas, rendering regular inspection practically impossible. The current state of the art relies on several online structural health monitoring (SHM) approaches that have been developed during the past decade.

Nondestructive techniques are the preferred approach. Such techniques have been adopted by several researchers to address the problem of bolt loosening detection in mechanical joints. Two main approaches predominate: impedance-based and vibrational techniques.

In impedance-based approaches, lead zirconate titanate (PZT), capable of converting electrical charges into mechanical strains and vice versa, is often bonded to an area of the structure to be inspected. Then, the vicinity of the inspection area is excited with transducers, acting as actuators. Any change in the mechanical impedance of the host structure caused by potential damages (such as reduction in the preload of a bolted joint) would alter the electrical impedance of the transducers [2]. Hence, registration and the subsequent analyses of the electrical impedance via impedance analyzer devices could pinpoint damage-sensitive features.

Afshari *et al.*[2] proposed an impedance-based method for the health monitoring of bolted joints used in railroad switches, in which frequency spectra of the real part of the impedance were adopted to establish the damage metric. The proposed damage index could successfully detect the loosening of a bolted joint with a minimum threshold level of 1/10th of a bolt turn, which corresponded to the condition where the bolt was loosened to 30% of the maximum specified torque. The extent of inspection capability, however, was limited to only one bolt, a downside of the method noted by the authors.

Ritdumrongkul *et al*. [3] developed a numerical model of a single lap bolted joints under the framework of the spectral element method (SEM). The bolted joint was modeled by a

spring-and-dashpot assembly that could account for the change in the stiffness and damping of the joint due to the loosening of the bolts. As opposed to the conventional finite element (FE) method, the model could accommodate the high-frequency content of the electrical impedance measurement of the bonded PZT. Moreover, in contrast to most impedance-based methods, they utilized the lower frequency content of the measured impedances. The study successfully discerned between the fully loosened state from the tight state of the bolted joints it examined. However, it produced low resolution when detection of in-between loosening (i.e. torque levels) of the joint's bolts was attempted.

Vibration-based techniques are divided into two categories: wave-propagation methods and modal methods. In the first approach, the acoustic or ultrasonic range (i.e. more than 20 kHz) of a structure's vibrations is excited and registered (usually via bonded piezoelectric transducers). In the second approach, referred to as the modal-based method, global properties of the structure (such as the natural frequencies and mode shapes) at lower vibration modes are interrogated. The use of modal parameters as damage indicators has been controversial [4]; from the practical point of view, exploring the natural frequencies as the modal parameter has been shown to be a fairly reliable method only when a severe damage (global type) has been introduced to the structure [5]. On the other hand, curvatures driven from the mode shapes have been shown to be more reliable candidates for identifying local damages [6]. However, the accurate measurement of mode shapes, especially at higher modes, would be a challenging task, as it requires a large number of sensors deployed on the structure [6].

Yang and Chang [7] investigated the efficiency of the attenuation-based method in health monitoring of bolted joints in a thermal protection system (TPS) of space operation vehicles (SOV). The attenuation-based method is categorized under the wave-propagation techniques and is based on the damping phenomena of the ultrasonic waves traveling across the bolted joints. The energy and the specific damping capacity (SDC) of the signals received by the piezoelectric patches were proposed as two damage-sensitive features. The micro-contact theory and structural/internal damping concepts were adopted to justify the behavior of the two damage-sensitive features with respect to the loss of preload in the bolted joints. They verified their methodology through a set of preliminary case studies. In continuation of their study, they applied the technique to identify the loosening of bolted

joints in a TPS prototype under simulated acoustic environments [8]. Smart washers, each embedding a PZT element, were designed and fabricated for sensing/actuation purposes. The results of the experiment revealed that the method was capable of identifying the torque levels of the joints.

Milanese *et al*. [9] introduced a mathematical model for sensing vibration of a beam hosting bolted joints. They explained the nonlinearity that would arise due to the bolt loosening by analyzing the dynamic behavior of a beam under broadband random vibration. Experimental studies were conducted on a composite/metal lap joint with bolted connections excited by a random force. The induced vibration was recorded by a fiber optic strain sensing system. Two statistical parameters were adopted in the damage detection algorithm; the two features were extracted from the frequency and time domain of the strain measurements, respectively. They concluded that their proposed strategy could distinguish between the fully tight state and finger-tight state of the bolts. However, the sensitivity of the method in detecting the in-between loosening states was not reported in their study.

Amerini and Meo [10] proposed three damage indices for detection of loosening/tightening of bolted joints in an aluminum single lap joint by acoustic/ultrasonic methods. The developed damage indices all proved to be efficient in distinguishing the difference in various torque levels that were applied to the bolts, especially in discerning the fully tight state and finger-tight state of the bolts. However, saturation of the proposed damage indices at higher torque levels, along with the imminent damage, optimization of excitation frequency, and maintenance of a high signal-to-noise ratio (SNR), was reported as a critical precaution.

Mickens *et al.* [11] studied the simulated loosening of rivets (using screws) in an aircraft joint. They established a damage index based on the deviation of the frequency spectrum of the joint caused by its degradation. A set of piezoelectric transducers were bonded strategically to the aircraft wing for sensing/actuation purposes. The authors concluded that their proposed damage index could effectively identify the presence and progression of loosened screws when the damage was located between the actuating and sensing elements. The other neighboring sensors could also predict the onset of damage, while they occasionally failed to predict its progression.

Despite the availability of numerous studies conducted on different bolted joint assemblies in the literature, the identification of bolt loosening in full-scale pipeline bolted flange joints has not been widely explored. Among this limited group, one could mention the study of Park *et al*. [12] who established a damage metric based on the electrical impedance measurements to interrogate the health of bolted flange joints in a small-scale pipeline. The piezoceramic patches were bonded onto the flanges of the joint for impedance measurements. Their proposed technique could successfully identify the presence and progression of the fully loosened bolted joints. Their method also showed a high level of sensitivity when 6 out of 12 bolts in a junction of the pipeline were completely loosened. However, no data were reported regarding the sensitivity of the method in discerning the in-between torque levels of the bolts. Trial-and-error optimization in choosing the most sensitive frequency range and the highly local nature of the approach due to the use of high-frequency measurements (up to 100 kHz) were noted as the downsides of the method by the authors. They also highlighted the fact that the high level of damping imposed by the implementation of the gasket between the mating surfaces of the flanges could affect the efficiency of their method, especially in the case of large-scale pipelines.

The loosening of bolts in flanges of joints in mating pipelines reduces the overall stiffness, thereby affecting the pipes' vibration response. This is accompanied by a change in the local damping resulting from the varying degrees of contact in the interfaces of the bolts and flanges, as well as the gasket placed between the flanges.

He and Zhu [13] developed a FE framework that could accurately predict the dynamic behavior of pipeline bolted joints. An optimization technique was then utilized to detect the loosening of the flange bolts with the use of the experimentally measured natural frequencies. Application of this method revealed that loosening of the bolts could be detected only when all the bolts were loosened. The ability of the method in determining the in-between torque levels in the bolts was not addressed.

Esmaeel *et al.* [14] applied a robust vibration-based strategy for health monitoring of bolted joints on a full-scale pipeline. The principles of their approach included excitation of the pipe assembly at a specified location near the joint and then capturing the vibration signals via a set of piezoceramic sensors bonded to the pipe and the flange. Finally, the digitized captured signals were analyzed with a signal processing toolkit, which embedded empirical

mode decomposition (EMD), to extract a damage-sensitive feature. The numerical simulations corroborated the integrity of their established approach in identifying the loosening of the bolted joints. It was also reported that this methodology could register the progression of damage in the bolted joint as a function of the varied torque levels applied to the bolts. These observations were verified qualitatively in the experimental study. However, major discrepancies were reported on tracking the damage progression. These were ascribed to inconsistent excitation imparted by the conventional manually operated instrumented hammer (MOIH) used to excite the assembly, as opposed to the consistent impact loads that were used in their numerical simulations.

While impedance-based methods are recognized for their high level of sensitivity in detection of imminent damages, their application has been limited to assessment of highly localized damage. This is due to the fact that one must explore the high-frequency range of the structural response, which dampens quickly over small regions. Therefore, the impedance-based method would be a wise choice if a relatively small area is to be inspected [2]. Vibration-based methods, on the other hand, can be used to inspect relatively larger areas, but at some cost to sensitivity. As stated earlier, the analysis of deviations of the natural frequencies associated with lower vibration modes has proven to yield poor indication of bolt loosening in pipelines' bolted flange joints [13]. On the contrary, compared to impedance-based methods, vibration-based methods that utilize wave-propagation techniques offer a relatively promising diagnostic practice [8], since they allow for noticeably larger inspection areas. This is achieved by implementation of a lower frequency range compared to the impedance-based methods. It is noteworthy that trial-and-error optimization of a suitable diagnostic frequency range seems to be a common pitfall among the vibration-based and impedance-based methods [11].

The present study is a continuation toward the enhancement of the novel vibration-based technique developed in the same research group [14, 15]. The aforementioned inconsistency in the experimental segment of the previous study [14] is addressed by utilizing an electric impact hammer accompanied by more refinements through implementation of a more effective signal conditioning stage. Additional efforts have been expended to enhance the predictive capability of the technique and improve its robustness. In this regard, a wireless data acquisition (WDAQ) has been adopted to provide a proof of

the concept on the capability of the technique for remote SHM. The numerical framework presented in our earlier study [14] has also been improved in an effort to more accurately represent the damage scenarios and obtain a better assessment of the integrity of the framework for conducting accurate and efficient parametric studies in the future.

3.3 EMD ENERGY DAMAGE INDEX

Huang *et al.* [16] introduced a novel technique for the time–frequency analysis of real signals. The method yields the time–frequency spectrum of a signal with a two-step procedure. The first step involves the decomposition of a signal into a set of oscillatory functions referred to as the intrinsic mode functions (IMFs) through an empirical method (i.e. the EMD). The empirically driven IMFs are independent of each other, and every individual IMF is time–frequency modulated and conveys important information about the signal [16]. In the second step, the Hilbert–Huang transform (HHT) is applied to the extracted IMFs to obtain the time–frequency representation of the original signal. The established time–frequency spectrum of the signal provides well-localized information about the signal, in both time and frequency domains; hence, it can accommodate nonlinear as well as non-stationary signals. The following paragraph briefly explains the application of EMD into a real signal to obtain the constituent IMFs of the signal:

- First, two cubic splines are fitted through the local maxima and minima of the time-signal, $x(t)$, to produce the upper and lower envelopes, respectively.
- Then, the average of these two splines (or envelopes) is calculated and subtracted from the original signal.
- The resultant signal is treated as a new signal and the aforementioned procedure applied onto this new signal. This iteration is repeated until reaching the stopping criterion [16]. The process is referred to as ‘‘sifting’’ (see Figure 3-1). The result of the first sifting process is referred to as the first IMF of the signal, c_1.
- If one wishes to obtain the subsequent IMF, the first IMF should be removed from the signal, and the sifting process performed on the residue to obtain the subsequent IMF of the signal.

- After extraction of all IMFs, the signal is decomposed into n empirical modes and a residue, r_n, which is monotonic in nature, representing the mean trend of the signal as per the following equation:

$$x(t) = \sum_{i=1}^{n} c_i + r_n \qquad 3\text{-}1$$

Using the above-mentioned technique for processing vibration signals, Cheraghi and Taheri [17] proposed a novel vibration-based technique for health monitoring of structures, formulated based on the energy of certain IMFs of a given structure's vibration signals. This generates a damage index (hereafter referred to as EMD energy damage index (EMD_EDI)). The procedure explained in the following (which, in this case, has been coded in the MATLAB environment) can be used for establishing EMD_EDIs of a given structure:

After a structure is excited (e.g. by means of an impact hammer), the dynamic response of the structure during its vibration, along with the hammer's output signal, is collected through appropriate sensors.

- The signals are then normalized with respect to the hammer's signal in order to minimize the inconsistency that would be inevitably caused using a manual hammer.
- Next, the normalized signals are passed through a band-pass filter to maintain the useful portion of the data. The normalized signals are then individually processed with the EMD method.
- After the IMFs of the normalized signals are established, the energy of the desired IMF , E , can be established by

$$E = \int_0^{t_0} (IMF)^2 \, dt \qquad 3\text{-}2$$

In Equation 3-2, t_0 is defined as the signal duration (which would be appropriately selected based on the structure's material type being tested). This duration is taken as a consistent

value for both the signals obtained from the structure in its healthy state, as well as in its damaged state. The above-mentioned procedure is repeated for the same structure at its damaged state to establish the energy stored in the associated signal of IMF.

- The last step is the application of the EMD–EDI to each sensor's signal; the index is calculated using the following equation:

$$EMD\_EDI = \left| \frac{E_{healthy} - E_{Damaged}}{E_{healthy}} \right| \times 100 \qquad 3\text{-}3$$

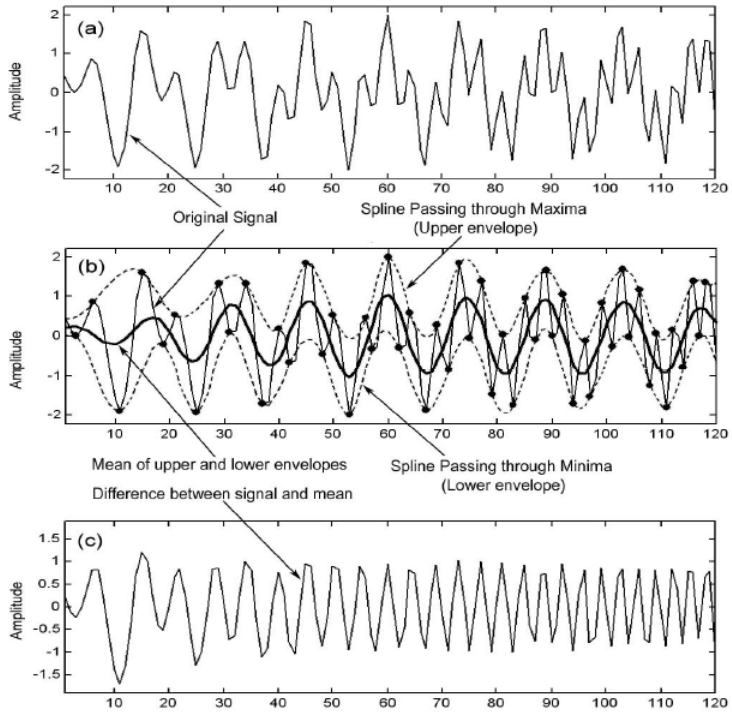

Figure 3-1: A schematic representation of the sifting process: (a) the original signal; (b) the signal in thin solid line, the upper and lower envelopes in dashed lines, and the mean in thick solid line; and (c) the difference between the signal and the mean [16].

Once the EMD_EDI is evaluated for each sensor, the existence and severity of the damage could be established. Sensors producing higher index values represent the presence and location of the damage. The progression and severity of the damage can also be established

by noting the increasing values of those indices as a function of time. The integrity of the described damage index has been verified through several case studies [14, 18, 19].

In summary, the EMD decomposes a signal into its oscillatory modes. The first two IMFs contain the oscillatory modes of higher frequencies of a given signal, which have been proven to be more sensitive to damage (see Razi *et al.* [18] and Loutridis [20] for further explanation).

3.4 EXPERIMENTAL STUDY

Consistent with the main objective of this study (i.e. to address and resolve the inconsistency issues pointed out in the experimental segment of the previous studies[14]), an electric impact hammer, rather than a conventional MOIH, has been used to excite the pipe in a more consistent manner. This study also presents a proof of the concept for the remote (wireless) application of this method, thereby enhancing the utility of the methodology. This is done by means of an experimental arrangement in which, a battery-powered WDAQ, a programmable logic controller (PLC) board and a battery-powered amplifier have been configured to simulate the control of the hammer and data acquisition from a remote location.

An American Society for Testing and Materials International (ASTM) compliant schedule 40 Grade B standard steel pipe (ASTM A53/A53M-07) was selected for the experimental verification segment of this study. Also selected were the American National Standards Institute (ANSI) forged steel flanges with the following specifications: nominal pipe size: 6 in, class: 150 lb, raised face, slip on, and material type A105N. Society of Automotive Engineers (SAE) Grade 5 unified national coarse (UNC) hex head bolts were used (diameter: 0.75" and length: 4"), with the corresponding sized nuts and washers. To create the mechanical joint in the pipe, the pipe was cut into two equal lengths, and the two flanges were welded onto the pipes' ends. The flanges were continuously welded to the pipe on the inside and outside of the joint with a small overlap over the pipe edge of approximately 23.0 mm. The pipe's main dimensions and properties are summarized in Table 3-1. The setup and the realistic photographs are depicted in Figure 3-2 and Figure 3-3.

Table 3-1: Pipe dimensions and properties.

Length (m)	3.52
Outer Diameter (mm)	168.3
Thickness (mm)	6.4
Density (kg/m^3)	7800
Young's Modulus (GPa)	200
Poisson's ratio	0.3

Piezoceramic sensors were used to monitor the pipe's vibration. Four piezoceramic sensors (PZT1:PZT4) were secured on one flange, and additional four sensors (PZT5:PZT8) were bonded onto the circumference of the pipe at equal distances, as shown in Figure 3-2. The piezoceramic sensors used for the experimental investigation were of type PZT-5H supplied by the Piezo Systems Inc. (Cambridge, MA, USA). The dimensions of each sensor are listed in Table 3-2. The material properties of the sensors have been presented in the numerical study.

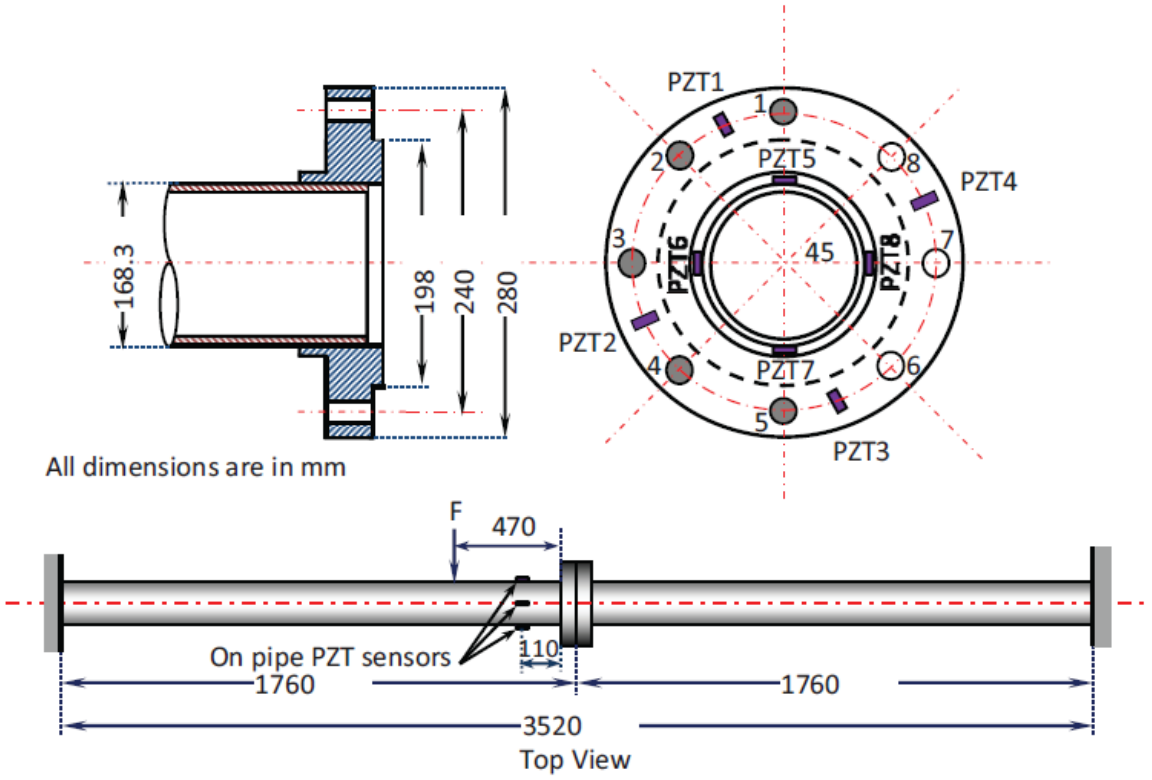

Figure 3-2: Schematic of the bolted joint showing dimensions and impact location.

For this specific configuration, maximum bolt torque was determined to be 124.7 N m. The procedure for tightening the bolts followed the industry standard, which was a crisscross pattern across the face of the flange, using a torque wrench, at increments of 30%, 60%, and then 100% of the maximum torque. The last step of tightening the joint was to go around the joint clockwise and verify that every bolt was at the maximum specified torque. The method used to loosen the bolts to a certain torque was achieved with the aid of a digital torque wrench set to the value that the bolt should be loosened to. The bolt was loosened using an adjustable wrench a slight amount and then tightened to a percentage of the maximum specified torque using the digital torque wrench. This procedure was repeated to achieve the subsequent desired torques.

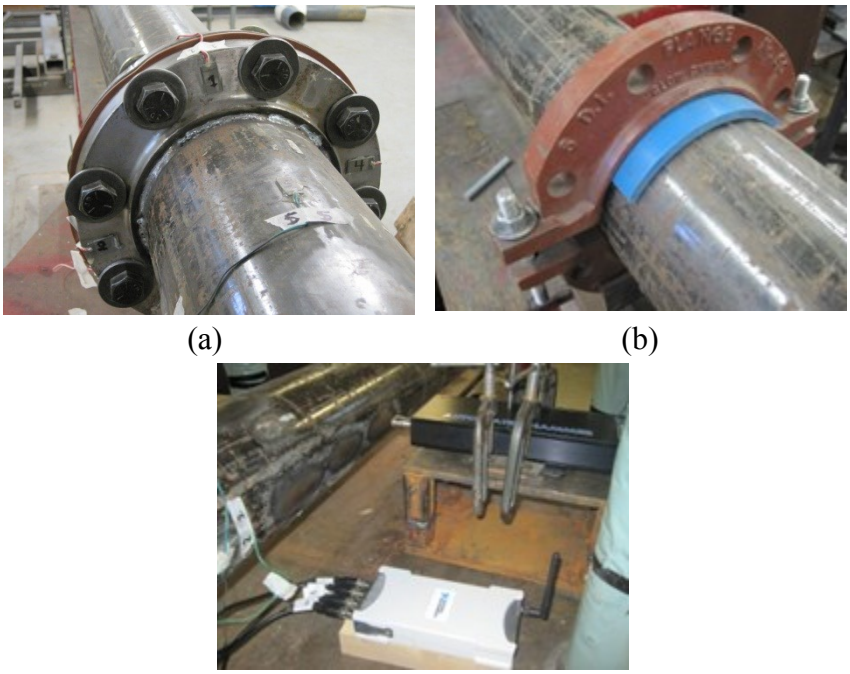

(a) (b)

(c)

Figure 3-3: Experiment setup: (a) the flange, (b) clamped support, and (c) WDAQ and hammer. WDAQ: wireless data acquisition.

A total of nine damage cases (DC1:DC9) were designated. The damage cases constituted the simultaneous reductions of the preload to predetermined specified levels (torques) in some of the bolts. The affected (loosened) bolts and the trial preloads/torques are tabulated in Table 3-3. As an example, the first three damage cases (DC1:DC3) correspond to the reduction of torque levels on bolt 3, from the fully tightened level of 120–20 N m, which corresponds to the most loosened state. This damage pattern (as outlined in Table 3-3) was

purposefully selected such that it could explore the minimum resolution by which the method could predict the existence of the damage as well as its progression.

As stated earlier, the process of damage detection starts with the excitation of pipe's vibration. The clamped–clamped pipe was excited at the specified location (see Figure 3-2) by an electric impact hammer (model AS-1220, Alta Solutions, Inc., San Diego, CA, USA) equipped with an aluminum tip, so that the higher modes could be excited more effectively. Since the method is an energy-based approach, the consistency of the excitation is of paramount importance to the integrity of the technique. As noted in previous studies, the use of the MOIH can adversely affect the consistency of the damage detection technique [14, 18, 21].

Table 3-2: Piezoceramic sensor dimensions.

Length (mm)	25
Width (mm)	12
Thickness (mm)	1

In real cases, the orientation, location, and amplitude of the impacts generated by a manual hammer could vary significantly through different impacts triggered by an inspector. The two latter issues were successfully addressed in our earlier study, and the adopted strategy (i.e. normalization of the signal, as discussed later in this article) effectively resolved most of the inconsistencies [21]. The variation in the orientation of the impact, which could impose some inconsistencies, could not be dealt with previously. The use of the electric hammer as incorporated in the present study effectively and collectively addressed all the above-mentioned factors, thereby generating consistent and reproducible vibration excitation.

Table 3-3: Description of the damage cases.

Bolt Set No.	**Loosened Bolts**	**Applied Torque** (N-m)	**Preload Force** (kN)
1	3	84	31.1
2	2-4	43.4	16.1
3	1-5	20	7.4

Moreover, as explained in our previous study, when a MOIH is used to excite a system, one should repeat the excitation procedure several times (depends on the consistency of the resulting vibration signals), so that a reasonable average value of the excitation signal could

be established. The use of the electric hammer eliminates the need for multiple excitations and the subsequent averaging process, thereby improving the efficiency and accuracy of the proposed methodology.

For each specified damage scenario, the in-house developed MATLAB code processed the data according to the routines briefly introduced in the previous sections. The steps of the processing are as follows:

Step 1. Both the electric hammer's signal and vibration signals registered by the bonded piezoceramics are digitized by a WDAQ (model WLS-9163, National Instruments Inc., Austin, TX, USA) at a sampling rate of 50 kHz. To the best knowledge of the authors, most of the commercially available wireless nodes cannot accommodate the required high sampling rate (this is so that the WDAQ system would offer lower power consumption). Most of the available WDAQ are therefore limited to a sampling rate of 10 kHz. The adopted WDAQ, however, can provide a sampling rate of 100 kHz. The WLS-9163 also embodies a 12 MB RAM, which ensures the secure transmission of the data; this feature enables the device to temporarily store 14 s of data (sampled at the maximum rate); this is a very important feature, in case the wireless network's transmission strength happens to weaken due to unpredictable and uncontrollable external factors. Wireless communication with the selected WDAQ could be successfully accomplished over relatively long distances (up to 100 m) in outdoor applications. However, the transmission becomes limited to 30 m in the case of indoor applications, since different structural materials would variably degrade the signal strength [22].

Moreover, the incorporation of a WDAQ with such a high sampling rate serves two main purposes as follows:

1. It enables one to capture higher vibration modes, which are more indicative of damage.
2. It would facilitate capturing of the electric hammer's signal with an acceptable accuracy and resolution, since any inaccurate record of the hammer's signal would adversely affect the efficiency of the normalization process that will be explained in the next section.

Typical hammer signals registered by different sampling rates, ranging from 10 to 50 kHz, are depicted in Figure 3-4. As it can be inferred, the impulse force occurs over

approximately 0.1 ms, requiring setting the sampling rate to at least 50 kHz (i.e. F_s=1/(0.1 ms/5)), or five times greater than the present harmonic of the signal [23]. Incorporation of a lower sampling rate may jeopardize the proper registration of the hammer's signal, from both the perspectives of shape and peak amplitude (Figure 3-4). Regarding the inconsistency noted in the calculated energies and the associated damage indices in our previously reported results, two factors were considered the main culprits [14]:

1. The lower sampling rate (i.e. 10 kHz), as adopted in capturing the MOIH's signal in our previous study;
2. The inevitable variation in the orientation of the impact forces that were imposed onto the system to excite it.

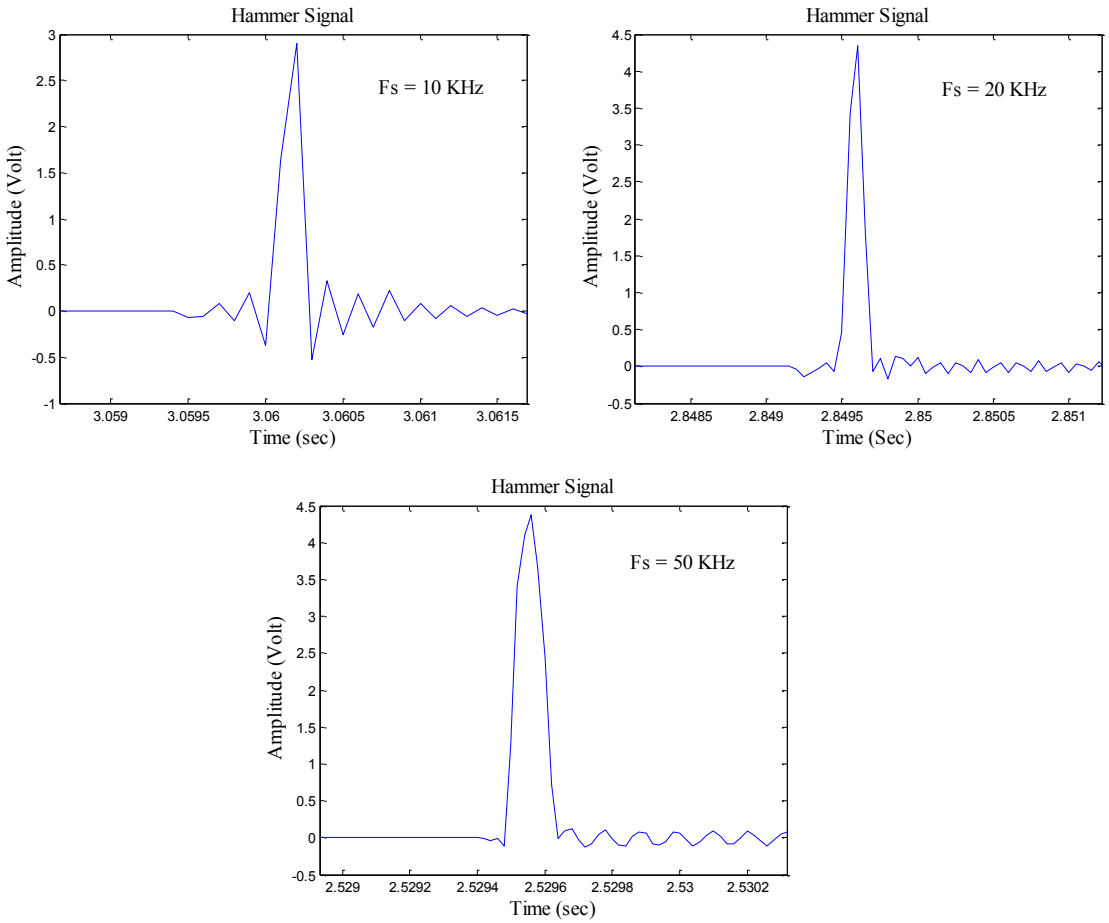

Figure 3-4: Electric Hammer's signal captured at different sampling rates.

Figure 3-5 sheds light on the tangible inconsistency (as high as 62%) in the calculated energy indices that could be potentially generated due to the incorporation of lower sampling rates.

Moreover, as a result of the inherently high damping associated with this type of joints, and the additional damping produced by the gasket integrated in-between the mating flanges, the gathered vibration signals would have to be conditioned and amplified with an appropriate signal conditioner. For this, a signal conditioner (model 482C16, PCB Piezotronics Inc., New York, USA) was used before their digitization within the WDAQ. In other words, this step is performed to magnify the voltage produced by the PZT, thereby maximizing the resolution of the digitized signals. In addition, this step also reduces the effect of the inherent noise embedded in the recorded data, thus generating more acceptable SNRs. This would in effect render more reliable signals, especially with respect to those produced by the sensors bonded to the flange.

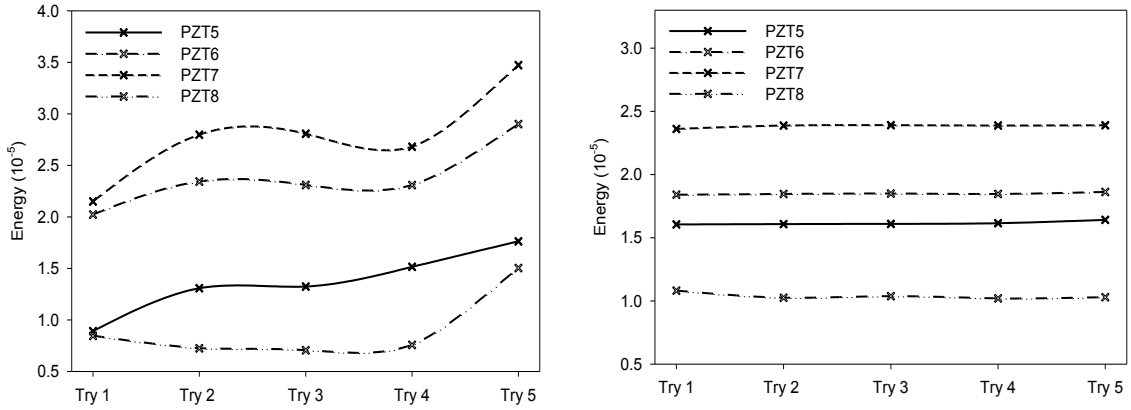

Figure 3-5: Calculated energy indices obtained from various sensors with different sampling rates of (a) 10 and (b) 50 kHz at various trials. PZT: lead zirconate titanate.

Figure 3-6 compares a typical signal generated by a PZT located on the flange before and after the amplification step is performed. The SNR values are calculated using the following equation:

$$SNR = 20\log\left(\frac{\sigma_{Signal}}{\sigma_{noise}}\right) \qquad 3\text{-}4$$

The increases in the actual values of the SNR of the signals obtained from PZTs located on the pipe and flange before and after the amplification are reported in

Table **3-4**. As it can be observed, the SNR value of the sensor bonded to the flange is relatively large. This is because the sensors on the flange experience more local damping. The digitized and treated data are then sent remotely to a computer station for analysis purposes through a reliable and secure communication link.

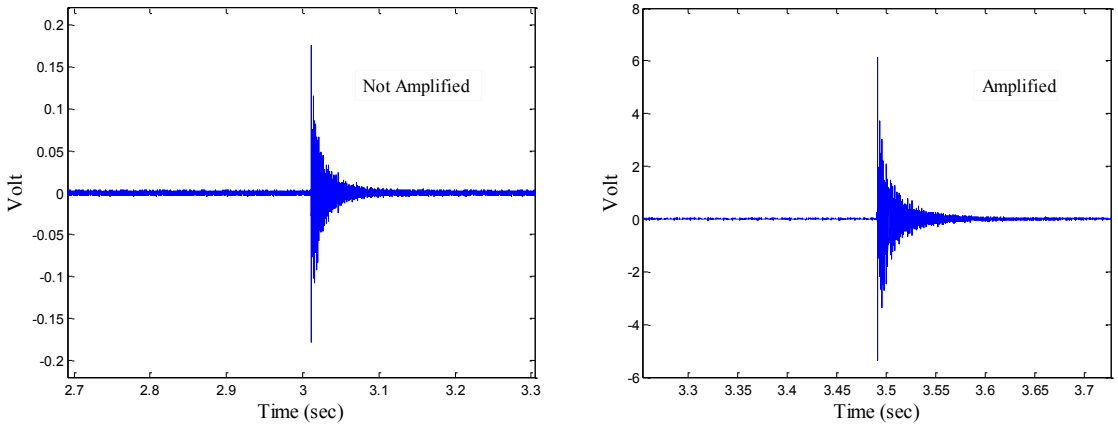

Figure 3-6: A typical output signal generated by a PZT bonded onto the flange (a) before and (b) after the amplification. PZT: lead zirconate titanate.

Table 3-4: Effect of amplification stage on the SNR.

SNR	Before Amplification	After Amplification
Sensors on the pipe	108	125
Sensors on the flange	55	121

SNR: signal-to-noise ratio.

Step 2. In this step, the sensors' signals are normalized with respect to the hammer's signal to maximize the consistency of the recorded data in the event of variable load amplitudes being produced using a manual hammer. It should be mentioned that the normalization step could be skipped when an electric hammer is used, as it produces consistent impacts from perspectives of both frequency and amplitude.

Accordingly, the sensors' signals are divided by the hammer's signal in the frequency domain. The resultant signal is transferred back into the time domain for further analysis.

Equation 3-5 describes the receptance function $\alpha(\omega)$ (the ratio of the response, x, to the excitation force F, in the frequency domain, ω, for a linear system [24]:

$$\left[\alpha(\omega)\right] = \frac{x(\omega)}{F(\omega)} = \left[K + i\omega C - \omega^2 M\right]^{-1} \qquad 3\text{-}5$$

where K, C, and M are the stiffness, damping (viscous), and mass matrices of a continuous system, respectively. This ratio is determined solely based on the physical characteristics of the system and is not influenced by the force amplitude, so long as the system remains linear. This feature, which justifies the use of the normalization, guarantees the consistency as the load amplitude may vary significantly when different operators using the same manual hammer.

Figure 3-7 shows the experimental energies calculated through different levels of the applied load for the healthy state of the pipe. As can be seen, both the sensors on the pipe and the flange yielded the same energies with varying load levels. This observation confirms the integrity of the normalization process implemented into the code and consequently correlates the changes in the energies to the onset and propagation of potential damages.

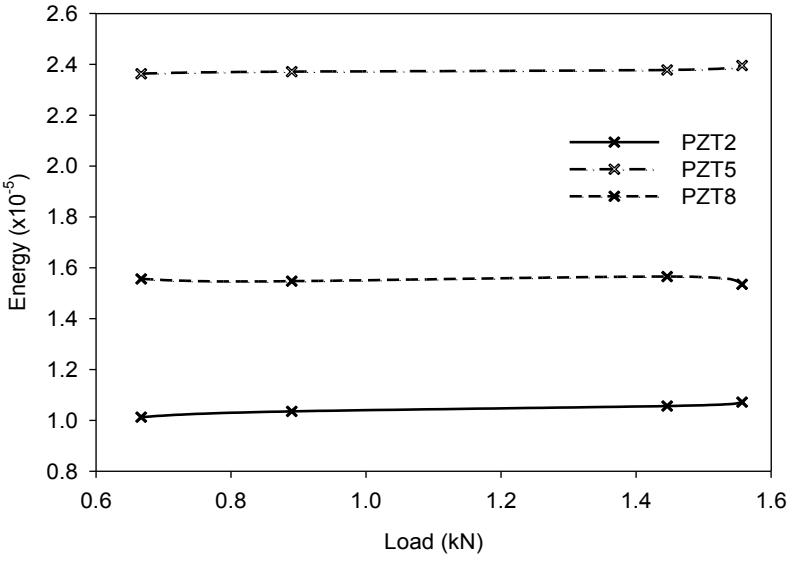

Figure 3-7: Computed energy indices with varying load amplitudes for sample sensors on the pipe and the flange in the healthy state of the pipe. PZT: lead zirconate titanate.

Although this step is not necessary when an electric hammer used, since the process does not consume a significant computational effort, it is recommended to be performed to maximize the consistency.

Step 3. The normalized signals are band-passed with a digital filter (i.e. the Butterworth filter) to maintain the useful portion of the data. In this study, the bandwidth was set to be 0–5 kHz. The bandwidth of the filter was selected such that it would yield digital signals whose shapes are very close to that of the analog ones having the same frequency content (i.e. up to 5 kHz).

It should be noted that the shape of the signal can be adequately reconstructed when the sampling rate is at least 5–10 times greater than the desired frequency content of the signal [23]. This rule of thumb may be applied to the energy-based approaches or the like, where the reconstruction of the signal is of paramount importance to the integrity of the method. In other words, the application of this rule ensures an upper limit for the reliable frequency content of a signal.

Moreover, the selected bandwidth would remove the portion of the signal that suffers from aliasing (i.e. in this case, the frequency content of the signal above 25 kHz (50 kHz/2)). Selection of the appropriate frequency bandwidth based on the explained rule of thumb (upper-band limit) would reduce the confusion and the subsequent trials and errors noted in the previous studies [14].

Step 4. Individual filtered signals are then processed with EMD [16]. After the first IMF is extracted for each signal, the program numerically calculates the energy of the IMF according to Equation 3-2. Finally, the damage indices are established by comparing the energies before and after the onset of damage. Figure 3-8 shows a typical signal obtained from one of the sensors and its constituents IMFs.

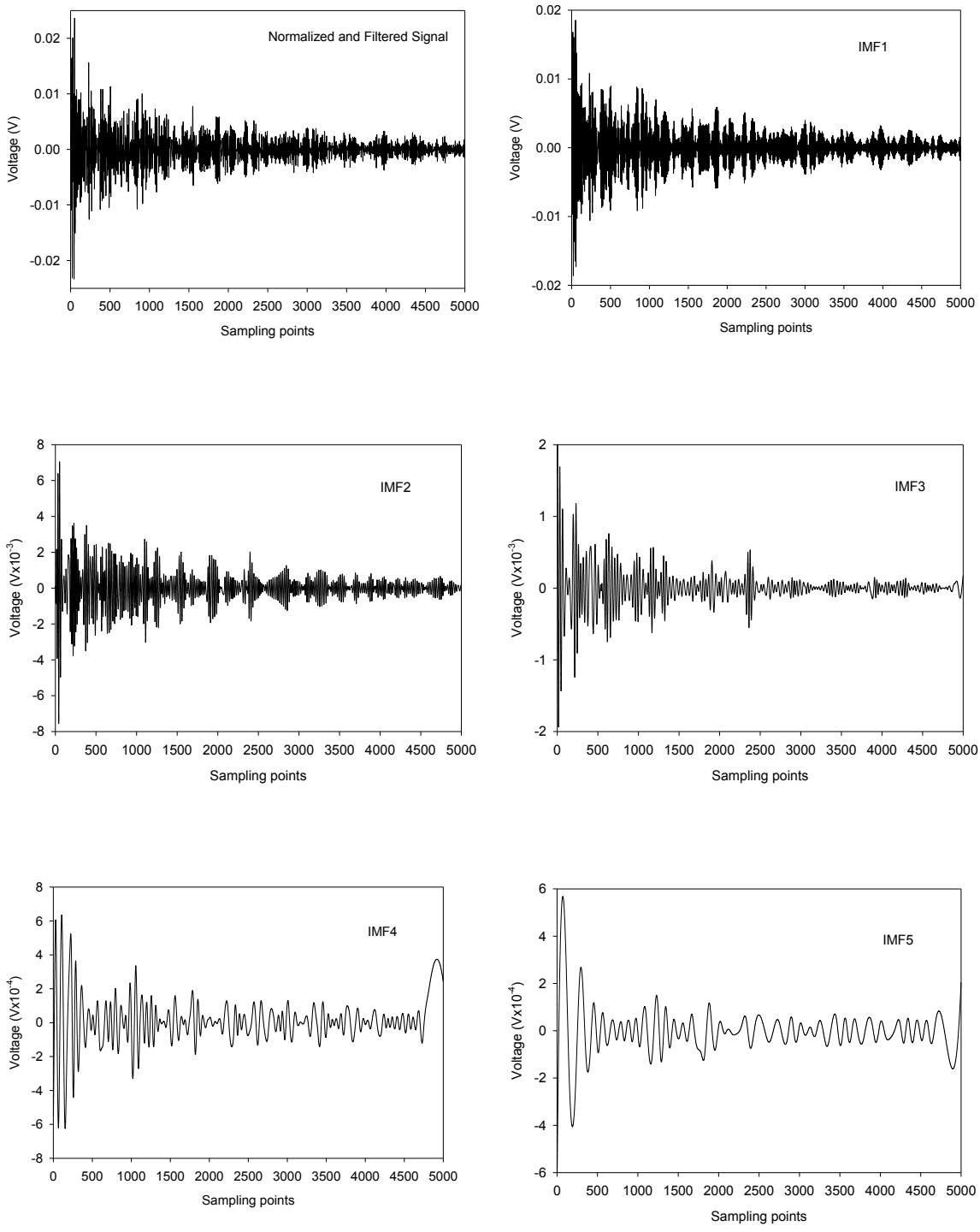

Figure 3-8: A typical signal of a piezoelectric sensor and its constituents IMFs. IMF: intrinsic mode function.

3.5 EXPERIMENTAL RESULTS AND DISCUSSION

The above-described data acquisition and signal processing routines were performed for each damage case as described earlier (see Table 3-3), as well as for the system at its healthy state. Reproducibility of the calculated energies from the generated signals is always an important and highly desirable feature when processing such signals and was determined to be over 97%. This means that all damage indices greater than 3% should warn the user of a potential damage in the bolted joint.

Figure 3-9 illustrates the evolution of the damage metric calculated based on the EMD_EDI of the signals generated by the sensors bonded onto the pipe. It can be clearly noted that not only could all the sensors bonded onto the pipe capture the existence of the bolt loosening (damage), but also its progression by producing reasonably discernible damage indices; the trends are consistent for all damage scenarios. For instance, the maximum damage index increases from almost 12% to 24% when the damage in bolt set 1 is compared to the one for bolt set 3 (Figure 3-9 (a) to (c)).

When comparing the increasing trend observed in the indices clearly noted in Figure 3-9 with our previously reported results, a marked improvement is apparent in the consistency and quality of the results [14]. This is believed to be due to the implementation of the signal conditioning procedure and the incorporation of the electric hammer that generated consistent vibration excitation of the system in a reproducible manner. Our previously reported effort, in which the manual hammer used to excite the system, succeeded in detecting the damage states but fell short of predicting accurately the progression of damage [14].

It should be noted that as bolts loosen in such joints, they give rise to several secondary phenomena that alter the vibration response of the system. Among the most important are the variation in the global stiffness of the pipe and the energy dissipation through the surface asperities that should vary as a function of the contact pressure [7]. It is believed that the sensors on the pipe sense the reduction in the system's stiffness more noticeably than they can in sensing the local energy dissipations imposed by the contact pressure-dependent surface asperities. It should also be emphasized that there is some small discrepancies in the pattern of damage progression. For instance, see the damage indices

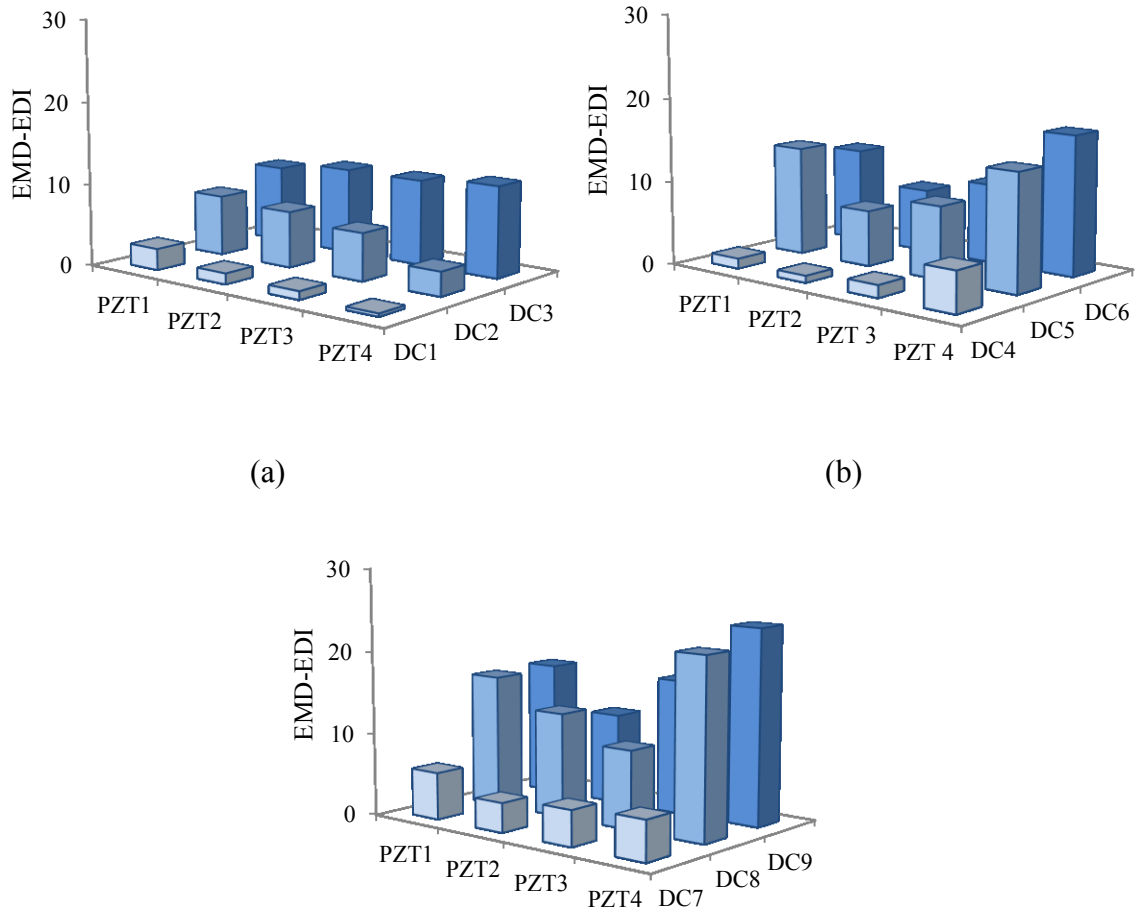

Figure 3-9: Damage indices based on the experimentally generated signals by the sensors located on the pipe for damage cases imposed on (a) bolt set 1, (b) bolt set 2, and (c) bolt set 3. PZT: lead zirconate titanate; EMD_EDI: EMD energy damage index.

generated from PZT5's signals, for damage cases DC5 to DC6; whereas one would expect to see a slightly larger damage index for DC6, the values still fall within the reproducibility threshold (i.e. within the established variation of indices of 3%). In addition, the damage metric calculated for set 1 bolts (i.e. bolt 3) indicates that the damage indices are well above the reproducibility threshold when bolt 3 is loosened to a medium torque level (40 N m). These findings suggest the minimum resolution of the health monitoring technique. Moreover, by observing the damage indices produced from the signals of the sensors

bonded onto the pipe, one can appreciate the fact that the use of only one sensor could handle the health monitoring of the joint.

On the other hand, the damage indices obtained through the sensors bonded onto the flange show higher values (by up to 50%) compared to those corresponding to sensors on the pipe (see Figure 3-10).

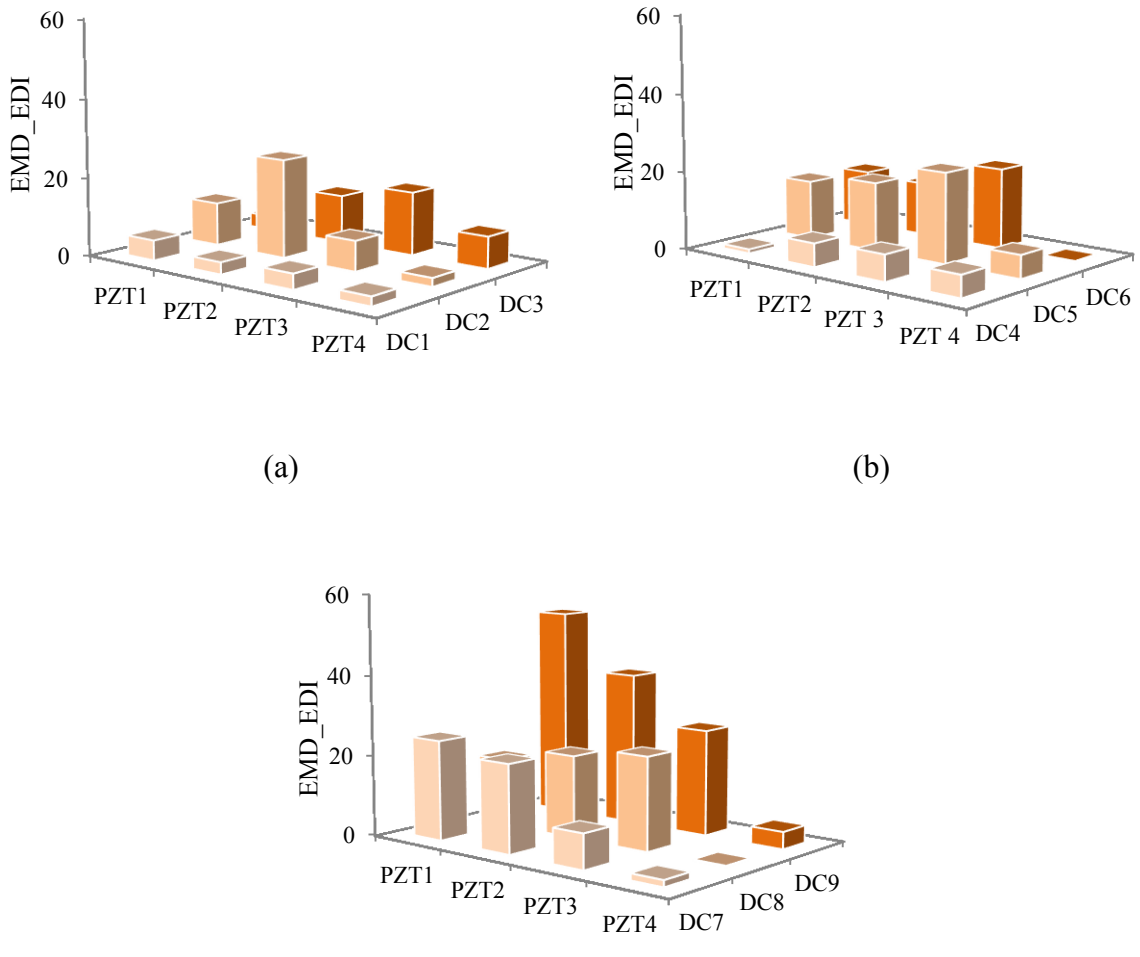

Figure 3-10: Damage indices based on the experimentally generated signals by the sensors located on the flange for damage cases imposed on (a) bolt set 1, (b) bolt set 2, and (c) bolt set 3. PZT: lead zirconate titanate; EMD_EDI: EMD energy damage index.

This is believed to be due to the fact that the sensors on the flange are closer to the damage zone. Similar to the results obtained through the sensors bonded to the pipe, the general progression trend of damage can be traced by the sensors on the flange. This trend is more tangible when comparing the damage indices corresponding to different damaged bolt sets. There are, however, some inconsistencies among the individual progression pattern of each bolt set damage cases.

It is believed that this inconsistent behavior is due to the unpredictable nature of the damping mechanisms, whose culprits were identified earlier.[7] Interestingly, PZT4, which is located farthest from the damage zone, yielded lower damage indices compared to the other three sensors located on the flange. Moreover, one may also conclude that the placement of only two sensors on the flange could efficiently facilitate the health monitoring of the joint, so long as they are bonded circumferentially, 180° away from one another.

In the next section, the details of the FE framework developed for simulating the damage detection technique are presented. The main goal of this part of the study is to develop a reliable tool by which one could conduct parametric studies for further streamlining the capability, accuracy, and the extent of the applicability of the proposed SHM technique.

3.6 FE MODEL

The FE model presented in our previous study was further refined [14]. In developing the FE model, for comparison purposes, the system dimensions and specifications were kept the same as those used in the experimental segment of this study. The thick rubber gasket (E = 1 GPa, ϑ = 0.5), which was used between the two flanges of the bolted joint, was also included in the FE model. The material properties of the PZT-5H sensors (obtained from Piezo Systems Inc., Cambridge, MA, USA) are described using the following matrices

$$S_E\left[\frac{m^2}{N}\right]=\left(10^{-12}\right)\begin{bmatrix} 16.5 & -4.78 & -8.45 & 0 & 0 & 0 \\ -4.78 & 16.5 & -8.45 & 0 & 0 & 0 \\ -8.45 & -8.45 & 20.7 & 0 & 0 & 0 \\ 0 & 0 & 0 & 43.5 & 0 & 0 \\ 0 & 0 & 0 & 0 & 43.5 & 0 \\ 0 & 0 & 0 & 0 & 0 & 42.6 \end{bmatrix}$$

$$d\left[\frac{C}{N}\right]=(10^{-12})\begin{bmatrix} 0 & 0 & 0 & 0 & 741 & 0 \\ 0 & 0 & 0 & 741 & 0 & 0 \\ -274 & -274 & 593 & 0 & 0 & 0 \end{bmatrix}$$

$$\varepsilon^{S}\left[F/m\right]=(10^{-9})\begin{bmatrix} 27.7 & 0 & 0 \\ 0 & 27.7 & 0 \\ 0 & 0 & 30.1 \end{bmatrix}$$

where S_E is the compliance matrix, d is the piezoelectric coupling matrix, and ε^S is the permittivity of the piezoceramic. These matrices are used to model the sensors in ABAQUS [25] using the three-dimensional eight-node piezoelectric element (C3D8E). The density of PZT-5H was taken as 7500 kg/m^3. ABAQUS's solid element C3D8R (continuum three-dimensional eight-node reduced integration element with three translational degrees of freedom per node) was used to model the pipes, flanges, and bolts. Tie multipoint constraints were used to connect the mating surfaces of the pipes and flanges, the contacting interfaces between bolts' heads/nuts and the flanges, and the sensors and flange interface.

The contact between the bolt shanks and the inside surfaces of flange holes was neglected. Within the resources available, inclusion of the contact in the model would render execution of the problem computationally formidable. Furthermore, the bolt and nut assembly was modeled as one part to remove the complexity arising from the contact between the threads of the bolt and the nuts. The ''surface to surface hard contact algorithm'' was used to model the contact mechanism between the rubber gasket and the flanges. It should be noted that this effort represents the enhancement of the numerical model presented in our earlier study, in which the ''tie constraint'' was used to approximate the interaction of the gasket and the flanges [14].

Details of the FE model and the mesh for all components are shown in Figure 3-11. Also, the impact hammer's force was simulated by the step impulse force with its amplitude, as shown in Figure 3-11. The mesh density was designed to produce an acceptable accuracy without making the problem computationally too expensive. Both the pipes and the flanges were modeled using at least two or three layers of elements through the thickness. The mesh was strategically refined at the sensor locations, at the bolt and flange interfaces, and between the mating surfaces of the flanges.

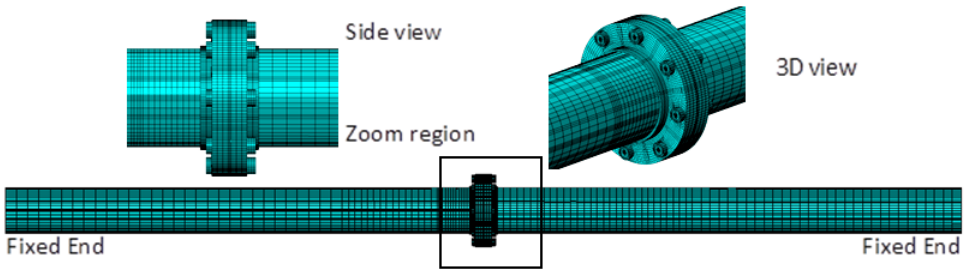

(a)

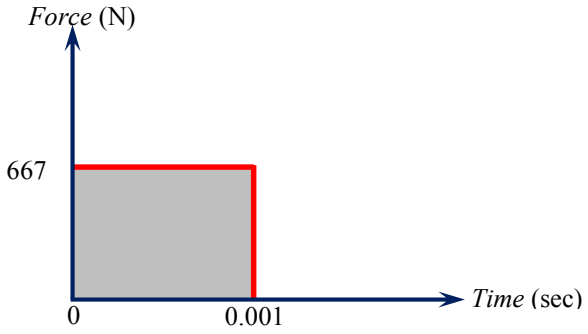

(b)

Figure 3-11: (a) Finite element model's details and (b) simulated impact hammer impulse force in the finite element model.

The pretension load applied to each bolt is calculated based on the actual torque applied to each bolt (measured during the experimental analysis) through the following standard relation

$$F = \frac{\tau}{k d_{bolt}} \qquad 3\text{-}6$$

where $k = 0.15$ is the nut factor used to account for the friction between the threads of the bolt and its nut [26].

The calculated pretension force was applied at a cross-sectional plane, located at the mid-height of each bolt. This method is recommended by the ABAQUS and will be further described later.

It should be noted that the considered damage scenarios are the same as the ones investigated in the experimental studies. However, the DC7:DC9 damage cases were removed from the numerical study because of convergence issues encountered when the simultaneous loosening of five bolts was attempted.

The analysis procedure for the healthy and damage states is conducted through several sequential steps in the ABAQUS, as follows:

Step 1. The pretension load is first applied onto each bolt. To account for the clamped boundary conditions, the translational degrees of freedom of the left and right edges of the pipes are restrained. Moreover, to prevent any initial electric potential that might affect the output voltage of the sensors, the bottom surface of each sensor (the surface in direct contact with the flange) is prescribed a zero electric potential as the initial condition. It should be noted that the pretension force of each bolt is varied appropriately when modeling the damage cases in separate runs.

Step 2. As stated, the pretension force should be applied to a plane at the mid-height of each bolt. Moreover, the degrees of freedom on that plane should be kept restrained. This is a requirement set by the ABAQUS, so that the influence of any other applied load (in this case, the influence of the impact load) could be transmitted across the bolts.

Step 3. A transient dynamic step within the ABAQUS/Implicit is performed, in which the pipe is excited by applying the step load shown in Figure 3-11 to simulate hammer's impact. Subsequently, each sensor's voltage signal is acquired during the first 0.1 s of the vibration event, at a sampling frequency of 10 kHz (i.e. time increment size of 0.0001 s).

3.7 NUMERICAL RESULTS AND DISCUSSION

After obtaining the sensors' signals from the healthy and damage state models, the EMD_EDIs were established according to Equation 3-3. Figure 3-12 and Figure 3-13 illustrate the damage indices established by the signals generated by the FE simulations. As can be seen, overall, the FE produced results corroborate with the experimental results. In other words, as observed from the experimental results, the indices produced from the signals of the sensors located on the pipe through the FE analysis could also capture the existence of the damage and could also trace its progression.

As stated earlier, it is believed that the sensors on the pipe sense the reduction in the stiffness more effectively rather than the local complex behavior at the joint. Therefore, it is expected that the assumptions made for the contacts of bolts-flange interfaces should not impose noticeable inconsistency between the numerical and experimental results. Accordingly, it can be seen (Figure 3-12) that the damage index values and their patterns

reasonably match those calculated from the experimental results. Interestingly, Figure 3-12 reveals that PZT5 and PZT7 sensors yield similar indices for the damages associated with the second bolt set. This is because of the fact that the two sensors are located symmetrically to the location of the simulated damages.

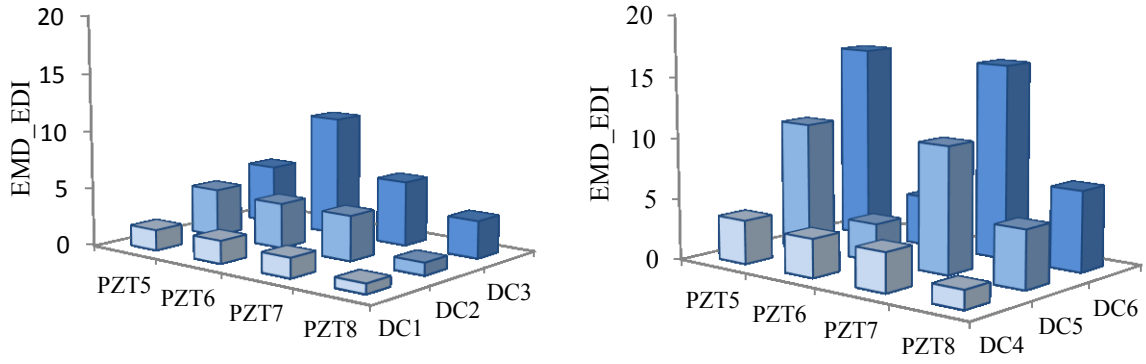

(a) (b)

Figure 3-12: Damage indices based on the FE signals generated by the sensors located on the pipe damage cases imposed on (a) bolt set 1 and (b) bolt set 2. FE: finite element; PZT: lead zirconate titanate; EMD_EDI: EMD energy damage index.

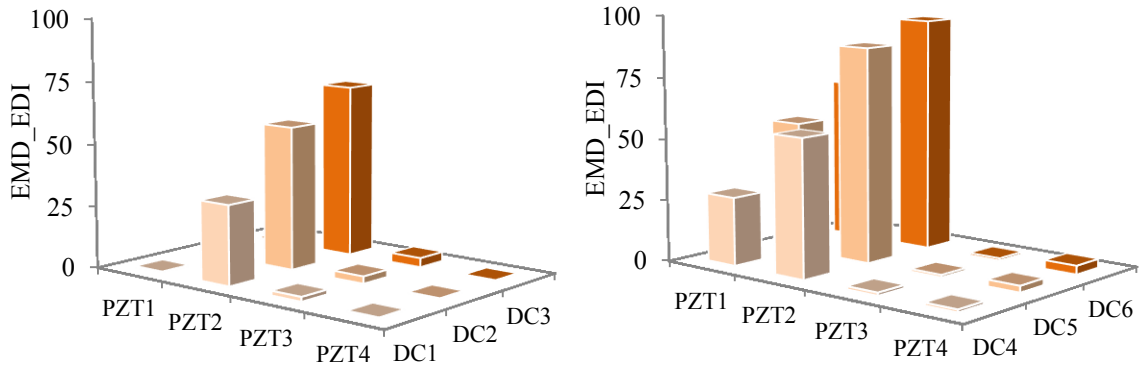

(a) (b)

Figure 3-13: Damage indices based on the FE signals generated by the sensors located on the flange damage cases imposed on (a) bolt set 1 and (b) bolt set 2. FE: finite element; PZT: lead zirconate titanate; EMD_EDI: EMD energy damage index.

This observation further highlights the integrity of modeling of the pipe/flange assembly. As expected, the analysis of the signals produced by the sensors bonded onto the flange yielded higher damage indices. However, it should be noted that the differences in the value of the damage indices from the numerical and experimental studies are believed to be due to the assumptions made in modeling the joint assembly. The real contacts between the bolts and flange interfaces, which are modulated by the different applied torques, have not been accounted for in the numerical modeling, thus causing the noted differences (differences in the value of damage indices) in the experimental and numerical results. It should be noted that the sensors on the flange are more sensitive to the erratic local response in the joint occurring at that region. However, as stated, modeling of such interactions would add formidable complexity to the model, which cannot be handled by our current resources.

3.8 REMARKS ON THE OPERATIONAL/ENVIRONMENTAL CONDITIONS

It should be noted that specific attentions should be paid to the in situ application of vibration-based damage detection (VBDD) methodologies, including the one utilized in this study. Inevitable noise sources (e.g. down sampling/aliasing of analog signals, environment, and electrical instrumentations), any variation in the boundary conditions, and sudden disturbance to the structure (e.g. in the case of pipes, disturbance due to a fluid hammer) could negatively affect the resolution of the method (in this case, in predicting progressing bolt loosening). The demonstrated repeatability in the results of our experiments (i.e. over 97%) highlights the fact that there could be a maximum of 3% variation in the calculated energies, which is believed to be specifically related to all the noise sources present in the laboratory. In an event when additional noise sources might be present (those that can be described as a harmonic function; for instance, the common 60 Hz electromagnetic noise associated with the nearby power cords), the specific harmonic can be minimized using an appropriate analog/digital band-pass filter.

On the other hand, a health monitoring session may coincide with the occurrence of sudden disturbances to the system (e.g. in the case of pipes, fluid hammer due to sudden closure of the valves or start-up induced abrupt pressure changes). In such cases, serious

inaccuracies may be resulted; thus, the use of vibration-based methodologies should be avoided in such circumstances.

Slight variations in boundary conditions of a system could also impact the accuracy of vibration-based methods. The current wave propagation/energy-based study is believed to be least sensitive to changes in the boundary conditions, so long as the boundary condition is far enough from the region of interest.

To examine the validity of the above-mentioned statement, the boundary condition at one of the pipe joints tested in our study (i.e. pipe's clamped ends) was disturbed, and the variations in the calculated energies were subsequently recorded. To this end, the level of torque applied to the bolts maintaining the clamping force on pipe's left support (see Figure 3-3(b)) was gradually reduced. The pipe was then impacted at each torque level (30–10 N m at 5 N m increment), and the signals from PZT2 and PZT6 were recorded simultaneously. The energies corresponding to each torque level were then calculated and normalized with respect to the maximum applied torque level (30 N m) for the two sensors. Figure 3-14 illustrates the result of this trial. As can be seen, a reduction of 66% in the applied torque used to maintain the clamping force of the support caused a maximum variation of approximately 4% in the resulting energies.

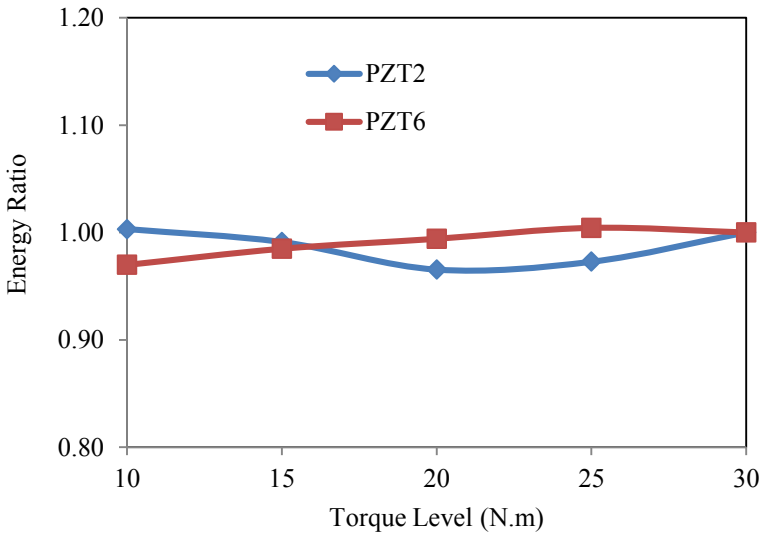

Figure 3-14: Variations in energies for different degrees of clamping force applied onto the left boundary. PZT: lead zirconate titanate.

Owing to the damping of the propagating waves, it is therefore postulated that these variations could be even smaller if the supports were situated farther away from the zone where the health monitoring was being conducted.

In summary, one should note that environmental conditions (if not controlled) could significantly affect the outcome of any vibration-based method, including the one used in this study. However, not only did the method used in our study produce fairly high damage indices for the case when the damage was quite severe (i.e. the case of almost fully loosened bolts), but also did a good job at tighter bolt situations (i.e. the cases in between fully tightened and loosened spectrums). This method can therefore be considered as an effective damage detection, especially as an initial alarm, prior to conducting a more thorough and extensive (thus costly) investigation.

3.9 CONCLUSION

This study examined and improved the integrity of a vibration-based approach for detection of bolt loosening in pipeline bolted joints. The numerical and experimental studies performed on a full-scale pipe corroborated the integrity of the technique. The reported inconsistencies in the previous effort [14] were addressed by employing an electric hammer and incorporating a robust signal conditioning protocol. The results presented in this part of the study demonstrated the successful detection of the onset of bolt loosening and its progression. Moreover, the concept of remote/wireless data collection was proven viable, hence enhancing the robustness of this damage detection approach. Also, the FE model presented in our earlier study was further improved, yielding more accurate results. The improved modeling approach will enable us to further investigate and improve the efficiency and extent of the applicability of the tested damage detection methodology by conducting cost-effective parametric studies. The development of a more versatile sensor and the implementation of the programmable wireless nodes are also the objectives of the ongoing research.

3.10 FUNDING

This study was financially supported by the Petroleum Research Atlantic Canada (PRAC) and the Natural Sciences and Engineering Council of Canada (NSERC).

3.11 REFERENCES

1. *Guidelines for the management of the integrity of bolted joints for pressurized systems*. 2007, Energy Institue: London.
2. Afshari, M., T. Marquié, and D.J. Inman. *Automated structural health monitoring of bolted joints in railroad switches*. in *Proceedings of ASME 2009 Rail Transportation Division Fall Conference*. 2009.
3. Ritdumrongkul, S., et al., *Quantitative health monitoring of bolted joints using a piezoceramic actuator–sensor.* Smart Materials and Structures, 2004. **13**(1): p. 20-29.
4. Carden, E.P. and P. Fanning, *Vibration based condition monitoring: a review.* Structural Health Monitoring, 2004. **3**(4): p. 355-377.
5. Farrar, C.R. and S.W. Doebling, *Damage detection II: field applications to large structures*, in *Modal analysis and testing (NATO science series)*, J.M.M. Silva and N.M.M. Maia, Editors. 1999, Kluwer Academic Publishers: Dordrecht. p. 1-29.
6. Chandrashekhar, M. and R. Ganguli, *Structural damage detection using modal curvature and fuzzy logic.* Structural Health Monitoring, 2009. **8**(4): p. 267-282.
7. Yang, J. and F.-K. Chang, *Detection of bolt loosening in C–C composite thermal protection panels: I. Diagnostic principle.* Smart Materials and Structures, 2006. **15**(2): p. 581-590.
8. Yang, J. and F.-K. Chang, *Detection of bolt loosening in C–C composite thermal protection panels: II. Experimental verification.* Smart Materials and Structures, 2006. **15**(2): p. 591-599.
9. Milanese, A., et al., *Modeling and Detection of Joint Loosening using Output-Only Broad-Band Vibration Data.* Structural Health Monitoring, 2008. **7**(4): p. 309-328.
10. Amerini, F. and M. Meo, *Structural health monitoring of bolted joints using linear and nonlinear acoustic/ultrasound methods.* Structural Health Monitoring, 2011. **10**(6): p. 659-672.
11. Mickens, T., et al., *Structural health monitoring of an aircraft joint.* Mechanical Systems and Signal Processing, 2003. **17**(2): p. 285-303.
12. Park, G., H.H. Cudney, and D.J. Inman, *Feasibility of using impedance-based damage assessment for pipeline structures.* Earthquake Engineering & Structural Dynamics, 2001. **30**(10): p. 1463-1474.
13. He, K. and W.D. Zhu, *A vibration-based structural damage detection method and its applications to engineering structures.* International Journal of Smart and Nano Materials, 2011. **2**(3): p. 194-218.
14. Esmaeel, R.A., J. Briand, and F. Taheri, *Computational simulation and experimental verification of a new vibration-based structural health monitoring approach using piezoelectric sensors.* Structural Health Monitoring, 2011. **11**(2): p. 237-250.
15. Cheraghi, N., M. Riley, and F. Taheri. *A novel approach for detection of damage in adhesively bonded joints in plastic pipes based on vibration method using piezoelectric sensors*. in *Systems, Man and Cybernetics, 2005 IEEE International Conference on*. 2005. IEEE.
16. Huang, N.E., et al., *The empirical mode decomposition and the Hilbert spectrum for nonlinear and non-stationary time series analysis.* Proceedings of the Royal

Society of London. Series A: Mathematical, Physical and Engineering Sciences, 1998. **454**(1971): p. 903-995.
17. Cheraghi, N. and F. Taheri, *A damage index for structural health monitoring based on the empirical mode decomposition.* Mechanics of Materials and Structures, 2007. **2**(1): p. 43-62.
18. Razi, P., R.A. Esmaeel, and F. Taheri, *Application of a robust vibration-based non-destructive method for detection of fatigue cracks in structures.* Smart Materials and Structures, 2011. **20**(11): p. 115017.
19. Rezaei, D. and F. Taheri, *Health monitoring of pipeline girth weld using empirical mode decomposition.* Smart Materials and Structures, 2010. **19**(5): p. 055016.
20. Loutridis, S., *Damage detection in gear systems using empirical mode decomposition.* Engineering Structures, 2004. **26**(12): p. 1833-1841.
21. Rezaei, D. and F. Taheri, *Experimental validation of a novel structural damage detection method based on empirical mode decomposition.* Smart Materials and Structures, 2009. **18**(4): p. 045004.
22. Kuo, W.-H., et al. *An intelligent positioning approach: RSSI-based indoor and outdoor localization scheme in Zigbee networks*. in *Machine Learning and Cybernetics (ICMLC), 2010 International Conference on*. 2010. IEEE.
23. Engelberg, S., *Signal reconstruction*, in *digital signal processing: an experimental approach*. 2008, Springer: London.
24. Ewins, D.J., *Theoretical basis, modal testing: theory, practice and application*. 2nd ed. 2000, Philadelphia: PA: Research Studies Press Ltd.
25. ABAQUS, *Dassault Systemes Americas Corp*. 2012.
26. Chambers, J.A., *Preloaded joint analysis methodology for space flight systems*. 1995, National Aeronautics and Space Administration (NASA), Lewis Research Center: Cleveland.

CHAPTER 4 ON THE VIBRATION SIMULATION OF SUBMERGED PIPES- STRUCTURAL HEALTH MONITORING ASPECTS

Pejman Razi, and Farid Taheri[1]

Department of Civil and Resource Engineering, Dalhousie University, 1360 Barrington Street, Halifax, NS, B3H 4R2, Canada

Submitted to the journal of Ocean Engineering.

4.1 ABSTRACT

This work aims to provide further insight into the modeling aspects and influence of some important parameters involved in the simulation of vibration of submerged pipes, especially in relation to vibration-based structural health monitoring (VB-SHM). Two widely-used techniques for modeling submerged pipelines, namely the "added mass" and "coupled acoustic-structural" approaches are compared and their limitations and advantages in the context of VB-SHM are highlighted. Moreover, the paper also presents a comprehensive study into the effect of operational variability on the accuracy of offshore pipelines' VB-SHM. It is demonstrated that the geometric stiffness produced by the operational variability (such as changes in the internal and external pressures of pipelines) could variably alter the overall stiffness of such submerged bodies, hence affecting their dynamic response. Depending on the pipe stiffness, the imposed variations could significantly affect the accuracy of VB-SHM trials.

Keywords: dynamic response, submerged structures, vibration-based structural health monitoring (VB-SHM), fluid-structure interaction (FSI), added mass, coupled acoustic-structural approach, geometric stiffness, operational variability.

Nomenclature

b	Width	$\boldsymbol{N}_u$	Shape functions for displacement
c	Speed of sound in the medium	$\boldsymbol{N}_p$	Shape functions for acoustic pressure
$\boldsymbol{C}$	Damping matrix	p_s	Static pressure
$\tilde{\boldsymbol{C}}$	Damping matrix for fluid	p	Dynamic/acoustic pressure
D_{ij}	Bending stiffness elements	$\tilde{\boldsymbol{p}}$	Acoustic pressure vector
E_{ij}	Elastic moduli	$\boldsymbol{Q}$	Coupling matrix
EI	Bending rigidity	r	Radius
$\boldsymbol{F}$	Force vector	$\boldsymbol{S}$	Mass matrix for fluid
g	Acceleration due to gravity	U	Velocity in lateral direction
G_{ij}	Shear moduli	$\boldsymbol{u}$	Displacement vector
h	Height of the fluid	$\tilde{\boldsymbol{u}}$	Nodal displacements vector
H	Stiffness matrix for fluid	V	Velocity
OD	Outer diameter	$X(t)$	Displacement in x-direction
K	Stiffness per unit length	Ω_f	Fluid domain
$\boldsymbol{K}$	Stiffness matrix	Γ_i	Boundary domain
M	Mass per unit length	ρ_f	Fluid density
$\boldsymbol{M}$	Mass matrix	ϕ	Velocity potential
$\boldsymbol{n}$	Unit normal vector	ν_{ij}	Poisson's ratio

4.2 INTRODUCTION

Vibration-based structural health monitoring (VB-SHM) of submerged structures has received several researchers' attention in recent years [1-7]. Some of these studies have included numerical simulations of their damage detection case studies in addition to their experimental verifications [1-4, 6]. In some of those numerical studies, the fluid-structure interaction (FSI) has been idealized by using the concept of "added mass" [1-3, 6]. While, others have adopted a more elaborate approach, namely the "coupled acoustic-structural" method, in their numerical simulations [4].

It has been shown that the idealization in representing the FSI could lead to erroneous predictions. For instance, Zeinoddini *et al.* [8] compared the performances of the added mass approach (AMA) against the "coupled acoustic-structural" approach (CASA) in predicting the seismic and harmonic responses of an offshore pipeline's free-spanning (a segment of a pipe that is suspended and does not have the seabed support). They showed that the conventional AMA generally provided more conservative predictions in comparison to the CASA. With the application of the AMA, the maximum mid-span deflection of the pipe was predicted to be about 6% higher than the one obtained through the CASA. The reason was postulated to be due to the fact that the AMA inherently overlooks the dynamic pressure wave travel, and therefore provides a more conservative predictions.

Moreover, the simple "added mass" term can only be formulated where the velocity potential function around a vibrating structure is mathematically definable [9]. Kramer *et al.* [10] adopted the "added-mass" term, which was originally formulated for analyzing the vibration of a submerged beam, to study the free vibration of submerged composite plates. They showed that the adoption of the AMA instead of CASA could yield inaccurate results in predicting the eigenvalues of the submerged plates with low aspect ratios (length/width). However, the predictions were in good agreements when the plates had larger aspect ratios (close to a beam-type geometry).

Therefore, one needs to gain a better understanding of the influence of such idealization in representing the associated FSI, in the context of VB-SHM of submerged structures.

In addition to the modeling aspects, VB-SHM of submerged structures could be adversely affected by certain combinations of operational variables. Specific to offshore pipelines, variation in the internal pressure (due to a drop and/or an increase in the internal fluid's pressure) or in the external pressure (upon possible changes in the depth of submergence) could variably modify the geometric stiffness of the pipes, thereby affecting their vibration. If deviance in the vibration characteristic is noticeable, it could lead to a false alarm in detecting damage. Therefore, the VB-SHM of submerged structures would be vulnerable in the presence of such operational variability.

Zou *et al* [11] reported negligible variation in the bending eigenvalues of a composite pipe subjected to a variable internal pressure. Ross *et al.* [12], however, observed significant

reductions in the eigenvalues of a submerged prolate dome (made of urethane plastic) when subjected to a variable external pressure.

Moreover, to the best authors' knowledge, the influence of such operational variability on the accuracy of VB-SHM has not been addressed [1-3, 6, 13-15].

The present study aims to investigate the effect of above-mentioned influential parameters on the accuracy of vibration-based damage diagnosis of submerged pipes. Accordingly, the main objectives of the current research can be itemized as follows:

(i) Identification of the more suitable approach (i.e., AMA or CASA) for numerical simulation of submerged structures with particular emphasis on VB-SHM. This is achieved by comparing the efficiency of the "added mass" and "coupled acoustic-structural" approaches in analyzing the vibration response of a submerged steel pipe.

(ii) Providing an insight into the influence of operational variability on the accuracy of VB-SHM of submerged structures. This is addressed by investigating the vibration response of submerged steel and composite pipes that are subject to variable internal and/or external pressures.

4.3 EVALUATION OF THE PERFORMANCE OF "ADDED MASS" AND "COUPLED ACOUSTIC-STRUCTURAL" APPROACHES IN THE CONTEXT OF VB-SHM

In this section, the theories of the AMA and CASA are first reviewed. Then, a submerged API-5L X65 steel pipe is numerically modeled by the two approaches, and its eigenvalues are investigated.

4.3.1 Theory of the Added Mass Approach

Consider a pipe vibrating in a body of water in the direction shown in Figure 4-1. The dynamic response of the pipe can be determined once the applied force acting on its surface is formulated. For this purpose, the pressure distribution around the pipe's circumference should be identified. Euler's equation [16] describes the relationship between the pressure gradient and velocity of the fluid in an unsteady flow (note that the lateral vibration of the pipe causes an unsteady flow around the pipe.). For an incompressible fluid, the Euler equation can be written as follows:

$$\frac{\partial \mathbf{V}}{\partial t} + (\mathbf{V}.\nabla)\mathbf{V} = -\frac{1}{\rho}\nabla p - g\nabla z \qquad 4\text{-}1$$

The above equation can be simplified as [9]:

$$\nabla\left(\frac{\partial \phi}{\partial t} + \frac{1}{2}V^2 + \frac{p}{\rho_f} + gz\right) = 0 \qquad 4\text{-}2$$

The above identity implies that the quantity in the parentheses is not a function of space. Therefore, for an arbitrary location within the fluid domain, one can assume:

$$p_s = -\rho_f \frac{\partial \phi}{\partial t} - \frac{1}{2}\rho_f V^2 - \rho_f gh \qquad 4\text{-}3$$

The above equation, which describes the static pressure as a function of the velocity potential is called the generalized Bernoulli equation.

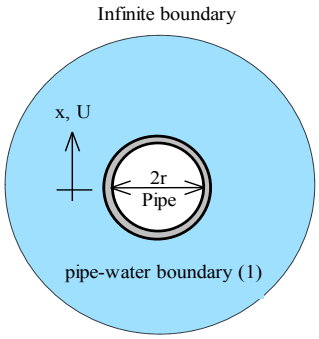

Figure 4-1: A pipe vibrating in a large body of fluid.

Bernoulli's equation is applicable to incompressible fluids and in parts of a flow in which the effect of viscosity is negligible [16]. As can be seen from Equation 4-3, in order to obtain the static pressure, the velocity potential has to be identified. Once that is done, the velocity vector can be subsequently identified by the following identity and its magnitude can be substituted in Equation 4-3 [16]:

$$\mathbf{V} = \nabla\phi \qquad 4\text{-}4$$

It has been shown that the velocity potential for a region around a cylinder vibrating laterally in a reservoir containing stationary fluid can be expressed by [9]:

$$\phi = \frac{U(t) r^2 \left[x - X(t) \right]}{\left[x - X(t) \right]^2 + y^2} \tag{4-5}$$

where x and y are the coordinates of points of interest.

Substituting the time derivative of Equation 4-5 into 4-3, then integrating the pressure term over the circumference of the pipe would yield the net force per unit length as given below:

$$\boldsymbol{F} = -\rho_f \pi r^2 \frac{dU(t)}{dt} \boldsymbol{i} \tag{4-6}$$

where $\boldsymbol{i}$ signifies the direction of the vector (here being along the x axis, shown in Figure 4-1). As can be seen, the force exerted by the fluid is opposing the pipe's motion since it is acting against the pipe's vibration.

It is very important to note that the term $\rho_f gh$ that represents the hydrostatic pressure in Equation 4-3 has no contribution to the net force. The hydrostatic pressure is assumed to be uniform around the pipe's circumference; thus, from the perspective of total net force, the finite forces generated by this term would cancel one another. However, this pressure could shift the eigenvalues of the pipe as will be explained in the following sections.

Assuming the motion of the pipe (cylinder) as a single-degree of freedom system, one can rearrange the equation of motion as:

$$\left(M + \rho_f \pi r^2 \right) \frac{d^2 X(t)}{dt^2} + KX(t) = 0 \tag{4-7}$$

In essence, the surrounding fluid imposes some extra mass to the structure, or equivalently, the cylinder imparts part of its acceleration to the surrounding medium. The term, $\rho_f \pi r^2$ is therefore referred to as the "added mass". Note that no structural damping is considered in Equation 4-7.

4.3.2 COUPLED ACOUSTIC-STRUCTURAL ANALYSIS

Free vibration of a pipe in an acoustic medium can be solved numerically by the standard Galerkin discretization approach applied to the weak form of the fluid equation [17]. The weak form of the dynamics of the acoustic medium can be written as:

$$d\Pi_f = \int_{\Omega_f} dp \left[\frac{1}{c^2}\ddot{p} - \nabla^2 p\right] d\Omega \qquad 4\text{-}8$$

Equation 4-8 expands to the following equation once the appropriate boundary conditions specific to vibration of a pipe in an infinite acoustic medium are applied:

$$\int_{\Omega_f} \left[\delta p \frac{1}{c^2}\ddot{p} - (\nabla \delta p)^T (\nabla p)\right] d\Omega + \int_{\Gamma_1} \delta p \rho_f n^T \ddot{u} d\Gamma + \int_{\Gamma_2} \delta p \frac{1}{c}\dot{p}\Gamma \qquad 4\text{-}9$$

The reader is referred to Zienkiewicz *et al.* [17] for derivation of the boundary conditions at the interface of solid-fluid (the second term), and the radiation boundary representing an infinite acoustic medium (the third term). Similarly, the weak form for the pipe can be established.

To solve the above equations in a discrete domain, the displacement and the nodal acoustic pressure are approximated by:

$$u = \boldsymbol{N_u}\tilde{\boldsymbol{u}}$$
$$p = \boldsymbol{N_p}\tilde{\boldsymbol{p}} \qquad 4\text{-}10$$

The discrete form of the structural and acoustic domains can be represented as follows:

$$\boldsymbol{M}\ddot{\tilde{\boldsymbol{u}}} + \boldsymbol{C}\dot{\tilde{\boldsymbol{u}}} + \boldsymbol{K}\tilde{\boldsymbol{u}} - \boldsymbol{Q}\tilde{\boldsymbol{p}} + \boldsymbol{F} = \boldsymbol{0} \qquad 4\text{-}11$$

and

$$\boldsymbol{S}\ddot{\tilde{\boldsymbol{p}}} + \tilde{\boldsymbol{C}}\dot{\tilde{\boldsymbol{p}}} + \boldsymbol{H}\tilde{\boldsymbol{p}} + \boldsymbol{\rho_f}\boldsymbol{Q^T}\ddot{\tilde{\boldsymbol{u}}} = \boldsymbol{0} \qquad 4\text{-}12$$

where,

$$Q = \int_{\Gamma_t} N_u^T n N_p d\Gamma$$

$$S = \int_{\Omega_f} N_p^T \frac{1}{c^2} N_p d\Omega$$

$$\tilde{C} = \int_{\Gamma_2} N_p^T \frac{1}{c} N_p d\Gamma \qquad \text{4-13}$$

$$H = \int_{\Omega_f} \left(\nabla N_p\right)^T \nabla N_p d\Omega$$

Free vibration of the coupled system could then be represented by the following matrices:

$$\begin{bmatrix} M & 0 \\ \rho_f Q^T & S \end{bmatrix} \begin{bmatrix} \ddot{u} \\ \ddot{p} \end{bmatrix} + \begin{bmatrix} K & -Q \\ 0 & H \end{bmatrix} \begin{bmatrix} \tilde{u} \\ \tilde{p} \end{bmatrix} = 0 \qquad \text{4-14}$$

It should be noted that the force and damping terms present in the original equations (i.e., Equations 4-11 and 4-12) have been ignored in the above equation; the only damping mechanism is therefore due to radiant energy loss. As can be noticed, the above equation is not a standard eigenvalue equation (i.e., the type with symmetric matrices). A simple method proposed by Ohayon [18] could, however, convert it to a standard eigenvalue problem.

4.3.3 NUMERICAL STUDY

This section provides details of the numerical models developed for the study of a submerged pipe's vibration. The models have been developed in the ABAQUS environment, a commercial finite element code [19]. The eigenvalues of the pipe obtained via the two theories described in the preceding sections are compared. An API-5L X65 steel pipe, commonly used for offshore oil and gas transportation, is considered in this study. Pipe's dimensions and mechanical properties are listed in Table 4-1. Figure 4-2 illustrates the cross section of the submerged pipe modeled via the two approaches. The pipe was modeled with C3D20R elements of ABAQUS (i.e., three dimensional 20 nodes reduced integration continuum element with three translational degrees of freedom per node). Fully-restrained boundary condition (clamped) was assigned to both ends of the pipe by restricting the translational degrees of freedom at the corresponding nodes.

A mesh convergence study, conducted on the pipe, tuned the mesh density for an acceptable convergence level with respect to the computed natural frequencies of interest. Accordingly, a total of 1600 elements connected by 2460 nodes constructed the pipe.

Table 4-1: Dimensions and mechanical properties of the pipe.

Mechanical properties of the pipe	
Elastic modulus (GPa)	206
Poisson's ratio	0.3
Density (kg/m^3)	7850
Yield strength (MPa)	450
Pipe's dimensions (mm)	
Length	2000
Outer Diameter (OD)	168.3
Wall thickness	11

As for the first approach, the total added mass was calculated to be 44.36 kg using Equation 4-7. This mass was evenly distributed on the outer surface of the pipe along its length via lumped masses assigned to the corresponding nodes (see Figure 4-2(a)).

Alternatively, the water surrounding the pipe could be modeled by AC3D20 (acoustic three dimensional 20 node element with one degree of freedom per node) of ABAQUS. The density and bulk modulus of the fluid must be defined as the material properties for the acoustic element. The corresponding values for water are taken as 997 kg/m^3, and 2.13 GPa , respectively. In addition, the boundary conditions had to be defined on both the acoustic-structural interfaces and infinite boundaries. Hence, a surface-based "TIE" constraint, defined in the interface region was implemented in the model to simulate the coupling between the pipe and water by correlating the pipe's displacement to the neighboring water elements' pressure degrees of freedom. Moreover, a radiation boundary was attributed to the exterior boundaries of water to approximate the infinite boundaries; this would facilitate the transmission of the acoustic waves across the boundaries with little reflection of energy back into the acoustic domain. The reflection from the boundary

becomes negligible once the boundary is located far enough from a vibrating structure [20]; Figure 4-2(b) elucidates the above-described details.

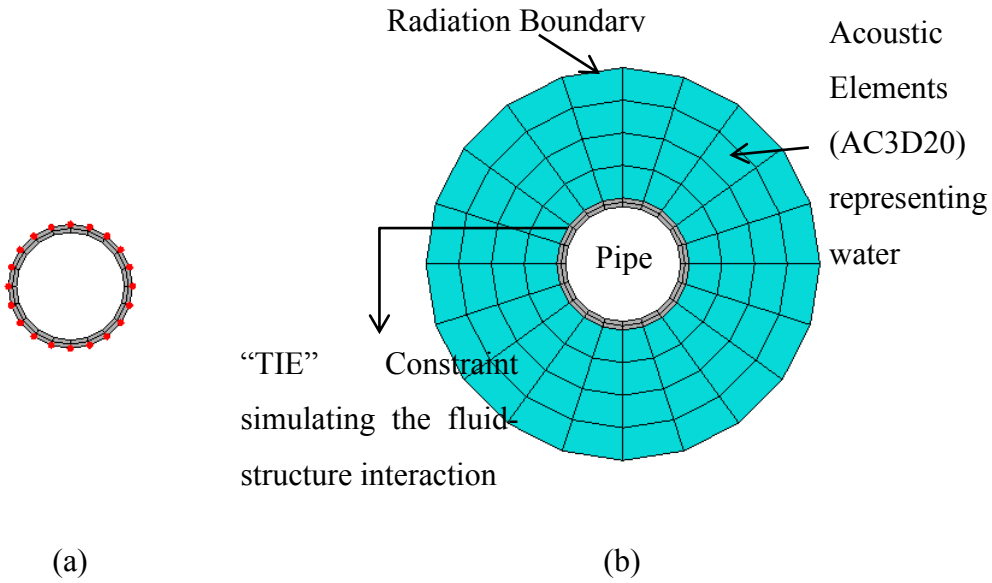

Figure 4-2: The submerged pipe's models (a) the added mass approach and (b) coupled acoustic-structural approach.

It should be noted that the extent of the distance that should be included within the acoustic domain in order for the solution to converge efficiently in various types of problems (i.e., eigenvalue, steady state dynamic or transient analyses) has been a controversial subject. To overcome this dilemma, the eigenvalues of a submerged pipe in a scaled depth of water were carefully investigated in our study. As such, the performances of the two boundaries as shown in Figure 4-3 were assessed and the results are shown in Figure 4-4. As can be seen, the first eigenvalue of the pipe converged to a constant value after a certain depth (distance), regardless of the type of the assigned boundary conditions. It was therefore concluded that there would be an effective water level (EWL) beyond which the reflection from the far-field boundary would become negligible. Accordingly, it was determined that modeling the surrounding water to a certain radius (in this case h/OD=4) would ensure the convergence of the first six eigenvalues, which are the main focus of this research. It should, however, be highlighted that the EWL may vary significantly depending on the intensity of disturbance caused by the nature of the load(s) within a given analysis (i.e., transient, or steady-state dynamic analysis).

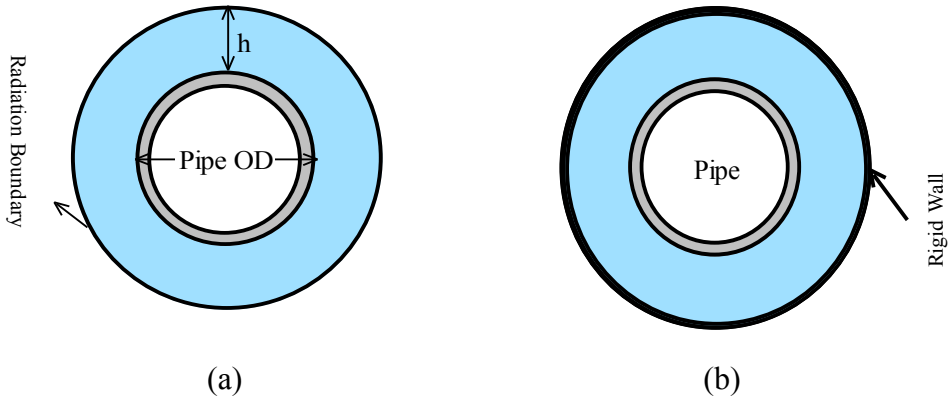

Figure 4-3: A submerged pipe with: (a) - radiation and (b) - rigid wall boundaries.

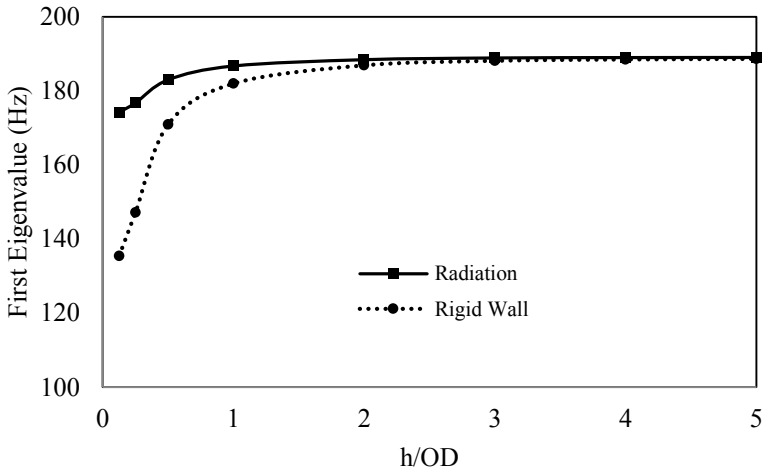

Figure 4-4: Convergence of the first eigenvalue.

4.3.4 Results and discussions

Table 4-2 compares the eigenvalues of the submerged pipe obtained via the two approaches. The results reveal a noticeable difference in estimation of the third eigenvalue (21% difference), while the variation among the other five eigenvalues is limited to approximately 2%.

The third eigenvalue corresponds to the first torsional mode of the pipe. In this mode, the pipe exchanges almost no energy to the surrounding water. Therefore, it is expected for the torsional modes to yield the same eigenvalues as if the pipe was in the air. The CASA could correctly simulate this condition. On the other hand, the AMA failed to accurately predict

the eigenvalues corresponding to the torsional modes. A careful examination of the derivation of the added mass term (presented in section 4.3.1) reveals that the velocity potential has been formulated for a submerged pipe that vibrates in the lateral direction [9]. Hence, the accuracy of this approach is maximized only when the bending modes are considered, and the contribution of the torsional modes is ignored.

Table 4-2: Comparison of the eigenvalues: AMA vs. CASA.

Mode	m	n	Pipe in air	Submerged pipe		% difference between the AMA and CASA
				AMA	CASA	
1	Bending		230.8	187.4	189	0.85
2	Bending		580.7	471.5	478.4	1.45
3	Torsiona		789.9	627.0	789.9	20.60
4	Bending		1033.2	838.5	855.4	1.98
5	1	2	1081.1	889.17	907	1.97
6	2	2	1126.5	926.3	947	2.20

m: number of longitudinal half waves
n: number of circumferential waves [21]
AMA: Added mass approach
CASA: Coupled acoustic-structural approach

Based on the above comparison, the following recommendation is offered for accomplishing successful numerical simulations of submerged pipelines in the context of VB-SHM:

As stated earlier, the AMA has been only formulated in consideration of only the lateral vibration of the pipe. Therefore, frequency-based VB-SHM approaches that only interrogate the bending eigenvalues of submerged pipes can reliably utilize AMA. The accuracy of signal-based (energy-based) VB-SHM approaches could also be adversely affected upon the contribution of the torsional, circumferential, and longitudinal mode shapes in the vibration response of the pipe. For instance, when a submerged pipe is excited by ambient vibration, all the mode shapes of the pipe can contribute to a pipe's vibration. Whereas, in the case of an applied impact force perpendicular to the pipe longitudinal axis, the contribution from the torsional and longitudinal mode shapes become negligible in a pipe's vibration response. Therefore, the use of the CASA is recommended when considering the VB-SHM of offshore pipelines.

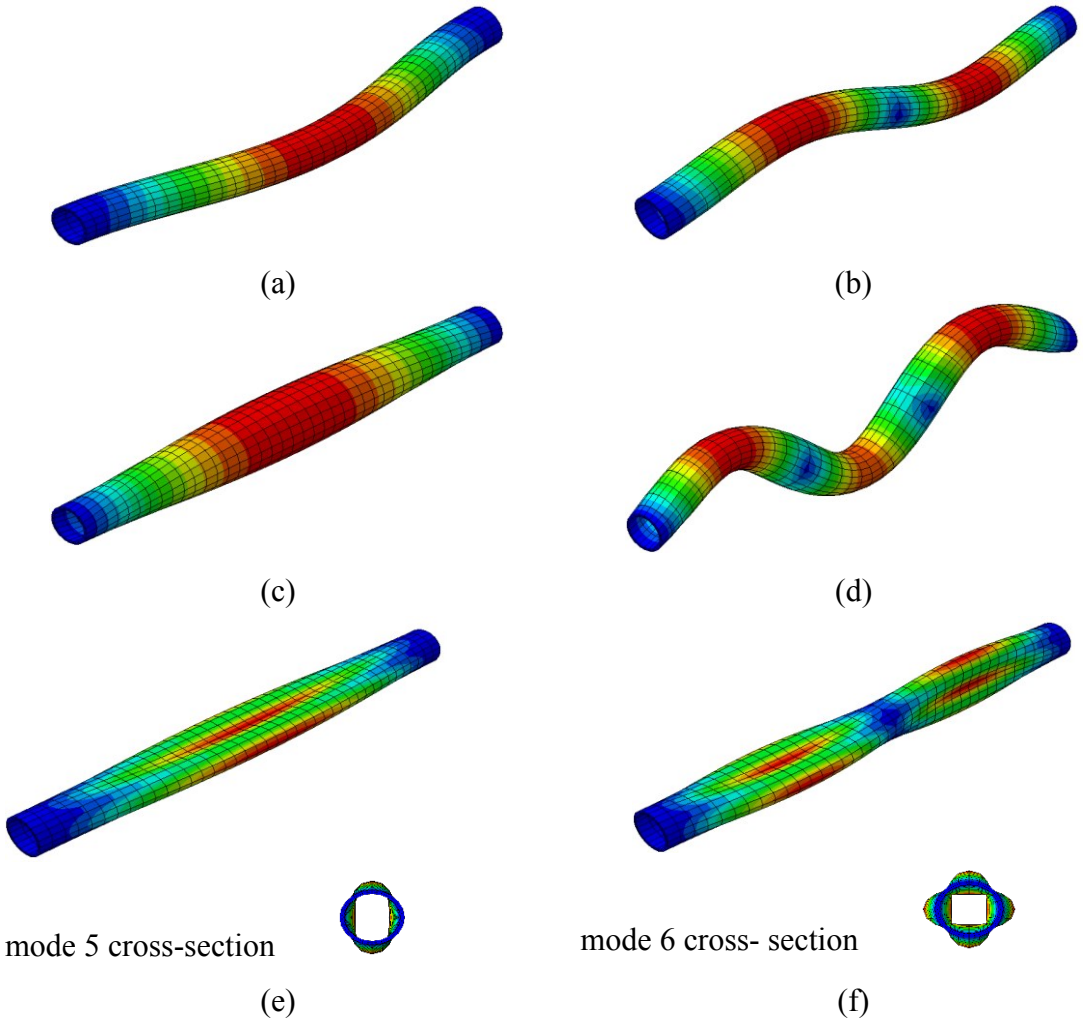

Figure 4-5: The first six eigenmodes of the steel pipe. (a) mode 1 (bending), (b) mode 2 (bending), (c) mode 3 (torsional), (d) mode 4 (bending), (e) mode 5 (m=1, n=2), and (f) mode 6 (m=2, n=2). Note: m: number of longitudinal half waves, and n: number of circumferential waves [21]

4.4 EFFECT OF OPERATIONAL VARIABILITY ON THE ACCURACY OF SUBMERGED STRUCTURES' VB-SHM

In general, any change in the internal or external pressure of a pipe would change its overall stiffness, and consequently changing its vibration response [22]. In this case, the equation for free vibration of a pipe is given by:

$$M\ddot{u} \quad C\dot{u} \quad K_G \quad K \; u = 0 \tag{4-15}$$

The stiffness introduced by the external loads is called the "geometric stiffness", K_G [23].

In the case of a submerged pipeline, the internal fluid's pressure or the external hydrostatic pressure would modify the pipe stiffness, thereby changing the pipe's eigenvalues and its dynamic response.

In VB-SHM techniques, deviations in the eigenvalues or dynamic response of a structure are attributed to the initiation of damage within the structure. Variation in the geometric stiffness (which in turn alters the eigenvalues) of the structure during a VB-SHM trial could cause false alarms. In the case of a submerged pipeline, such variations could be developed by a sudden drop in the internal fluid's pressure or variation in the depth of submergence (which changes the magnitude of the external hydrostatic pressure).

This section investigates the effect of such operational variability on the eigenvalues and dynamic response of submerged steel and composite pipes. For this purpose, eigenvalues of the pipes when subject to various combinations of internal and external pressures are evaluated. The external pressure on the pipes was varied between 0 to 3 MPa to account for the variable hydrostatic pressure experienced by the pipes as the depth of submergence varies between 0 to 300m. The internal pressure was assumed to vary between 3 to 0 MPa to simulate an internal pressure drop of 3MPa.

4.4.1 Effect of operational variability on pipes eigenvalues

The steel pipe described in the previous section was first considered and modeled using CASA. Figure 4-6 shows the variation of the submerged pipe's eigenvalues due to the external and/or internal pressures. As can be seen, variations in the eigenvalues corresponding to bending and torsional modes are negligible. However, the mode shapes with longitudinal and circumferential waves (see Figure 4-5) experienced a maximum of 2% variations in their eigenvalues.

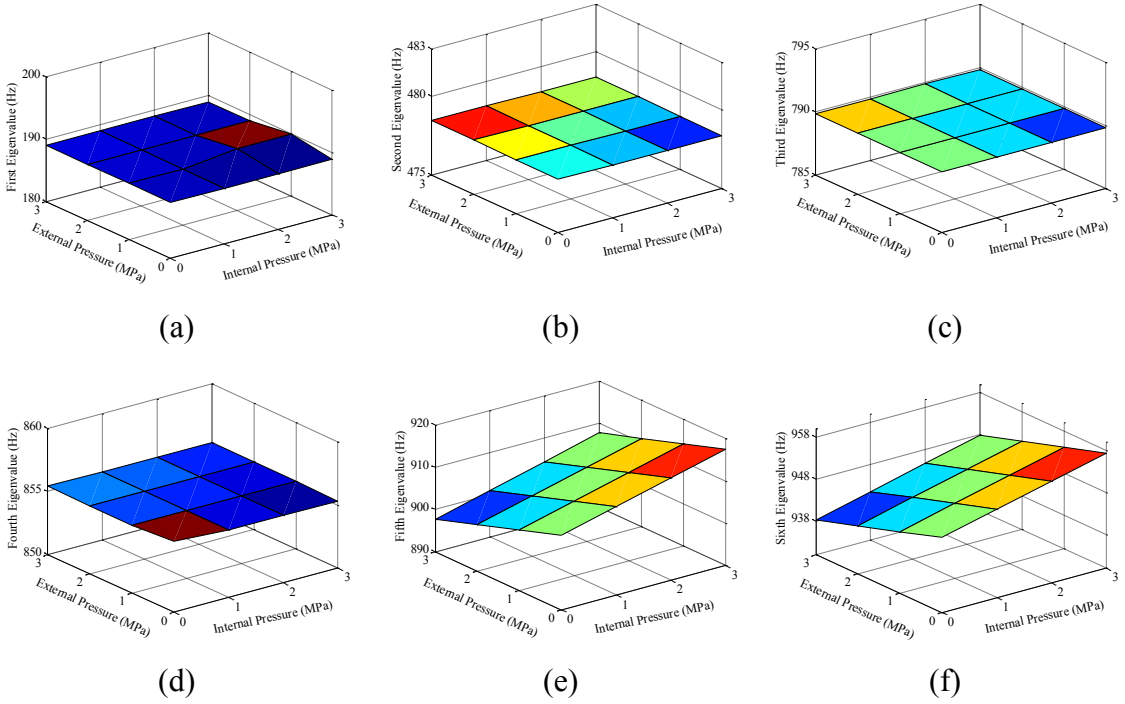

Figure 4-6: Variation in the eigenvalues of the submerged steel pipe due to varying external and/or internal pressures (buckling pressure (P_{cr}) = 392 MPa): (a) mode 1 (bending), (b) mode 2 (bending), (c) mode 3 (torsional), (d) mode 4 (bending), (e) mode 5 (m=1, n=2), and (f) mode 6 (m=2, n=2). Note: m: number of longitudinal half waves, and n: number of circumferential waves [21]

The increase in the external pressure (in the presence of a constant internal pressure) causes a decrease in the eigenvalues of the latter modes, While, the internal pressure acts in an opposite fashion. The reason is postulated to be due to the fact that the latter modes include local deformations; therefore, the geometric stiffness, $\boldsymbol{K}_G$, produced by the internal pressure increases the total stiffness of the pipe, hence providing more resistance against formation of circumferential and longitudinal waves. The external pressure, however, decreases the overall stiffness of the pipe, thereby facilitating the appearance of local deformations. In summary, the geometric stiffness, $\boldsymbol{K}_G$, developed as a result of the applied external and/or internal pressures would more affect the overall stiffness of the latter modes (the fifth and sixth modes).

To further examine the effect of the geometric stiffness on pipes' eigenvalues, two submerged pipes made of FRP composites were also considered. One pipe was made of

carbon-epoxy and the other was an E-glass epoxy pipe. The lay-up configuration, dimensions, and mechanical properties of the composite pipes are tabulated in Table **4-3**. The pipes were modeled with S4R element of ABAQUS (i.e., a 4-node doubly curved thin or thick shell with finite membrane strains and reduced integration, with the hourglass control option). Fully-restrained boundary condition (clamped) was assigned to both ends of the pipe by restraining the translational and rotational degrees of freedom of the corresponding nodes. A mesh convergence study was conducted for the pipes based on evaluating the pipes' natural frequencies with the criterion of yielding an acceptable convergence level of 95% with respect to the theoretical values. Accordingly, a total of 800 elements connected by 820 nodes were used to construct the pipe. The surrounding water domain was constructed by 8000 acoustic elements (AC3D8) connected by 9020 nodes.

Table 4-3: Dimensions and lay-up of the FRP pipes (m).

	Pipe 1	**Pipe 2**
Material	Carbon/epoxy	E-glass/epoxy
Length	2	2
Outer diameter	0.1467	0.1545
Wall thickness	0.0036	0.0075
Lay-up	$[90/\pm45]_{3,s}$	$[90/\pm45]_{5,s}$
Mechanical properties of composite materials		
	Carbon/epoxy	**E-glass/epoxy**
E_{11} (GPa)	138	38.6
E_{22} (GPa)	8.96	8.27
ν_{12}	0.30	0.26
G_{12} (GPa)	7.10	4.14
ρ (kg/m^3)	1600	1800

The pipes' lay-ups were selected such that the pipes could sustain a design pressure of 15 MPa (external/internal) with the same safety factor based on the Hashin damage criterion. Figure 4-7 and Figure 4-8 demonstrate the variations in the FRP pipes' eigenvalues against the internal/and or external pressures. As seen, similar to the results obtained from the previous eigenvalue analysis, the bending and torsional modes' eigenvalues of the FRP pipes experience negligible variations upon applying the net external and internal pressures. The internal pressure generates an effective compressive axial force (see Figure

4-9), which causes a decrease in the lateral stiffness of the pipe, thereby reducing the eigenvalues corresponding to the bending modes [24]. Conversely, the external pressure generates an effective tensile axial force, thereby increasing the eigenvalues corresponding to the bending modes. The other modes' eigenvalues undergo significant variations upon applying the external/and or internal stresses. The trend in variation is also similar to what was observed for the steel pipe. However, the rate of increase/decrease in the eigenvalues is more severe in the case of the FRP pipes. For instance, the third mode (m=1, n=2) of the FRP pipe made of carbon/epoxy experiences 84 % change in its eigenvalues (from 280 to 44 Hz) as the external pressure increases to 3 MPa (assuming an internal pressure of 0 MPa). For the FRP pipe made of E-glass/epoxy, however, the variation in the eigenvalues is less severe. For instance, under the same loading condition, the same mode's (m=1, n=2) eigenvalue undergoes 21% reduction (from 383 Hz to 301 Hz).

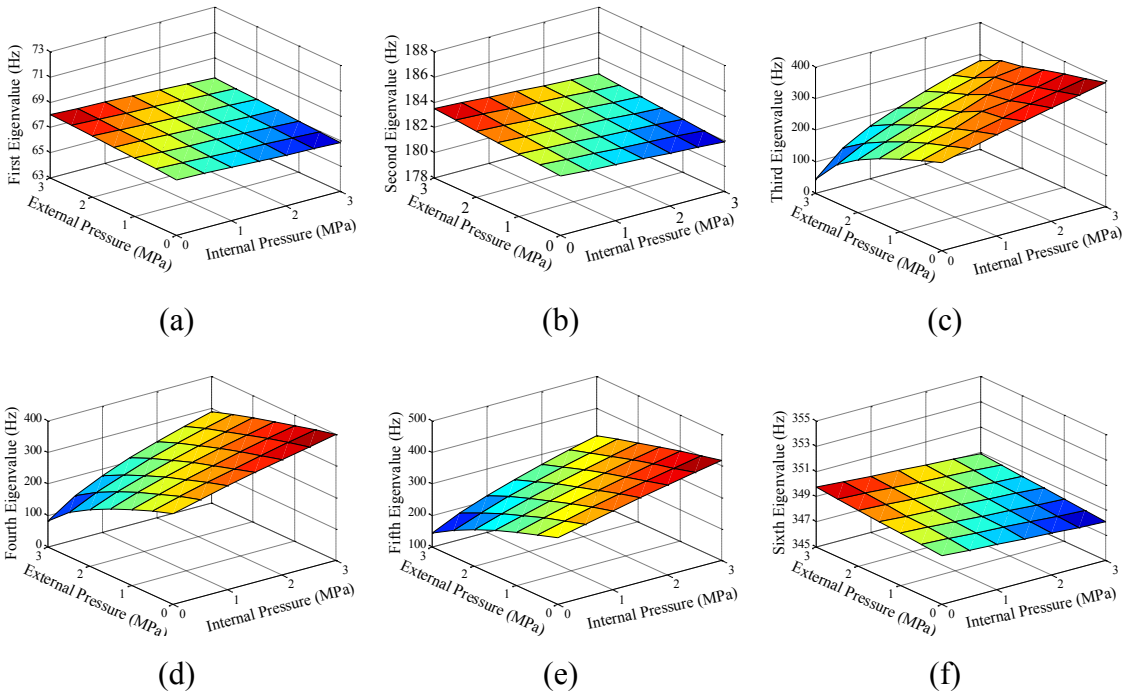

Figure 4-7: Variation in the eigenvalues of the submerged carbon/epoxy pipe varying due to external and/or internal pressures (design pressure = 15 MPa): (a) mode 1 (bending), (b) mode 2 (bending), (c) mode 3 (m=1, n=2), (d) mode 4 (m=2, n=2), (e) mode 5 (m=3, n=2), and (f) mode 6 (bending). Note: m: number of longitudinal half waves, and n: number of circumferential waves [21]

These observations imply that the variation in geometric stiffness produced by the presence of the external loads has variably affected the overall stiffness of the FRP pipes. To elaborate on this observation, the local stiffness (bending rigidity) of the FRP pipes were calculated based on the Classical Laminate Theory (CLT) according to the following equation [25]:

$$EI = b\left(D_{11} - \frac{D_{12}^2}{D_{22}} \right) \qquad 4\text{-}16$$

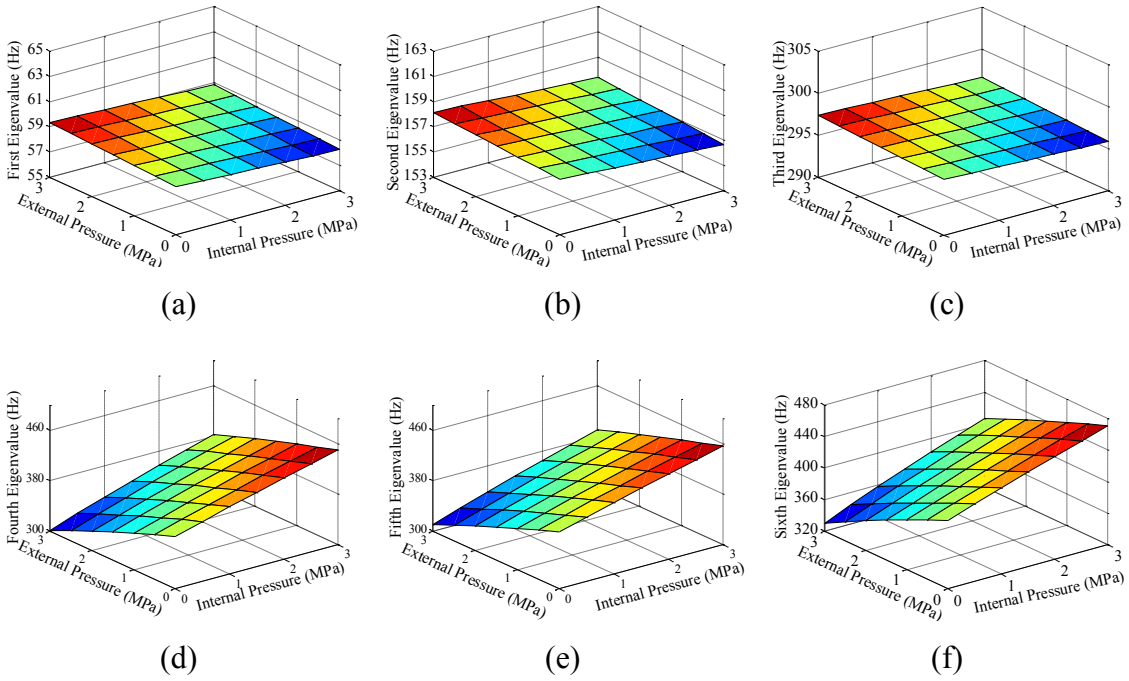

Figure 4-8: Variation in the eigenvalues of the submerged E-glass/epoxy pipe due to varying external and/or internal pressures (design pressure = 15 MPa): (a) mode 1 (bending), (b) mode 2 (bending), (c) mode 3 (bending), (d) mode 4 (m=1, n=2), (e) mode 5 (m=2, n=2), and (f) mode 6 (m=3, n=2). Note: m: number of longitudinal half waves, and n: number of circumferential waves [21]

Table 4-4 compares the local bending rigidity of the two FRP pipes and the steel pipe described in the previous section. The local bending rigidity of the pipe made of E-glass/epoxy (wall thickness of 0.0075 m) is approximately four times that of the carbon/epoxy pipe (with wall thickness of 0.0036), which justifies the rate of reduction in

the investigated modes' eigenvalue (i.e., 21% as opposed to 84% reduction in the eigenvalue of the mode (m=1, n=2), for the E-glass/epoxy and carbon/epoxy pipes, respectively.). On the other hand, the relatively higher stiffness of the steel pipe explains the minor observed variations in the pipe's eigenvalues (i.e., approximately 2% in mode five (m=1, n=2), and six (m=2, n=2)).

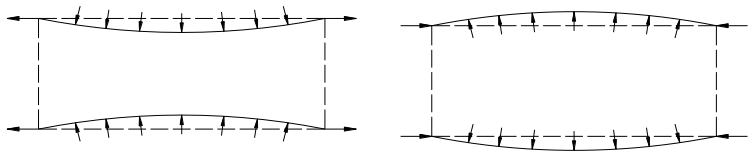

(a) (b)

Figure 4-9: Free body diagram of the pipe with clamped-clamped boundary condition. (a) pipe under external pressure, and (b) pipe under internal pressure .

Table 4-4: Bending rigidity (EI) of the FRP and steel pipes.

	FRP pipes		**Steel pipe**
Bending rigidity ($Pa.m^4$)	Carbon/epoxy	E-glass/epoxy	
	98	427	2318

The findings of this study can be summarized as follows:

- The accuracy of the frequency-based VB-SHM methods could be adversely affected by the presence of operational variability, depending on the stiffness of the pipe and the severity of variability.
- Accordingly, frequency-based VB-SHM of the pipes with high stiffness (e.g., the steel pipe considered in this study) that are subject to operational variability could be successfully accomplished. On the other hand, the VB-SHM of less stiffer pipes (such as the FRP pipes considered in this study), should be conducted with diligence and cautiously, since their eigenvalues are quite sensitive to the operational variation.

4.4.2 Effect of operational variability on the transient dynamic response of pipelines

The transient dynamic responses of pipes would also be affected as a result of a change in their stiffness. For instance, the same carbon/epoxy pipe examined earlier is subjected to an impact load in the form shown in Figure 4-10, under the conditions described in the insert of Figure 4-11. The pipe was impacted at 0.5 m from its left end, and the acceleration time-history (a_y) of a point on the pipe, located at 0.6 m from the left end, was collected (see Figure 4-10). As can be seen in Figure 4-11, the existence of the external pressure (3 MPa) on the pipe tangibly alters the transient response of the pipe, both in terms of the amplitude and energy.

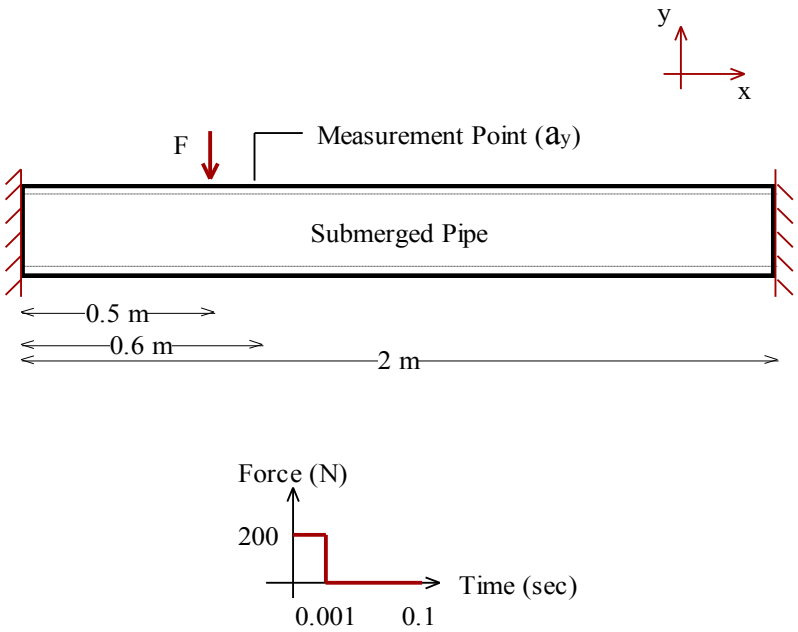

Figure 4-10: Schematic of the submerged pipe and the transient applied load.

Several VB-SHM methods' damage-sensitive features are based on the time-domain vibration response of the system being monitored [2, 6, 13, 14]. As demonstrated earlier, the vibration response of pipelines could be significantly affected as a result of operational variability (i.e., variation in either the internal fluid's pressure or external hydrostatic pressure or both). Neglecting such an influential parameter could significantly affect the accuracy of VB-SHM methods. Therefore, since the SHM of interest to us is a signal-based

as well as a vibration-based approach, it would be instructive to evaluate the degree of sensitivity of the methodology to such operational variability.

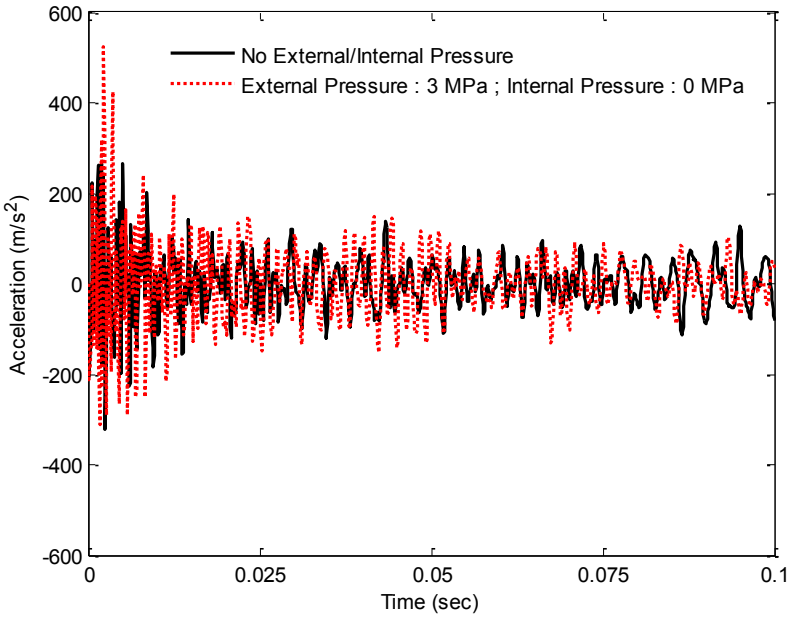

Figure 4-11: Acceleration time history of a selected point on the FRP pipe (made of carbon/epoxy) due to an impact load.

The VB-SHM technique that has been developed in our research group [14, 15], is based on the examination of the energy of the first intrinsic mode function (IMF) of the time-domain vibration response of a given structures. This quantity is used as a damage-sensitive feature, and is mathematically represented by the following equation:

$$E = \int_0^{t_0} (IMF1)^2 \, dt \qquad 4\text{-}17$$

where t_0 is the signal duration. The IMFs of a typical vibration response can be obtained by applying the empirical mode decomposition (EMD), a signal processing technique, applied to the time-domain vibration response of the system. Evaluation of the above term during a structures' service life enables detection of damage within the structures by using the following damage index formulation:

$$EMD\_EDI = \left| \frac{E_{healthy} - E_{Damaged}}{E_{healthy}} \right| \times 100 \qquad 4\text{-}18$$

where $E_{healthy}$ and $E_{damaged}$ correspond to the energy of the first IMF of the vibration response evaluated at the structure's healthy and damaged states. If the calculated index is larger than zero, the presence of damage is indicated. As noted, however, the energy term, E, could be affected by the presence of operational variability explained earlier. The consequence could be false alarms in detection of damage.

To investigate the sensitivity of the EMD_EDI to the operational variability, the time-histories of the vibration responses of the FRP and steel pipes due to an impact load (see Figure 4-10) were considered. The operational variability consisted of changes in the external or internal pressures. Two scenarios were considered, as follows.

(i) Variable internal pressure, $P_{Internal}$ = 0 to 3 MPa, varying at 0.5 MPa increment, while $P_{External} = 0$

At each internal pressure level, the acceleration time-history of the pipe was collected at the location shown in Figure 4-10. Subsequently, the energy term, E, was calculated according to Equation 4-17.

(ii) Variable external pressure, $P_{External}$ = 0 to 3 MPa, varying at 0.5 MPa increment, while $P_{Internal} = 3$

The same procedure as described in the first scenario was followed in this scenario as well.

Figure 4-12 illustrates the variations of the energy in the pipes under the first scenario. Note, that the energies are normalized with respect to the energy of the pipes with no internal pressure (i.e., $P_{Internal}$ = 0 MPa).

The results indicate that the steel pipe's acceleration response remains insensitive to the imposed variation. The FRP pipes' vibration response, on the other hand, show considerable sensitivity to the variation in pressure. The sensitivity is believed to be due to the fact that the steel pipe's stiffness was notably higher than the FRP pipes' stiffness (see Table 4-4). As a result, the contribution of the geometric stiffness ($\boldsymbol{K}_G$) to total stiffness was negligible for the steel pipe.

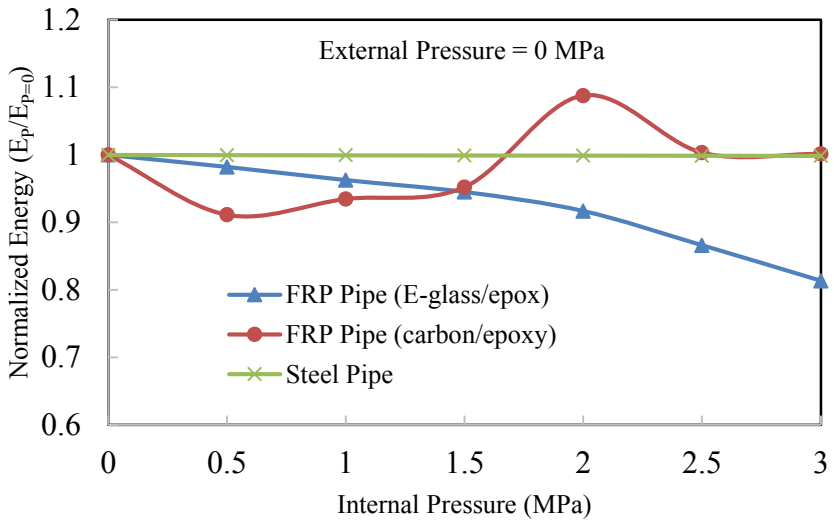

Figure 4-12: Variation in the energy of the acceleration time-history's first IMF against the internal pressure.

Moreover, as seen, the vibration response of the FRP pipe made of E-glass/epoxy (wall thickness of 0.0075 m) shows a constant decrease in its IMF1's energy as the internal pressure is increased. This is because the internal pressure increases the overall stiffness of the pipe, as a result, suppressing the pipe's vibration amplitude. The dynamic response of the FRP pipe made of carbon/epoxy (wall thickness of 0.0036 m), however, showed an erratic behavior. This is because of the noticeable contribution of the geometric stiffness (produced by the internal pressure) to the overall stiffness of the pipe. As can be visually inferred from the results presented in Figure 4-7, the pipe's mode shape sequence was altered as the internal pressure increased to 3 MPa (with the external pressure at 0 MPa); for instance, the eigenvalue of the third mode (m=1, n=1) dropped below the first mode's (bending mode's) eigenvalue. It is believed that the change in the eigenmodes, which occurs due to the gradual increase in the internal pressure of the pipe, in turn changes the contribution of the eigenmodes to the vibration response of the pipe. Therefore, a non-linear trend in the energies of the pipe made of carbon/epoxy can be expected.

Figure 4-13 demonstrates the variations of IMF1's energy as a function of the variation of external pressure (i.e., the second scenario). Similar to the results observed in the previous scenario, the steel pipe's vibration response was proved to be insensitive to the variation in the external pressure. The dynamic response of the FRP pipes, however, showed notable variations to the variation in the loading.

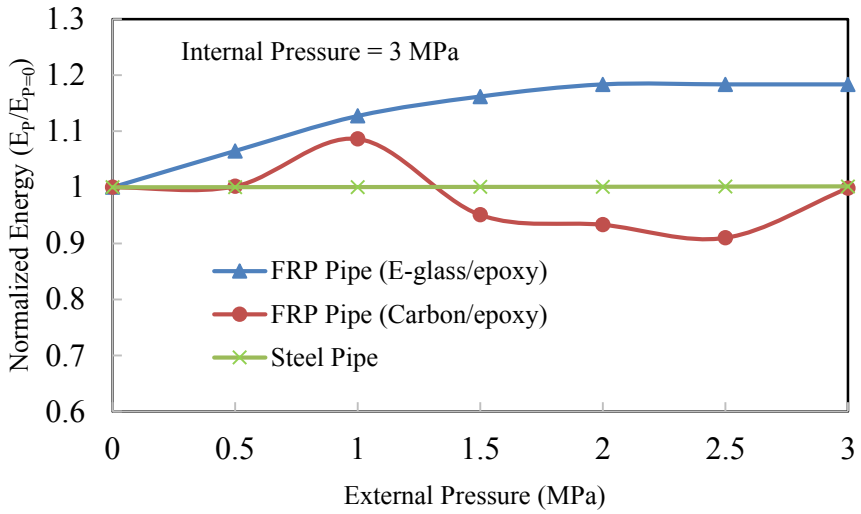

Figure 4-13: Variation in the energy of the acceleration time-history's first IMF against the external pressure.

The results from this part of the study can be summarized as follows:

- The integrity of the energy-based (or signal-based) VB-SHM methodologies, when investigating the health of an offshore pipeline, could be greatly affected depending on the pipe's stiffness and extent of the operational variability experienced during a VB-SHM trial.
- The VB-SHM of submerged stiff pipes (e.g., the steel pipe considered in this study) using the EMD_EDI method can be accomplished with good level of confidence if the pipe experiences a sudden drop in its internal pressure (up to 3MPa according to this study's result), or when the depth of submergence changes within 300 m (i.e., 3 MPa change in the external pressure). The results of EMD_EDI method applied to less stiff pipes (i.e., the FPR composite pipes considered here), indicate that SHM of such pipes would be a challenging task. This is mainly due to the fact that their vibration response could undergo a significant change under imposed operational variability.

4.5 CONCLUDING REMARKS

The performance and accuracy of the two widely-used approaches for modeling the dynamic response of submerged structures (namely, the "added mass" and "coupled acoustic-structural" approaches) in the context of VB-SHM were investigated. The

investigation included the evaluation of the eigenvalues of an offshore pipeline modeled by the two approaches. The differences were limited to below 2% in the lateral modes, whereas for the torsional mode, the differences approached to 20%. The large discrepancy was attributed to the limitation involved in the formulation of the "added mass" approach. It was therefore recommended to adopt the coupled acoustic-structural approach to conduct successful VB-SHM of submerged structures.

Subsequently, the effect of operational variability on the accuracy of a VB-SHM of offshore pipelines was studied. Such operational variability could rise due to the change in the pressure of the fluid the pipe is pressurized with or the change in the external hydrostatic pressure upon submergence of the pipe in various depths. For this purpose, vibration response of steel and FRP composite pipes were examined against incremental variations in the internal and external pressures. It is concluded that:

- The accuracy of VB-SHM could be adversely affected by the presence of operational induced variability, with the level of accuracy depends to the stiffness of the examined offshore pipeline and the extent of the variability.
- Accordingly, it was determined that VB-SHM of the steel pipe considered in this study could be successfully conducted under the examined operational variability. On the other hand, the VB-SHM trial should be conducted with diligence for less stiffer pipes such as the FRP composite pipes considered in this study, as their vibration response showed notable sensitivity to the operational variability.

4.6 ACKNOWLEDGEMENT

This study was financially supported by the Petroleum Research Atlantic Canada (PRAC) and the Natural Sciences and Engineering Council of Canada (NSERC).

4.7 REFERENCES:

1. Peng, X.-L. and H. Hao, *A numerical study of damage detection of underwater pipeline using vibration-based method.* International Journal of Structural Stability and Dynamics, 2012. **12**(03): p. 1250021.
2. Peng, X.-L., H. Hao, and Z.-X. Li, *Application of wavelet packet transform in subsea pipeline bedding condition assessment.* Engineering Structures, 2012. **39**: p. 50-65.

3. Zhu, X., H. Hao, and X. Peng, *Dynamic assessment of underwater pipeline systems using statistical model updating.* International Journal of Structural Stability and Dynamics, 2008. **8**(02): p. 271-297.
4. Chen, J., Z. Su, and L. Cheng, *Identification of corrosion damage in submerged structures using fundamental anti-symmetric Lamb waves.* Smart Materials and Structures, 2010. **19**(1): p. 015004.
5. Na, W.-B. and T. Kundu, *Underwater pipeline inspection using guided waves.* Transactions-American Society of Mechanical Engineers Journal of Pressure Vessel Technology, 2002. **124**(2): p. 196-200.
6. Bao, C., H. Hao, and Z. Li, *Vibration-based structural health monitoring of offshore pipelines: numerical and experimental study.* Structural Control and Health Monitoring, 2012.
7. Rizzo, P., J.-G. Han, and X.-L. Ni, *Structural health monitoring of immersed structures by means of guided ultrasonic waves.* Journal of Intelligent Material Systems and Structures, 2010. **21**(14): p. 1397-1407.
8. Zeinoddini, M., G.A.R. Parke, and S.M. Sadrossadat, *Free-spanning submarine pipeline response to severe ground excitations: water-pipeline interactions.* Journal of Pipeline Systems Engineering and Practice, 2012. **3**(4): p. 135-149.
9. Blevins, R.D., *Flow-Induced Vibration*. 2nd ed. 2001, Malabar: Krieger.
10. Kramer, M.R., Z. Liu, and Y.L. Young, *Free vibration of cantilevered composite plates in air and in water.* Composite Structures, 2013. **95**: p. 254-263.
11. Zou, G., N. Cheraghi, and F. Taheri, *Fluid-induced vibration of composite natural gas pipelines.* International journal of solids and structures, 2005. **42**(3): p. 1253-1268.
12. Ross, C.T.F., et al., *Vibration of a thin-walled prolate dome under external water pressure.* Ocean Engineering, 2007. **34**(3-4): p. 560-575.
13. Bao, C.X., H. Hao, and Z.X. Li, *Vibration-based damage detection of pipeline system by HHT method.* Applied Mechanics and Materials, 2011. **99**: p. 1067-1072.
14. Rezaei, D. and F. Taheri, *Health monitoring of pipeline girth weld using empirical mode decomposition.* Smart Materials and Structures, 2010. **19**(5): p. 055016.
15. Razi, P., R.A. Esmaeel, and F. Taheri, *Improvement of a vibration-based damage detection approach for health monitoring of bolted flange joints in pipelines.* Structural Health Monitoring, 2013. **12**(3): p. 207-224.
16. Cengel, Y.A. and J.M. Cimbala, *Fluid Mechanics: Fundamentals and Applications*. 2006, New York: McGraw-Hill.
17. Zienkiewicz, O.C., R.L. Taylor, and J.Z. Zhu, *The Finite Element Method: Its Basis and Fundamentals*. 6th ed. 2005, Burlington: Butterworth-Heinemann.
18. Ohayon, R., *Symmetric variational formulation of harmonic vibrations problems by coupling primal and dual principles. Application to fluid-structure coupled systems.* La Recherche Aérospatiale, 1979. **3**: p. 207-211.
19. ABAQUS, *Dassault Systemes Americas Corp*. 2012.
20. Corporation, D.S.A. *ABAQUS 2011 Version 6.10 User Manual*. 2011 [cited 2011; Available from: www.abaqus.com.
21. Ustundag, B., *On the Free Vibration Behavior of Cylindrical Shell Structures*, in *Mechanical Engineering*. 2011,

Massachusetts Institute of Tehcnology: Cambridge, MA.

22. Rao, S., S, *Mechancial Vibrations*. 2011, Upper Saddle River: Prentice Hall.
23. Cook, R.D., *Finite Element Modeling for Stress Analysis*. 1998, Canada: Wiley & Sons.
24. *Recommended practice DNV-RP-F105 : free spanning pipelines*. 2009, DNV Det Norske Veritas (DNV): Oslo.
25. Wiesshaar, T.A. and B.L. Foist, *Vibration Tailoring of Advanced Composite Lifting Surfaces.* Aircraft. **22**(2): p. 141-147.

CHAPTER 5 A VIBRATION-BASED STRATEGY FOR HEALTH MONITORING OF OFFSHORE PIPELINES' GIRTH-WELDS

Pejman Razi, and Farid Taheri

Department of Civil and Resource Engineering, Dalhousie University, 1360 Barrington Street, Halifax, NS, B3H 4R2, Canada

Submitted to the journal of Smart Materials and Structures.

5.1 ABSTRACT

This study presents numerical simulations and experimental verifications of a vibration-based damage detection technique. Health monitoring of a submerged pipe's girth-weld against an advancing notch is attempted. Piezoelectric transducers are bonded on the pipe for sensing or actuation purposes. Vibration of the pipe is excited by two means: (i) an impulsive force; (ii) using one of the piezoelectric transducers as an actuator to propagate chirp waves into the pipe. The methodology adopts empirical mode decomposition (EMD), which processes vibration data to establish energy-based damage indices. The results obtained from both the numerical and experimental studies confirm the integrity of the approach in identifying the existence, and progression of the advancing notch. The study also discusses and compares the performance of the two actuation units in damage detection.

Keywords: vibration-based damage detection, empirical mode decomposition (EMD), submerged pipelines, girth-weld, piezoelectric transducers, energy-based damage index.

5.2 INTRODUCTION

Offshore pipelines are susceptible to initiation of various types of defects, including corrosion, induced dents, and cracking/leakage, especially in their mating interfaces (e.g. girth-welds, and bolted joints). Therefore, periodic visual inspections are carried out by skilled divers or remote operating vehicles (ROVs) [1]. Such inspections are usually

followed by more advanced examinations (e.g., automated ultrasonic technique (AUT) and eddy current method), once any suspected areas are detected.

Health monitoring of a large network of offshore pipelines, even at a preliminary stage (i.e., visual inspection), is usually a cumbersome and costly practice. Vibration-based approaches have therefore been developed and been proven to be relatively successful in detecting such damages [1-4]. Therefore, they could potentially reduce the requirement of summoning skilled divers for performing the initial examinations, thus facilitating quicker and more cost-efficient inspection.

To the best knowledge of the authors, there have been very few studies conducted on damage detection of submerged structures; some of the noteworthy ones are briefly mentioned here. Na and Kundu [1] applied the guided wave technique for detection of mechanical defects (e.g., a dent, and removed material) in a scaled submerged pipe. The health monitoring of the scaled pipe was achieved by a transmitter and a receiver, each located on either ends of the pipe. The relatively long range of inspection was noted as the advantage of the method. However, adjustment of the transmitter angle (in a trial and error fashion) was required to achieve a reliable identification of damage in the submerged pipe. Rizzo *et al.* [5] developed a method for health monitoring of a submerged plate hosting a notch and corrosion. A non-contact pulsed laser unit introduced stress waves into the plate. Two immersion non-contact sensors, made of piezoelectric materials, captured the reflected waves. The plate was scanned along its length by a pulse/sensing unit at discrete locations. The continuous wavelet transform (CWT) was used to extract a damage sensitive parameter from the joint time-frequency domain of the sensors' signals. The method could identify the location of damage by producing relatively large damage indices as the sensing probes passed across the defect regions. They marked the inclination angle along with the relative location of their adopted transducers-damage, and the proximity of the sensors as the influential parameters in the damage detection of the submerged plate.

A research team also conducted a series of extensive numerical and experimental studies to identify free-spanning and corrosion along offshore pipelines [6-9]. In their study, damage detection was facilitated mainly via two approaches: (i). observation of a pipeline's eigenvalues, and (ii). processing of the acceleration data gathered along the pipe as the pipe underwent random vibrations. The team could successfully identify the location of damage.

However, there were some inconsistencies in quantifying damage size. Moreover, the free-spanning of pipelines was more reliably detected rather than the corrosion. Also, in some cases, they failed to detect small corrosions; however, free-spanning of pipelines sizing more than 5% of the pipe's length was confidently identified.

Chen *et al.* [10] developed a strategy for health monitoring of a submerged plate against corrosion. They used piezoelectric transducers to generate and receive lamb waves. The received signals were processed within a probability-based diagnostic imaging approach to identify the damage. The numerical and experimental verifications of the method yielded successful results in identifying the damage location.

In the present work, numerical simulations and experimental verifications of a vibration-based damage detection methodology (developed in our research group [11]) for health monitoring of a submerged pipe's girth-weld against a propagating notch are presented. The pipe's response while carrying two different pressurized fluids is examined. The study begins with providing a brief introduction about the adopted vibration-based damage detection strategy. Details of the developed numerical model and the experimental setup are presented in the next sections. That is followed by a discussion on the outcome of the damage detection.

5.3 EMD ENERGY DAMAGE INDEX (EMD_EDI)

Huang *et al.* [12] introduced a robust signal processing technique in 1998, which was referred to as the empirical mode decomposition (EMD). The EMD decomposes a time-signal into its oscillatory components referred to as the intrinsic mode functions (IMFs). The decomposition is accomplished through the so-called "sifting process", which is an empirical and data-driven algorithm [12]. The reader is referred to [13] for a detailed explanation on how the IMFs of a typical signal recorded during a vibration event is extracted. Hilbert transform (HT) is then applied to the IMFs to unveil their time-modulated frequency components. The HT outperforms the wavelet transform (WT), in the sense that it can accommodate non-linear systems. In addition, it is a data-driven signal processing algorithm, thus its performance would not be affected by pre-defined functions typically used in the fast Fourier transform (FFT) or WT.

Thereafter, the EMD has been used in interpreting data in various disciplines [12]. For instance, it has been shown that the first two IMFs extracted from vibration data of a system would be sensitive to presence of damage [13, 14]. On the same basis, Cherghai and Taheri [11] introduced the energy of the IMFs as an efficient and robust damage indicator, defined as follows:

$$E = \int_0^{t_0} \left(IMF \right)^2 dt \tag{5-1}$$

where t_0 is the signal duration. Subsequently, damage indices can be established as follows:

$$EMD\_EDI = \frac{\left| E_{Healthy} - E_{Damaged} \right|}{E_{Healthy}} \tag{5-2}$$

$E_{Healthy}$, and $E_{Damaged}$ are the energy terms calculated from vibration signals of individual sensors gathered at healthy and damaged states of a given structure, respectively. Sensors producing relatively higher damage indices infer the location of damage. Progression of damage can also be quantified by noting the increasing value of damage indices as a function of time. Several experimental case studies accompanied by numerical simulations were conducted to verify the integrity and effectiveness of the proposed methodology [15]. This method, which was developed in our research group, is therefore adopted in the current study.

5.4 FINITE ELEMENT MODELING

5.4.1 Modeling of a submerged pipe equipped with piezoelectric transducers

An aluminum pipe was considered in the current study. The material properties and dimensions of the pipe are listed in Table 5-1. The pipe was modeled with a total of 33,440 solid elements using the ABAQUS's element C3D8R (continuum three dimensional eight-node reduced integration with three translational degrees of freedom per node). Using the same elements, a mid-span girth-weld was modeled in the pipe model (see Figure 5-1). A

bulge with 10 mm width and 2 mm height was used to model the girth-weld over the pipe circumference, taking into account the local stiffening introduced by the weld material. To account for a clamped-clamped boundary conditions, the translational degrees of freedom of the elements located at both ends of the pipe were restrained.

Table 5-1: Dimensions and mechanical properties of the aluminum pipe.

Mechanical properties	
Elastic modulus (GPa)	68.9
Density (kg/m^3)	2700
Poisson's ratio	0.33
Dimensions (m)	
Length	1
Outer diameter	0.06
Wall thickness	0.0052

To monitor the pipe's vibrations, eight piezoelectric sensors were bonded onto the pipe, 5mm away from either sides of the girth-weld as depicted in Figure 5-1. The sensors dimensions were measured to be $(45\times 20\times 0.15)\ mm$. A total of 64 three-dimensional eight-node piezoelectric elements (C3D8E) were used to model each piezoelectric sensors. The "TIE" constraints were used to connect the sensors and the pipe at their interfaces. The sensors were made of piezoceramics (model: PZT-5H) with the following electro-mechanical properties:

$$S_E\left[\frac{m^2}{N}\right]=\left(10^{-12}\right)\begin{bmatrix} 16.5 & -4.78 & -8.45 & 0 & 0 & 0 \\ -4.78 & 16.5 & -8.45 & 0 & 0 & 0 \\ -8.45 & -8.45 & 20.7 & 0 & 0 & 0 \\ 0 & 0 & 0 & 43.5 & 0 & 0 \\ 0 & 0 & 0 & 0 & 43.5 & 0 \\ 0 & 0 & 0 & 0 & 0 & 42.6 \end{bmatrix}$$

$$d\left[\frac{C}{N}\right]=(10^{-12})\begin{bmatrix} 0 & 0 & 0 & 0 & 741 & 0 \\ 0 & 0 & 0 & 741 & 0 & 0 \\ -274 & -274 & 593 & 0 & 0 & 0 \end{bmatrix}$$

$$\varepsilon^S\left[F/m\right]=(10^{-9})\begin{bmatrix} 27.7 & 0 & 0 \\ 0 & 27.7 & 0 \\ 0 & 0 & 30.1 \end{bmatrix}$$

where S_E is the compliance matrix, d is the piezoelectric coupling matrix, and ε^S is the permittivity of the piezoceramic. The density of the piezoceramic was taken as 7500 kg/m^3. Individual piezoelectric transducers could serve as a sensor and an actuator. They could turn into an actuator once a surface charge is defined for one of their surfaces.

ABAQUS's acoustic element, AC3D8 (an eight-node three dimensional acoustic element) was used to model surrounding water and the internal fluid in the computational domain. 1280 and 640 elements constructed the surrounding water and the internal fluid, respectively. Density and bulk modulus of water were taken as 997 kg/m^3, and 2.13 GPa, respectively, and 1.2 kg/m^3 and 101000 Pa for air. "TIE" constraints were defined at the pipe-water and pipe-internal fluid interfaces. The constraints correlated the pipe's surface displacement degrees of freedom to the neighboring fluid elements' pressure degrees of freedom [16].

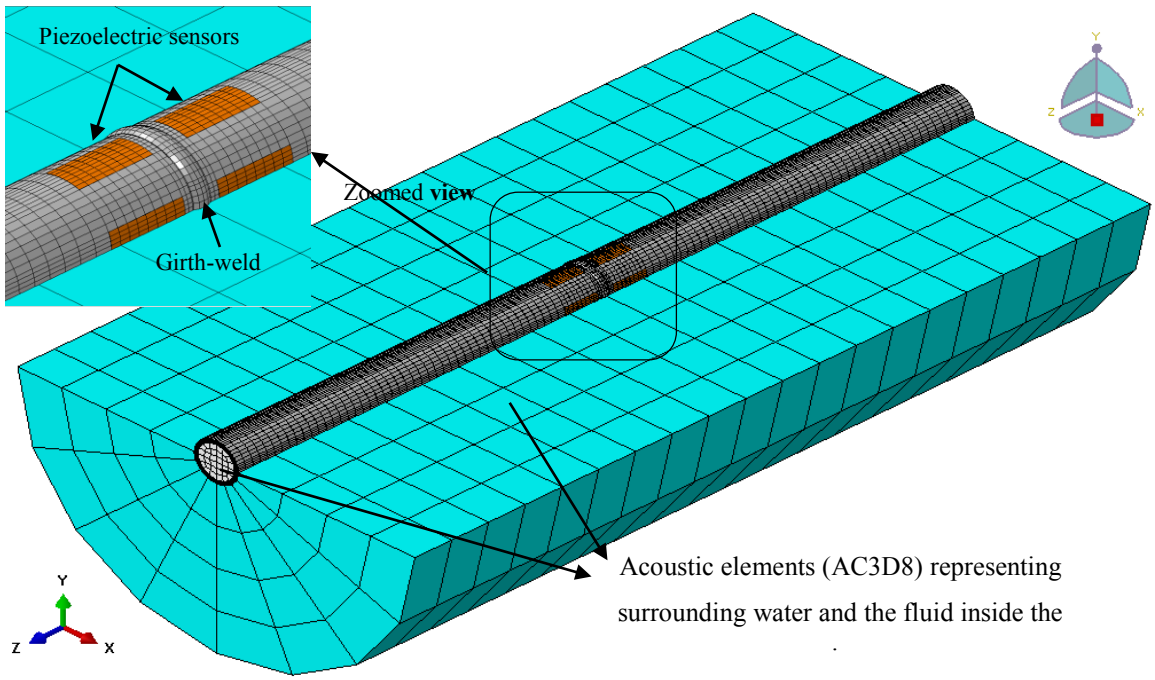

Figure 5-1: Finite element model of the submerged pipe incorporating piezoelectric sensors.

It was pondered whether an effective water level (EWL) could be established in order to avoid modeling of a large medium of water, hence reducing the computational cost without

sacrificing the accuracy. EWL could be limited to a boundary such that the reflected waves from that would not affect the pipe's vibration. The reflection from the boundary would become negligible once the boundary is located far enough from a vibrating structure [16]. To determine an EWL, two different boundary conditions were considered on the exterior boundaries of water; they were (i) radiation and (ii) rigid-wall (see Figure 5-2). The radiation boundary would facilitate transmission of the acoustic waves across the boundaries with little reflection of energy back into the acoustic domain. On the other hand, the acoustic waves reflect back into the acoustic domain after they hit the rigid-wall boundary [16]. Subsequently, the variation of the first-three natural frequencies of the submerged pipe against the step-wise levels of submergence, h/OD, was observed. Here, h is the height of water above the pipe, and OD is the pipe outer diameter.

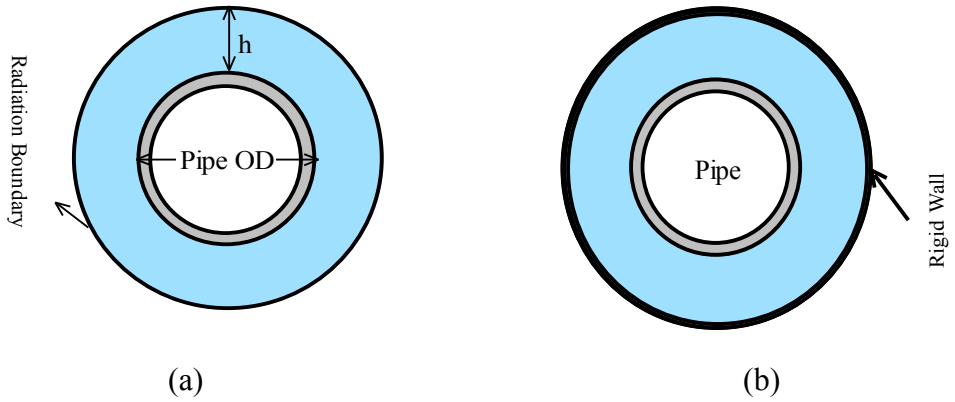

Figure 5-2: A submerged pipe with: (a) radiation and (b) rigid wall boundaries.

From the results shown in Figure 5-3, one could assume the EWL to be four times the outer diameter of the pipe; beyond this level, the boundary-type would not affect the natural frequencies of the pipe. Hereafter, the $EWL = h/OD = 4$ is therefore considered for the rest of the study.

For the accurate representation of the submerged pipe model, a mesh convergence study was conducted. The mesh density was increased to a level such that the variation in the first-three eigenvalues remained below 1%.

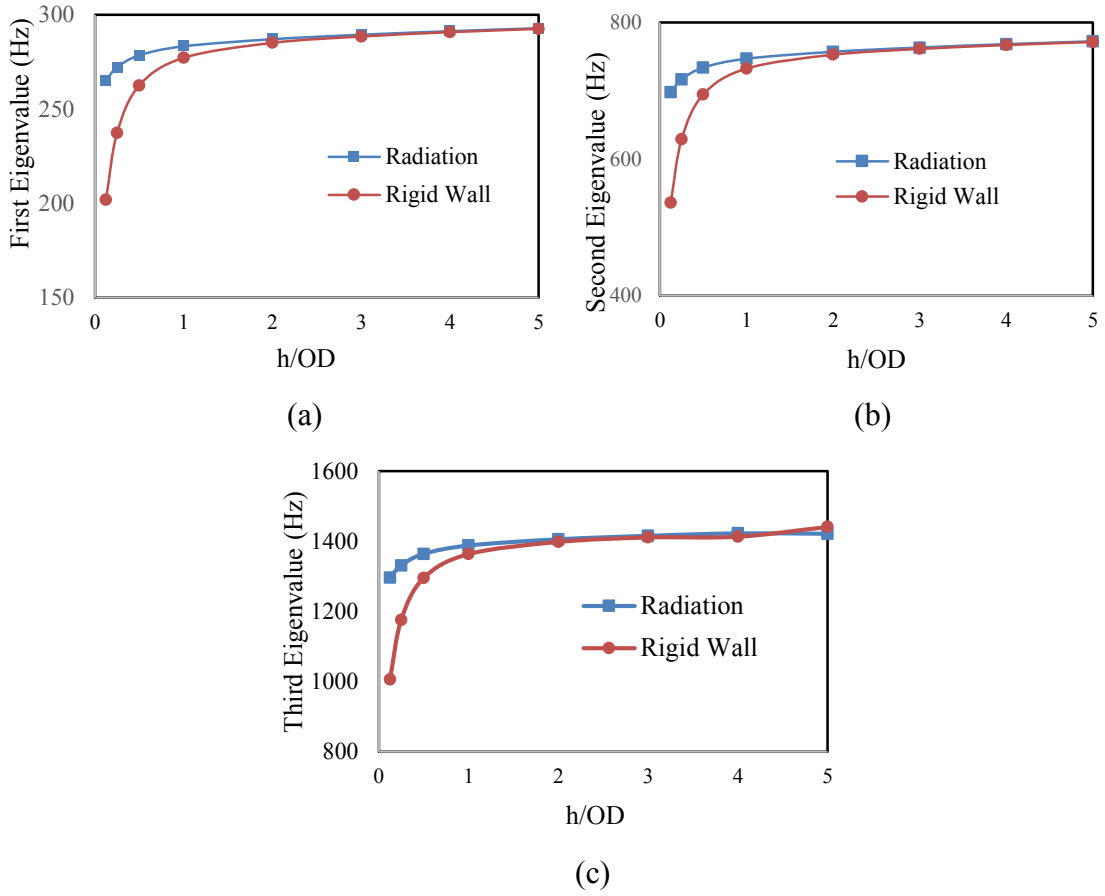

Figure 5-3: Evolution of the pipe's eigenvalues: (a) first eigenvalue, (b) second eigenvalue, (c) third eigenvalue.

5.4.2 Transient analysis

Health monitoring of the submerged pipe was accomplished by conducting transient dynamic analyses solved by the implicit analysis algorithm of ABAQUS. Two excitation approaches were adopted in the damage detection practice. An impulsive force, as produced by a pneumatic hammer in the experiment, was simulated in ABAQUS by defining a force of magnitude 1000N, acting over a short period of time (0.0003 sec). The other alternative was to employ one of the piezoelectric transducer as an actuator, which propagated a chirp signal into the pipe. The adopted chirp, defined as a surface charge in the piezoelectric actuator, contained a frequency range of 10-5kHz, which was linearly varied over 0.05 sec. Schematic representations of the actuation units are elucidated in Figure 5-4.

The analysis was performed with an increment of 0.00002 sec. In other words, the pipe's vibration was sampled at 50 kHz (1/0.00002 sec), so that it could accommodate the highest excitation frequency (i.e., 5 kHz) through the chirp. The pipe's vibration was registered via the piezoelectric sensors' output, which were measured in voltage.

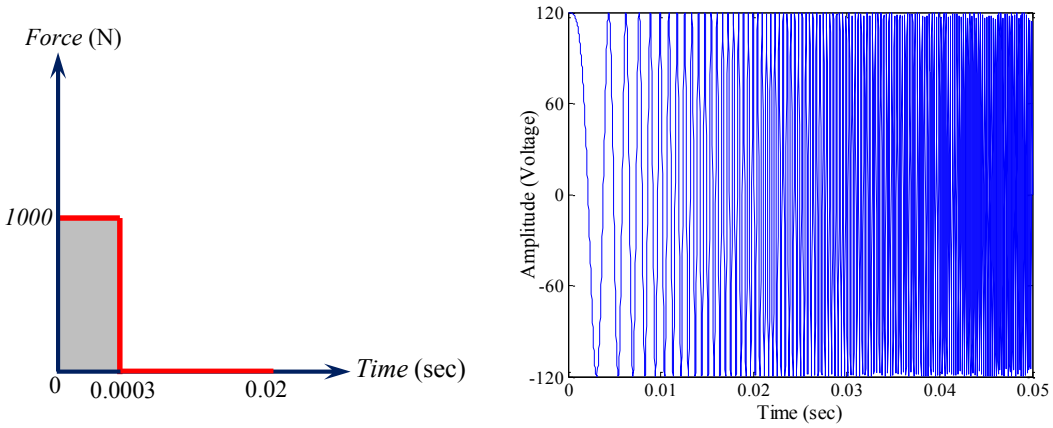

Figure 5-4: Schematic representations of (a) the impact and (b) the chirp excitations.

The analysis run-time was set to 0.02 sec and 0.05 sec for the tests conducted by the impact and the chirp excitation methods, respectively. It should be mentioned that a chirp signal with the same frequency content, but varying over 0.5 sec (similar to the experimental study), was initially considered. However, the result of a time-sensitivity analysis was performed and revealed the insensitivity of the damage detection's outcome to the selected time modulation of the chirp signal. Therefore, the aforementioned chirp was applied over 0.05 sec in order to reduce the computational cost without sacrificing the accuracy.

5.5 EXPERIMENT FRAMEWORK

An aluminum pipe with the same material properties and dimensions listed in Table 5-1 was considered for the experimental segment of the work. The tests were conducted in a $2.45 \times 1.12 \times 0.78$ m^3 laboratory tank. The pipe was clamped at both ends as shown in Figure 5-5. A pressure gauge, mounted on the pipe's cap, was used to monitor the internal fluid pressure.

Eight flexible piezoelectric actuator/sensors (model: pa16n, available through Mide Technology Corporation, Medford, Massachusetts) were bonded onto the pipe in either

sides of the girth-weld as shown in Figure 5-5(b). The transducers were enclosed by waterproof coating. However, the electrical connections were sealed manually by applying a generous amount of silicon, and then securing individual connections by heat shrinks.

A waterproofed pneumatic hammer was designed and fabricated in-house to generate the required impulsive forces. Figure 5-6 shows the symbolic design of the pneumatic hammer. An air regulator assured the flow of air with a constant pressure, thus it secured the consistency of the impacts. A flow control tuned the intensity of the impacts. Back and forth strikes of the piston was controlled by a solenoid valve through an electrical switch. The cylinder and piston assembly was waterproofed by incorporating a plexiglass box. An O-ring sealed the box/piston gap. A close-up of the fabricated hammer is shown in Figure 5-5(b).

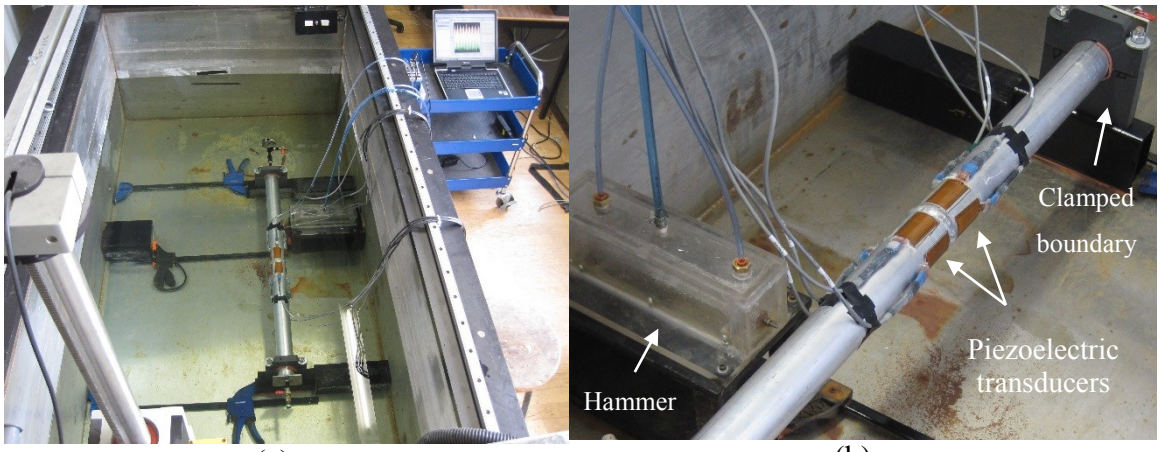

(a) (b)

Figure 5-5: (a) Experiment setup, and (b) close-up of the sensors' arrangement and the pneumatic hammer

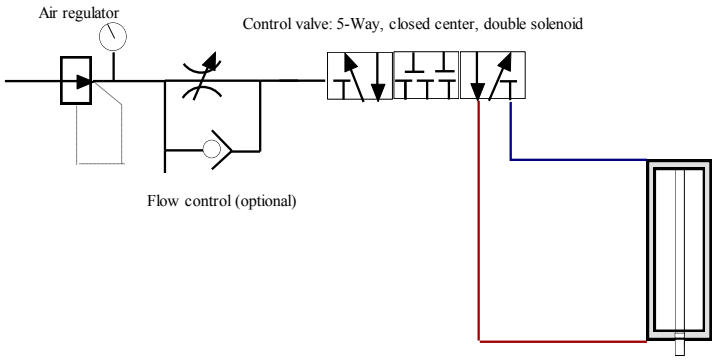

Figure 5-6: Schematic design of the pneumatic hammer.

The second actuation unit adopted one of the piezoelectric transducers as an actuator, thus propagating chirp waves in the pipe. A signal generator (model 33210A, available from Agilent Technologies, Santa Clara, California) was used to generate the chirp signals. The signals were then amplified via a power amplifier (model: 790 series available from PCB Piezotronics, Inc., Depew, New York) before being injected to the piezoelectric actuator. The chirp signals contained frequency range of 10 to 5 kHz which varied linearly over 0.5 sec.

The piezoelectric-based actuation unit provides the following main advantages over the impulsive excitation typically generated by impact hammers:

i. It easily secures the consistency of excitation, thus repeatability of the measurements is improved. On the other hand, the application of an impulsive hammer is vulnerable to severe inconsistencies due to several factors, including small deviations in the impact location, and magnitude of the generated force.
ii. It allows exploitation of a wide range of frequencies, and selection of various types of excitation signals (i.e., chirp, burst, and random)

Vibration signals gathered through the sensors were digitized by a data acquisition system (NI-9215 in a compact chassis manufactured by National Instrument Inc., Austin, Texas). The sampling rate was set to 50 kHz.

5.6 DAMAGE SCENARIOS

Health monitoring of the pipe's girth-weld was attempted by the proposed damage detection algorithm explained in section 6.3. A notch of 1mm depth (19% of the wall thickness) was introduced adjacent to the girth-weld and propagated to a depth of 4mm (77% of the wall thickness) by a step of 1mm. In the numerical model, a canoe-shape notch was made by an extrude-cut along the pipe with a width of 0.5mm. In the experiments, the notches were cut by a jeweler saw. Two different conditions were considered for the internal surface stress in the pipe: (i) the pipe pressurized with air (P=1 MPa) and, (ii) with water (P=5 MPa).

Figure 5-7 depicts the notch locations and the arrangements of sensor/actuators in the four damage scenarios considered in this study. The tests' framework enabled comparison of the two actuation units' performances.

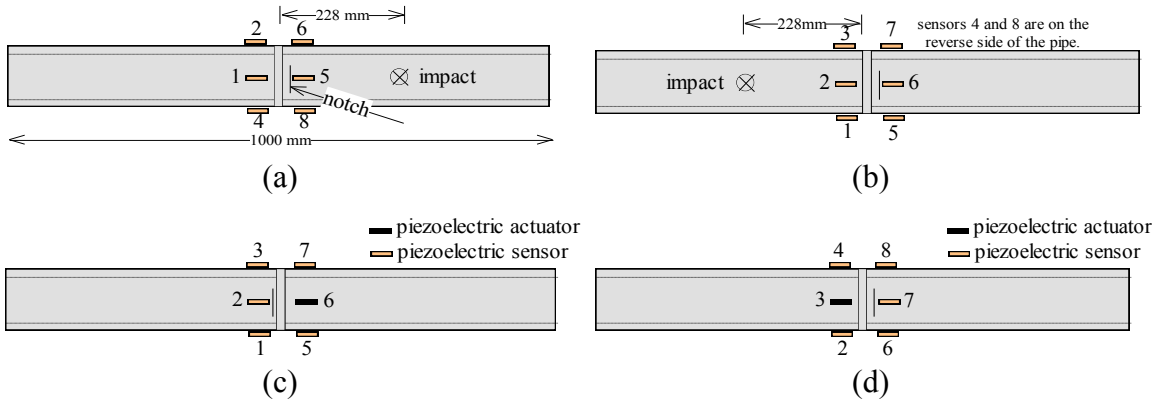

Figure 5-7: Schematic view of damage scenarios. The pipe was pressurized by air ((a) and (c)) and by water ((b) and (d)). Note: drawing not to scale.

5.7 RESULTS AND DISCUSSIONS

An experimental study was conducted in our laboratory tank to verify the integrity of the developed numerical model before beginning the damage detection process. For that, the experimentally measured eigenvalues of a submerged pipe were compared against those obtained from the numerical model. The aluminum pipe was hung in the tank by soft elastic ropes emulating a free-free boundary condition. One of the piezoelectric transducers was used to propagate the chirp signal along the pipe. The pipe's vibration was recorded by one of the piezoelectric sensors, whose output was a voltage-signal. The experiment was simulated by the numerical model described earlier. The eigenvalues of the submerged pipe were determined by applying an FFT to the pipe's forced vibration signals obtained from the experimental study and the numerical model.

The first-three eigenvalues of the submerged pipe, obtained via the two approaches, were compared as tabulated in Table 5-2. The reasonable agreement between the experimental and numerical measurements corroborated the integrity of the developed numerical model. Having established the integrity of the numerical model, a transient analysis as explained earlier was executed for the pipe at its healthy and damaged states for each damage scenarios shown in Figure 5-7.

Table 5-2: Eigenvalues of the submerged pipe.

Eigenvalues	Experiment	Numerical model	Difference (%)
$f_{1(Hz)}$	200.0	198.5	0.7
$f_{2(Hz)}$	542.8	533.0	1.8
$f_{3(Hz)}$	1030.6	1002.5	2.7

The vibration signals were then recorded through the sensors. An in-house developed MATLAB-code implemented the adopted damage detection algorithm (EMD_EDI) on the vibration data by performing the following tasks:

(i) Filtering the signals (the code applied low-pass filters of [0-1000] Hz and [0-5000] Hz to the signals obtained from the impact and chirp tests, respectively.)

(ii) Extracting the IMFs of vibration signals through EMD (see Figure 5-8)

(iii) Calculating the first IMF's energy (Equation 5-1)

(iv) Establishment of the damage indices (Equation 5-2)

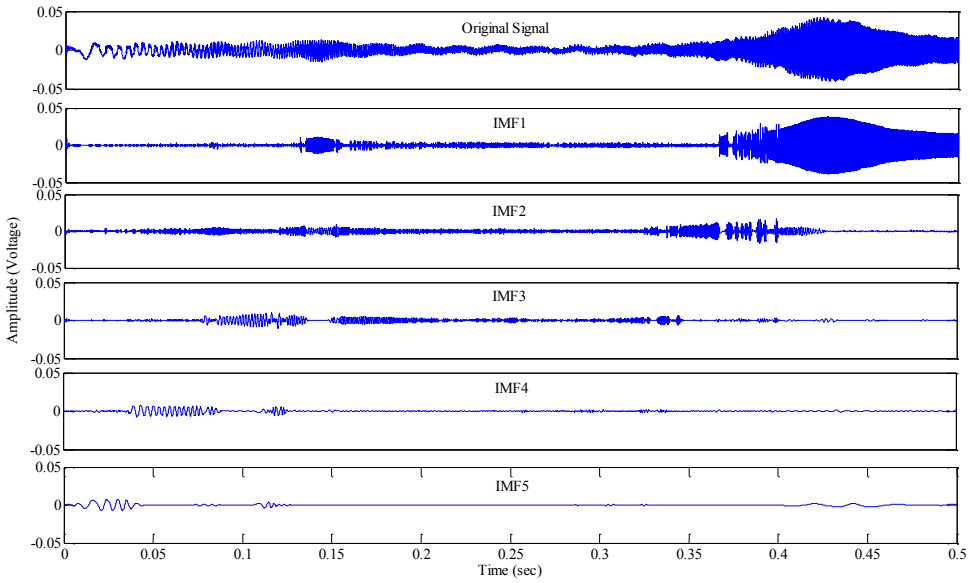

Figure 5-8: One of the sensor's vibration response to the chirp (original signal) and its first five IMFs obtained through EMD.

The charts shown in Figure 5-9 illustrate the results of the damage detection conducted via the numerical model. Figure 5-9(a) and (b) present the first two damage detection trial results, in which the impulsive force was employed as the actuator (Figure 5-7(a) and (b)). Figure 5-9(c) and (d), on the other hand, present the EMD_EDIs for the cases that the chirping method served the actuation unit (Figure 5-7(c) and (d)). The results are compared with those obtained in the experimental part of the study (see Figure 5-10).

The results obtained from both the numerical and experimental studies indicated that at least half of the sensors could detect the existence and progression of damage. The advancement of the notch could be noticed as the method yielded higher damage indices as the notch depth increased. The only exception would be the case shown in Figure 5-10(b). In that case, the existence of the notch was identified with notably large indices, while its progression was underestimated at its final depth. The rest of the sensors also discerned the existence of damage, however, they occasionally failed to predict its advancement.

It can be inferred from the results that the relative location of the sensor and actuators with respect to the notch is responsible for the variability seen in the results. Those sensors receiving their vibration waves passing through the notch outperformed the rest of the sensors in terms of damage detection accuracy. This statement can be further explained by referring to Figure 5-9(b), which presents the results of damage detection for the damage scenario considered in Figure 5-7(b). The figure shows that the sensors 5 to 8 were able to track the damage advancement, while the sensors 1 and 3 failed to do so. In Figure 5-9(a), the sensors 1-4, which satisfy the stated condition, produced noticeably higher damage indices, as well as providing a more clear indication of damage progression.

The behavior was more vividly seen in the experimental results. For instance, one can consider as shown in Figure 5-10(c), the outcome of the damage detection for the damage scenario considered in Figure 5-7(c). In this case, not only did the sensors receiving the waves that had passed through the notch (sensors 1-4) produce noticeably larger indices, but could also track the advancement of the notch more accurately.

It is therefore postulated that the diagnostic capability of half of the sensors are affected by the reflection of the waves from the notch. More parametric studies on pipes with larger diameters could shed more light on the observed behavior and the noted postulation.

The diagnostic capability of the method in damage localization was also investigated. As can be seen from the results of the numerical simulations, the closest sensor to the damage produced the highest damage index, hence an accurate damage localization could also be produced by this method. The exception only applied to the first damage scenario (see Figure 5-9(a)).

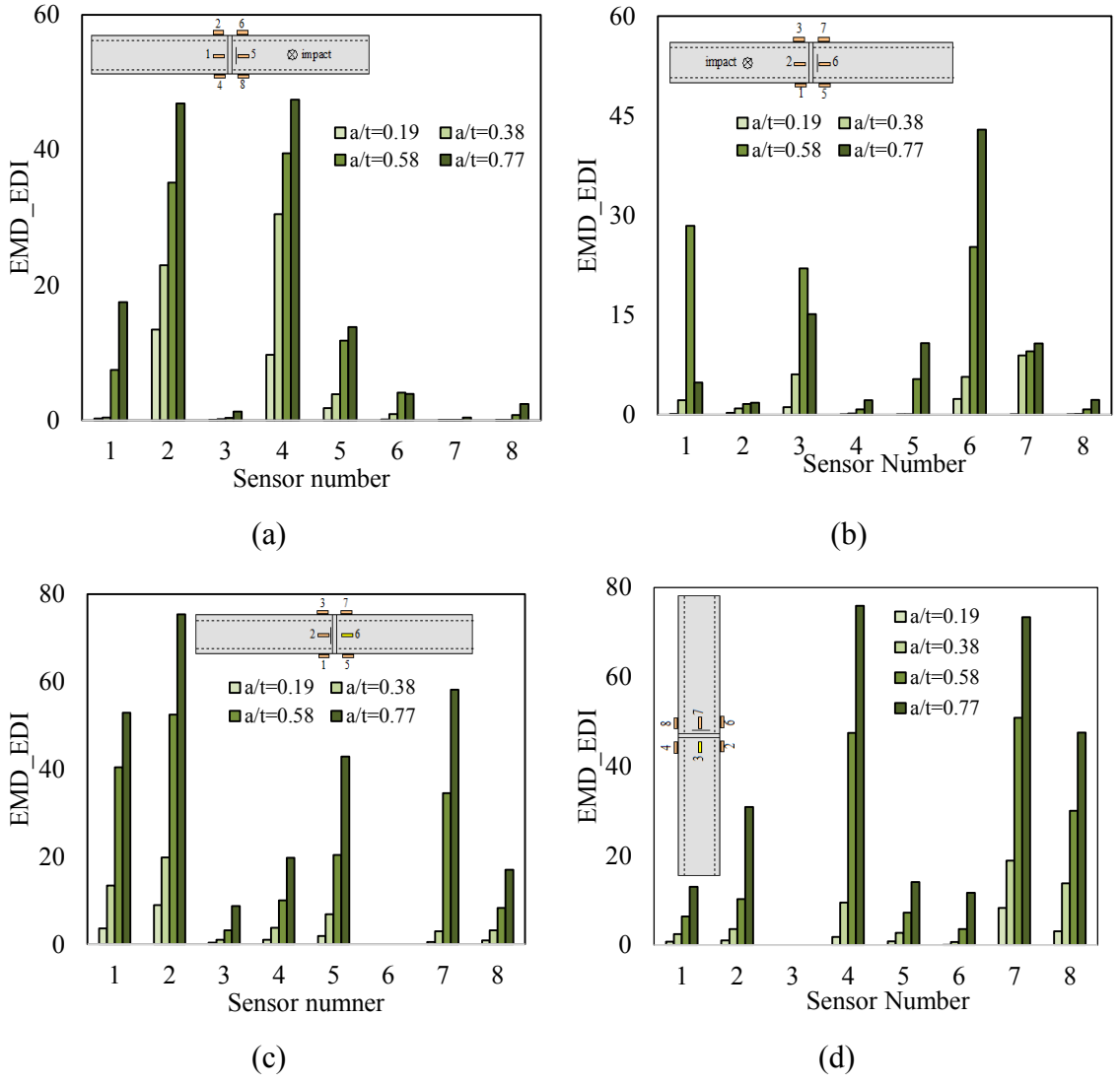

Figure 5-9: Damage indices obtained from the numerical study on the corresponding damage scenarios shown in Figure 5-7. Note that a/t is the ratio of notch's depth to pipe's wall thickness.

In that case, the closest sensor to the damage (i.e., sensor 5) was located in-between the source of excitation and the notch, thus a low diagnostic capability was already anticipated based on the observations explained in the previous paragraph. Nonetheless, the notch's

approximate location (being on the right-hand side of the girth-weld) was confidently identified by the opposite side's sensors, which produced the largest indices, thereby highlighting the fact that the propagated wave has passed the notch.

In comparison, the experimental investigations, however, provided somewhat controversial results in terms of damage localization. The results presented in Figure 5-10(c) show that the sensor 2 (the closest sensor to the damage) yielded the largest indices, hence identifying the exact location of the notch on the pipe's circumference. For the rest of the damage scenarios, only the approximate location of the notch (be it on the left or right-hand side of the girth-weld) could be discerned.

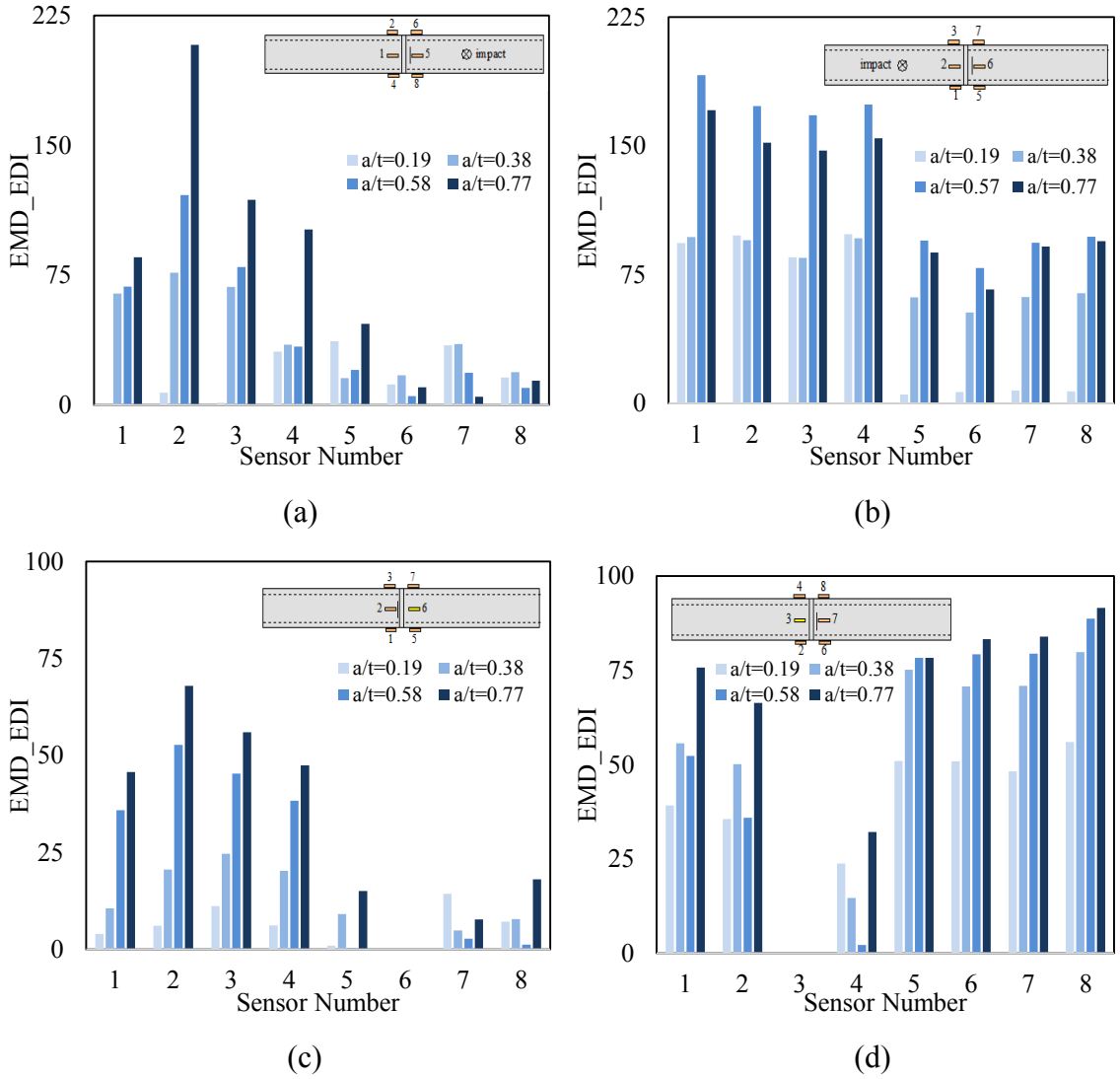

Figure 5-10: Damage indices obtained from the experimental study on the corresponding damage scenarios shown in Figure 5-7. Note that a/t is the ratio of notch's depth to pipe's wall thickness.

It is postulated that the inevitable uncertainties involved in the experiments (e.g., the variable pipe/sensors bond-strength, and the minute inequalities in sensors/girth-weld distances, which occurred unintentionally during the process of bonding the sensors to the pipe) could have affected the damage localization accuracy.

Taking the above observations into account, it could be suggested that a minimum of one piezoelectric bonded on each sides of the girth-weld is required for accurate health monitoring of such damage conditions. A more effective health monitoring, however, could be achieved by conducting two separate trials using either of the excitation techniques. In the case of generating vibration excitation by means of an impulsive force, the two tests would consist of impacting the pipe at both sides of the girth-weld, and recording the associated vibration of each impact. In the case of chirping, the piezoelectrics can alternate their tasks in the form of a sensor and actuator, respectively. Upon completion of the two tests, the location (be on the left or on right-hand side of the girth-weld) and severity of damage could be more effectively discerned by noting the highest damage indices obtained from the two trials. The conclusion also holds true for the numerical model, so long as the chirp excitation method is used as the actuation unit. Otherwise, at least four sensors (two on each side of the girth-weld) are required for a successful damage identification, since it was observed that some of the sensors failed to notice the existence of damage (see Figure 5-9(a) and (b)).

In all, both the numerical and experimental studies provided satisfactory results on identification of an advancing notch, regardless of the type of fluid the pipe carried. It can therefore be concluded that the additional damping introduced by the presence of water inside the pipe would not weaken the method's diagnostic capability.

The chirp excitation method proved to outperform the commonly-used impulsive force excitation technique, in terms of both damage localization and prediction of its advancement. The experimental studies warned the onset and advancement of damage with larger damage indices compared to the indices obtained through the numerical simulations, as seen from the results presented in Figure 5-10(a) and (b). The reason could be due to the actual magnitudes of the applied force in the two studies. It should be noted that there

was no direct means to measure the magnitude of the force in the experiment. Therefore, an approximate amplitude (based on our previously conducted trials with a modal hammer) was selected for the impulsive force used in the numerical study.

5.8 REMARKS ON THE OPERATIONAL/ENVIRONMENTAL CONDITIONS

In the experimental investigation, the repeatability of the measurements (in terms of comparing the energy terms) for ten trials was calculated to be 92% and 98% when the pneumatic hammer, and piezoelectric actuator were adopted, respectively. The deviations in the measurements were believed to be due instrumentation noise and inevitable minor inconsistencies produced during hammer impacts.

It was also of interest to examine the simultaneous effects of noise and disturbance on the boundary condition (which could happen in real applications) on the repeatability of the measurements. For that purpose, the clamping torque of the bolts securing the collar on one of the pipe's ends (see Figure 5-5) was reduced from (40 to 20) N.m in increments of 5 N.m. The precise reduction of clamping force on the bolted assembly was facilitated via a digital torque meter. At these individual torque levels, a chirp-type wave was propagated via the piezoelectric 5, and the vibration was recorded by the first four sensors (sensor 1-4). The energy of each sensor's vibration signal at the specified clamping force was calculated according to Equation 5-1, and was subsequently normalized with respect to its energy at the maximum torque level (i.e., 40 N.m).

Figure 5-11 reports the average of ten measurements at specified torque levels. As can be seen, the maximum variation in the calculated energies is only 6%. Implicitly therefore, in a damage detection trial, damage indices above 6 % would indicate the existence of a damage. Damage indices below this threshold could not be confidently attributed to the presence of damage, as the disturbance to the boundary could result in a damage index of 6 %. Owing to the damping of the propagated waves, it is anticipated that those variations would be smaller for cases where the supports are located farther from the inspection zone.

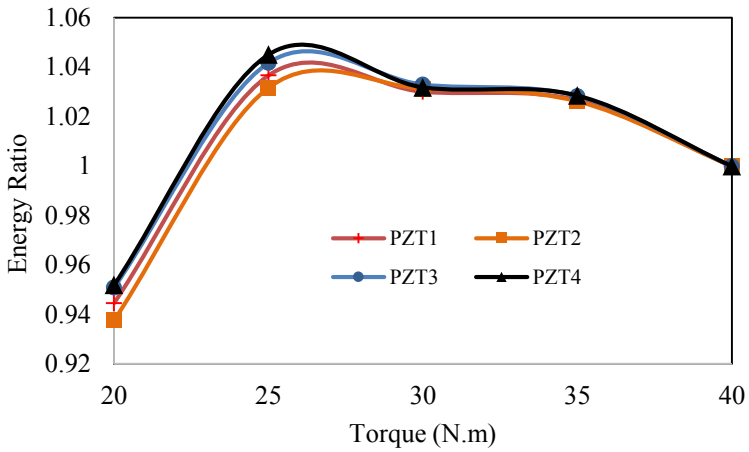

Figure 5-11: the normalized energy as a function of the clamp torque level.

5.9 CONCLUSIONS

Numerical simulations and experimental verifications of a vibration-based damage detection strategy for health monitoring of submerged pipelines' girth-welds was presented. The simulations incorporated piezoelectric transduces serving as sensors and actuators. The methodology applied the empirical mode decomposition (EMD) onto the recorded vibration signals to establish the energy-based damage indices (EMD_EDIs). The effectiveness of the technique was evaluated by detection of an advancing notch in a girth-weld of an aluminum pipe. The results of the numerical study were compared by those obtained from the experimental examinations investigations. Reasonable agreement in terms of damage detection was found between the two studies. Examination of the damage indices revealed encouraging results on detection, localization, and sizing the damage. The method was capable of identifying the damage, regardless of the type of fluid by which the pipe was pressurized with. It was concluded that health monitoring of the submerged pipe's girth-weld could be efficiently accomplished with a minimum of one sensors/actuators bonded on each side of the girth-weld.

5.10 REFERENCES

1. Na, W.-B. and T. Kundu, *Underwater pipeline inspection using guided waves.* Transactions-American Society of Mechanical Engineers Journal of Pressure Vessel Technology, 2002. **124**(2): p. 196-200.

2. Rezaei, D. and F. Taheri, *Experimental validation of a novel structural damage detection method based on empirical mode decomposition.* Smart Materials and Structures, 2009. **18**(4): p. 045004.
3. Rezaei, D. and F. Taheri, *Health monitoring of pipeline girth weld using empirical mode decomposition.* Smart Materials and Structures, 2010. **19**(5): p. 055016.
4. Razi, P., R.A. Esmaeel, and F. Taheri, *Improvement of a vibration-based damage detection approach for health monitoring of bolted flange joints in pipelines.* Structural Health Monitoring, 2013. **12**(3): p. 207-224.
5. Rizzo, P., J.-G. Han, and X.-L. Ni, *Structural health monitoring of immersed structures by means of guided ultrasonic waves.* Journal of Intelligent Material Systems and Structures, 2010. **21**(14): p. 1397-1407.
6. Bao, C., H. Hao, and Z. Li, *Vibration-based structural health monitoring of offshore pipelines: numerical and experimental study.* Structural Control and Health Monitoring, 2012.
7. Peng, X.-L. and H. Hao, *A numerical study of damage detection of underwater pipeline using vibration-based method.* International Journal of Structural Stability and Dynamics, 2012. **12**(03): p. 1250021.
8. Peng, X.-L., H. Hao, and Z.-X. Li, *Application of wavelet packet transform in subsea pipeline bedding condition assessment.* Engineering Structures, 2012. **39**: p. 50-65.
9. Zhu, X., H. Hao, and X. Peng, *Dynamic assessment of underwater pipeline systems using statistical model updating.* International Journal of Structural Stability and Dynamics, 2008. **8**(02): p. 271-297.
10. Chen, J., Z. Su, and L. Cheng, *Identification of corrosion damage in submerged structures using fundamental anti-symmetric Lamb waves.* Smart Materials and Structures, 2010. **19**(1): p. 015004.
11. Cheraghi, N. and F. Taheri, *A damage index for structural health monitoring based on the empirical mode decomposition.* Mechanics of Materials and Structures, 2007. **2**(1): p. 43-62.
12. Huang, N.E., et al., *The empirical mode decomposition and the Hilbert spectrum for nonlinear and non-stationary time series analysis.* Proceedings of the Royal Society of London. Series A: Mathematical, Physical and Engineering Sciences, 1998. **454**(1971): p. 903-995.
13. Razi, P., R.A. Esmaeel, and F. Taheri, *Application of a robust vibration-based non-destructive method for detection of fatigue cracks in structures.* Smart Materials and Structures, 2011. **20**(11): p. 115017.
14. Loutridis, S., *Damage detection in gear systems using empirical mode decomposition.* Engineering Structures, 2004. **26**(12): p. 1833-1841.
15. !!! INVALID CITATION !!!
16. Corporation, D.S.A. *ABAQUS 2011 Version 6.10 User Manual*. 2011 [cited 2011; Available from: www.abaqus.com.

CHAPTER 6 APPLICATION OF A ROBUST VIBRATION-BASED NON-DESTRUCTIVE METHOD FOR DETECTION OF FATIGUE CRACKS IN STRUCTURES

Pejman Razi, Ramadan A Esmaeel and Farid Taheri

Published online the journal of Smart Materials and Structures, 20, 2011.
doi:10.1088/0964-1726/20/11/115017

6.1 ABSTRACT

This paper presents the application of a novel vibration-based technique for detecting fatigue cracks in structures. The method utilizes the empirical mode decomposition method (EMD) to establish an effective energy-based damage index. To investigate the feasibility of the method, fatigue cracks of different sizes were introduced in an aluminum beam subjected to a cyclic load under a three-point bending configuration. The vibration signals corresponding to the healthy and the damaged states of the beam were acquired via piezoceramic sensors. The signals were then processed by the proposed methodology to obtain the damage indices. In addition, for the sake of comparison, the frequency and damping analysis were performed on the test specimen. The results of this study concluded with two major observations. Firstly, the method was highly successful in not only predicting the presence of the fatigue crack, but also in quantifying its progression. Secondly, the proposed energy-based damage index was proved to be superior to the frequency-based methods in terms of sensitivity to the damage detection and quantification. As a result, this technique could be regarded as an efficient non-destructive tool, since it is simple, cost-effective and does not rely on analytical modeling of structures. In addition, the capability of the finite element method (FEM) in mimicking the experiments, and hence for consideration as an effective tool for conducting future parametric studies, was also investigated.

6.2 INTRODUCTION

Fatigue is considered as one of the major causes of failures in various mechanical, marine, aerospace and civil structures. As a result, several non-destructive test (NDT) methods (e.g. ultrasonic, magnetic and radiography) have been developed with the aim of detecting fatigue cracks at an early stage of their lives. To evaluate the integrity of a structure by the above methods, one needs to locally scan the entire structure, which consumes considerable effort and cost. Moreover, the application of these methods requires access to the entire structure or the regions of interest, which could at times be impossible in practice (e.g. buried structures or a structure exposed to harsh environmental conditions). These two main issues could render the application of such methods often impractical and/or too costly. Hence, considerable efforts have been expended by researchers to develop 'global' and cost-effective NDTs. These methods often incorporate smart materials/sensors to determine certain characteristics of a given structure (e.g. vibration), thereby monitoring the structure's health. This new era of damage detection is referred to as structural health monitoring (SHM) [1].

Over the past three decades, of the various SHM methods, the vibration-based methods have gained significant popularity among academia and the aerospace industry, as they offer a relatively simple and cost-effective approach. As an example, it has been theorized that the presence of a crack within a structural system would affect the physical parameters of the system (i.e. mass, stiffness and damping), and consequently would affect the vibration response of the structure. Based on these facts, vibration-based detection of cracks has been widely addressed in the literature, either as a 'forward' or 'inverse' problem [2].

Rizos *et al* [3] incorporated the linear elastic fracture mechanics (LEFM) to replace a crack with an equivalent rotational spring whose stiffness was a function of the crack size. Based on the model, they successfully identified the location and size of a crack in a beam by measuring the vibration response of two points along the beam at one of the beam's mode shapes. That model was also adopted by Lele and Maiti [4] to predict a crack in a thick beam by a few experimentally measured natural frequencies.

Kim and Stubbs [5] established an algorithm based on the modal sensitivity concept to estimate the crack location in a beam-type structure using a few natural frequencies of the

system. The method was highly successful, especially in predicting the crack location. Nahvi and Jabbari [6] incorporated the experimentally driven mode shapes as well as the corresponding natural frequencies of a cracked cantilever beam in the model proposed by Qian *et al* [7] in order to locate and quantify the crack. The model proposed a new stiffness matrix for an element that included a crack by incorporating LEFM. Rezaei and Taheri [8] experimentally validated a novel approach developed by Cheraghi and Taheri [9] to identify a small edge crack in a cantilever beam. Their method, referred to as EMD_EDI, takes advantage of the empirical mode decomposition (EMD) to establish an effective energy damage index (EDI). The results of the study corroborated that the method could be superior over the common frequency-based methods. Rezaei and Taheri [10] further extended the application of their method to a full-scale pipe in an effort to detect and quantify a penny-shaped notch in a girth weld of the pipe. Their experimental results showed a good agreement with the results obtained through their numerical model.

In all the above experimental, computational and theoretical studies, however, the researchers have investigated the influence of a notch instead of a sharp crack on the structures' vibration response. One of the reasons is that, in these studies, the crack(s) had been assumed to have remained open during the vibration of the monitored structure. This assumption, however, does not hold true for the case of real sharp cracks, whose surfaces are completely or partially in contact during a vibration [11].

To the best knowledge of the authors, there are very few research works that have experimentally validated the integrity of the proposed theoretical vibration-based models for detecting actual fatigue cracks. Cawley and Ray [12] compared the reduction in the natural frequencies of a beam due to a fatigue crack and those of a slot (or notch). They concluded that the fatigue crack lowered the natural frequencies of the beam, depending on the width to depth ratio of the notch as the notch dimensions approach those of the crack. Modena *et al* [13] reported their findings on the changes in the natural frequencies and damping ratio of a precast hollow concrete floor panel due to a crack. Their results revealed that the natural frequencies were very insensitive to the presence of the crack. The damping ratio, on the other hand, showed a higher level of sensitivity to the presence of the crack. Andreaus and Baragatti [14] studied the effect of a propagating fatigue crack on the fundamental frequency and damping ratio of an aluminum bar. The fundamental

frequency of the beam experienced a minute change to the fatigue crack at its final length, while the damping ratio exhibited more sensitivity to the presence of the crack. Consequently, they suggested the evaluation of the structural response at higher modes, which was postulated to yield more distinct and sensible changes in the corresponding natural frequencies. Zhang and Testa [15] studied the closure effect of fatigue cracks on the vibration response of a T-beam. They concluded that both the natural frequencies and damping ratio exhibited a nonlinear behavior with respect to different levels of dynamic loads (i.e. impulse excitations). The frequency varies very slightly as the fatigue crack grew. However, the damping ratio proved to be more sensitive to the crack growth variation. They also observed the so-called 'beating' phenomenon when the applied impulse load was above a certain magnitude, thereby causing the interaction of the crack surfaces during the resultant vibration. Rezaee and Hassannejad [16] established a theoretical model for a beam hosting a fatigue crack. They considered both the structural damping and the locally induced damping due to the presence of a crack. Moreover, the local stiffness of the beam at the crack location was represented by a nonlinear amplitude-dependent function to accommodate the nonlinear behavior of the cracked beam. The validity of their proposed model was verified through a set of experiments. The authors finally concluded that neglecting the nonlinear behavior imposed by the fatigue cracks could be a considerable source of error when evaluating the dynamic characteristic of cracked structures. Furthermore, like the other researchers, they noticed the beating phenomena in the vibration signal of the cracked beam.

In summary, a major conclusion that could be extracted from the earlier studies conducted by other researchers in relation to damage detection of fatigue-induced cracks would be that the frequency-based methods could not be regarded as an effective tool for detecting such cracks. Therefore, the promising capability of the EMD_EDI technique motivated the authors to examine the effectiveness of the method for detecting a fatigue crack mainly due to two reasons:

- EMD can accommodate nonlinear signals resulting from nonlinear phenomena [17]; the vibration of a structure hosting a fatigue crack could fall under this category [11].

- It has been proven that the EMD–EDI technique provides a higher and more distinct measure of changes in the structural response due to the presence of damage (i.e. by producing damage indices with large magnitude) in comparison to the frequency-based methods (exhibited through the investigation of a notch-type damage [8]).

Consequently, this work focuses on assessing the sensitivity of the EMD_EDI technique for detecting the presence of an initial sharp crack and its propagation. In this paper, a brief review of the EMD–EDI is first presented. It is then followed by an experimental study, which quantifies the capability of the proposed EMD-based damage index in predicting both the presence and growth of a sharp fatigue crack in an aluminum beam. The sensitivity of the EMD_EDI is compared with that of the commonly used frequency-based method. Moreover, a complete FE model, which included the actual piezoelectric sensors, was constructed to determine whether the sensors' signals obtained through FEM could accurately mimic the actual vibration response of the beam having various crack sizes. The establishment of the integrity of the computational approach will enable us to conduct effective parametric analyses in the future.

At the outset, it should be emphasized that the intention of the proposed strategy is not to compete with the conventionally used NDT methods, such as the ultrasonic one. It is believed that the strategy could be used as a 'first line of defense (FLD)'. This is because the use of the more precise NDT techniques usually requires skilled operators and specialized (usually expensive) equipment. The adaptation of the proposed strategy as an FLD can save a considerable amount of money for owners and operators of oil and gas pipelines and other pertinent industries. The proposed strategy can be effectively used as an 'alarm' in plants or other circumstances, as a means of providing a warning to operators that more in-depth NDTs (such as ultrasonic) should be employed to further assess the situation.

6.3 EMD ENERGY DAMAGE INDEX (EMD–EDI)

Huang *et al* [17] introduced a novel technique for the time–frequency analysis of real signals. The method yields the time– frequency spectrum of a signal with a two-step procedure. The first step involves the decomposition of a signal into a set of oscillatory

functions referred to as the intrinsic mode functions (IMFs) through an empirical method (i.e. the empirical mode decomposition (EMD)). The empirically driven IMFs are independent of each other and every individual IMF is time–frequency-modulated and conveys important information about the signal [17]. In the second step, the Hilbert–Huang transform (HHT) is applied to the extracted IMFs to obtain the time–frequency representation of the original signal. The established time–frequency spectrum of the signal provides well-localized information about the signal both in time and frequency domains; hence it can accommodate nonlinear as well as non-stationary signals. The following paragraph briefly explains the application of EMD into a real signal to obtain the constituent IMFs of the signal.

Two cubic splines are fitted through the local maxima and minima of the time-signal, $x(t)$, to produce the upper and lower envelopes, respectively. The average of these two splines (or envelopes) is calculated and subtracted from the original signal. The resultant signal is subsequently treated as a new signal and the aforementioned procedure is applied onto this new signal. A stopping criterion, as proposed by Huang *et al* [17], is used to terminate the above process (which is also referred to as the 'sifting process'; see Figure 6-1). The result of the first sifting process is referred to as the first IMF of the signal, c_1. It should be noted that, if one wishes to obtain the subsequent IMF, then the first IMF should be removed from the signal and the sifting process be performed on the residue to obtain the subsequent IMF of the signal. After extracting all IMFs, the signal is decomposed into n empirical modes and a residue, r_n, which is monotonic and represents the mean trend of the signal, as per the following equation:

$$x(t) = \sum_{i=1}^{n} c_i + r_n \qquad 6\text{-}1$$

Based on this technique, Cheraghi *et al* [9, 18] proposed a novel vibration-based technique for health monitoring of structures, which is formulated based on the energy of certain IMFs of a given structure's vibration signals, thereby producing a damage index (hereafter referred to as EMD–EDI). The procedure explained below (which, in our case, has been

coded in the MATLAB environment) can be followed for establishing EMD–EDIs of a given structure.

(i) After a structure is excited (e.g. by means of an impact hammer or the like), the dynamic response of the structure during its vibration, along with the hammer's output signal, are collected through appropriate sensors.

(ii) The signals are then normalized with respect to the hammer's signal in order to minimize the inconsistency that would be inevitably caused using a manual hammer.

(iii) Next, the normalized signals are passed through a band-pass filter to maintain the useful portion of the data. The normalized signals are then individually processed with the EMD method.

After the IMFs of the normalized signals are established, the energy of the desired IMF can be established by:

$$E = \int_0^{t_0} \left(IMF \right)^2 dt \qquad 6\text{-}2$$

In the above equation, t_0 is defined as the signal duration (which would be appropriately selected based on the type of structure's material being tested). This duration is taken as a consistent value for both the signals obtained from the structure in its healthy state as well as in its damaged state.

(iv) The above procedure is repeated for the same structure at its damaged state to establish the energy stored in the associated signal's IMF.

(v) The last step is the application of the EMD–EDI to each sensor; the index is calculated by:

$$EMD\_EDI = \left| \frac{E_{healthy} - E_{Damaged}}{E_{healthy}} \right| \times 100 \qquad 6\text{-}3$$

Once the EMD–EDI is evaluated for each sensor, the existence and severity of the damage may be established. Sensors producing higher index values represent the presence and location of the damage. The progression and severity of the damage can also be established by noting the increasing values of those indices as a function of time.

In summary, the EMD decomposes a signal into its oscillatory modes. The first two IMFs contain the oscillatory modes of higher frequencies of a given signal, which are believed to be more sensitive to damage (see [10, 19] for further explanation). However, if one uses the original signal, the outcome would be less sensitive for damage detection, since the original signal would contain all the IMFs. This would especially hold true in the case of monitoring crack propagation, in such cases when a crack's surfaces do not come into contact during the excitation (in which case the difference between the vibration signals obtained before and after the damage would not be discernible).

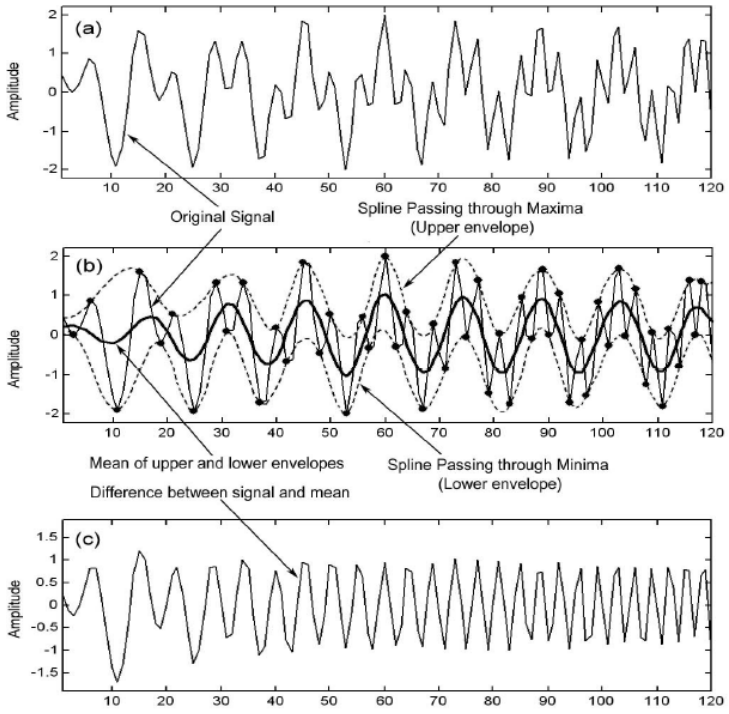

Figure 6-1: A schematic representation of the sifting process. (a) The original signal; (b) the signal in a thin solid line, the upper and lower envelopes in dashed lines; the mean in a thick solid line and (c) the difference between the signal and the mean [17].

6.4 EXPERIMENTAL STUDY

An experimental framework was designed to assess the capability of the proposed method in sensing the presence of a fatigue crack in a beam, as well as its propagation. As stated, the work was also carried out to establish the capability of the FEM in mimicking the actual

experiment and establishing whether the damage can also be established using the signals produced by the piezoelectric elements of the model. To this end, an aluminum beam with a square cross section was selected as the test specimen (see Figure 6-2). The physical and mechanical properties of the beam are also tabulated in Table 6-1. A fatigue crack was introduced at 240 mm from the beam's left end. For that, a notch of 1.5 mm depth was first introduced in the beam at the specified location by a jeweler's saw. The surfaces of the beam were mirror polished in the vicinity of the notch to monitor the crack growth by a 20x magnifying camera lens mounted on a moving vernier with a precise movement capability.

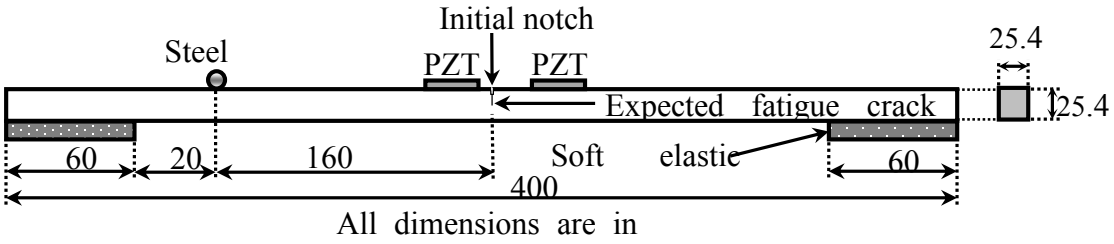

Figure 6-2: Configuration of the beam and its basic dimensions.

Table 6-1: Material properties of aluminum 6061-T6.

Property	Value
Cross-section dimensions (mm × mm)	25.4×25.4
Length (mm)	400
Young Modulus (GPa)	68.9
Density (Kg/m^3)	2700
Yield Strength (MPa)	280
Ultimate Strength (MPa)	325
Fatigue crack growth threshold ΔK_{TH} (MPa-m$^{1/2}$)	3
Fracture Toughness (MPa-m$^{1/2}$)	29
Poisson's ratio	0.33

The beam was then subjected to a cyclic load in a three-point bending configuration (Figure 6-3(a)), controlled by an Instron machine under a load-control condition. The cyclic loading amplitudes and its frequency are tabulated in Table 6-2.

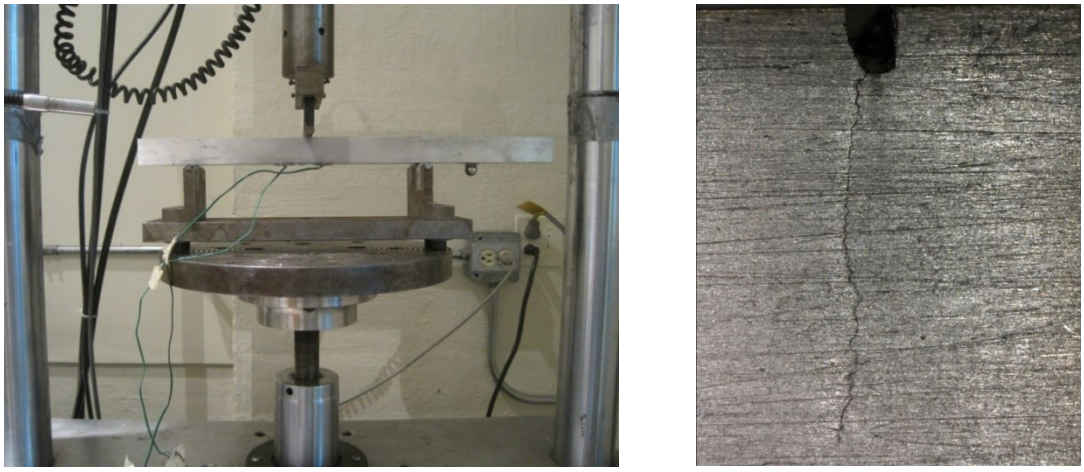

(a) (b)

Figure 6-3: (a) Fatigue crack propagation test set-up and (b) close-up of the fatigue crack.

Table 6-2: Specifications of the applied cyclic load.

P_{max} (N)	6048
$R=P_{max}/P_{min}$	15
Frequency (Hz)	20

It should be noted that the extreme values of the load were tuned such that the difference between the resultant stress intensity factors remained above the threshold for the crack to initiate (i.e. $\Delta K = 6.4 \succ$ $m^{1/2}$), yet well below the fracture toughness of the material. Note that the stress intensity for a given crack length, *a*, was calculated using the following equation [20]:

$$K = \sigma\sqrt{\pi a}F\left(\frac{a}{H}\right) \qquad 6\text{-}4$$

where σ and H represent the average stress and beam's height, respectively, and F is a geometric parameter, which can be calculated using the following relationship [20]:

$$F\left(\frac{a}{H}\right) = 1.106 - 1.552\left(\frac{a}{H}\right) + 7.71\left(\frac{a}{H}\right)^2 - 13.53\left(\frac{a}{H}\right)^3 + 14.23\left(\frac{a}{H}\right)^4 \qquad 6\text{-}5$$

Under the specified loading condition (as tabulated in Table 6-2), it took 140 000 cycles for the initial sharp fatigue crack to initiate. After this stage, additional loading cycles were

applied to propagate the crack. The crack length was frequently monitored by the microscope/camera. The loading was interrupted after the crack length reached predetermined intervals (i.e. a/H = 0.171, 0.266 and 0.413). At every damage state (i.e. after the crack length reached the stated intervals), the test specimen was removed from the set-up for vibration testing and analysis purposes, and was subsequently replaced back in the set-up for the application of additional loading cycles (i.e. further crack propagation). Figure 6-3(b) depicts the propagated fatigue crack at its final length.

For vibration analysis purposes, the beam was supported on two soft elastic pads to simulate the free–free boundary condition (see Figure 6-4). The free–free boundary condition was selected with the aim of eliminating any potential discrepancy in the boundary condition that could occur at various stages of the damage detection procedure.

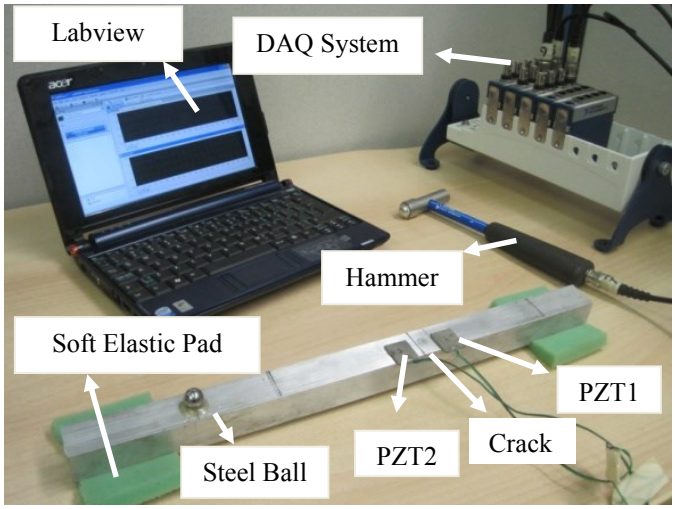

Figure 6-4: Vibration test set-up.

The discrepancy could occur due to the disturbance of the original boundary condition of the structure when removing the structure from its original configuration for vibration excitation [8]. As stated, the excitation is required for the establishment of the EDI. An impact hammer (model 5800B5 manufactured by Dytran Instrument Inc. (Chatsworth, CA)), with an aluminum tip, was used to excite the bending modes of the beam. The aluminum tip was specially selected to more effectively excite the higher modes of the beam, as the higher modes are generally better indicators of damage. Since the consistency of the impacts is an important factor that affects the results in the EMD–EDI method, a

small steel ball was bound to the beam with a two-part epoxy adhesive, Araldite 2011 (supplied by Huntsman Advanced Materials Americans Inc., Los Angeles, CA), and the beam was excited by applying an impact at this location. For each damage scenario then, the gathered signals are normalized with respect to the hammer signals to facilitate the comparison of the computed energies. As explained later, the normalization procedure, coded and embedded in our developed software, removes inconsistencies in the computed energies that could arise from any potentially inconsistent load magnitude and excited frequency range (therefore ensuring consistency in both the magnitude and frequency).

The vibration of the beam was monitored via two piezoceramic sensors, namely PZT1 and PZT2, which were polarized through the thickness and bound securely to the beam by the same adhesive, just adjacent to the crack location.

Table 6-3: Theoretical and experimental bending natural frequencies of the intact beam.

Natural Freq. (Hz)	**Theory**	**Experiment**	**Error**
f_1	812	808	0.5
f_2	2182	2161	1.0
f_3	4128	4081	1.1
f_4	6538	6481	0.9

The induced voltages in the PZT1, PZT2 and the hammer (due to the impact) were all recorded simultaneously with a data acquisition system. This system consisted of an analog input module NI-9215 in a compact chassis, cDAQ-9172, manufactured by National Instrument Inc. (Austin, TX). The LabView Signal Express 2010, coded by National Instrument Inc., provided the graphical interface for displaying and recording the individual signals. During the experiment, the sampling rate was set to be 20 kHz in order to take advantage of including the higher modes of vibration. The recorded signals were stored in ASCII text files for post-processing. The experimental set-up and the relevant instruments are shown in Figure 6-4.

It is worth noting that in general the vibration characteristics of structures (e.g. natural frequencies or mode shapes) could provide important global information about the integrity of a given system. Therefore, placement of a PZT sensor at a larger distance from the damage could still effectively capture the resulting reduction in the natural frequencies.

This is especially true for lightly damped structures in which the wave can travel quite far from the impacted area. It is believed that the incorporation of the proposed signal processing scheme could also be effective on occasions in which signal processing-based quality control tests are conducted on production lines.

Table 6-3 compares the first four theoretical bending natural frequencies of the healthy beam with the ones obtained experimentally after performing the fast Fourier transform (FFT) on the acquired signals from the piezoceramic sensors. The analytical natural frequencies of a beam can be determined using the following equation:

$$f_i = (\frac{1}{2\pi})\lambda_i^2 \sqrt{\frac{EI}{\rho A L^4}} \qquad 6\text{-}6$$

where E, I, ρ, A and L represent the modulus of elasticity, area moment of inertia, density, cross-sectional area and the length of the beam, respectively. λ is a parameter that depends on the boundary condition of the beam. For the free–free boundary condition, $\lambda_{(i=1:4)}$ = 4.730, 7.853, 10.996 and 14.137.

The results tabulated in Table 6-3 confirm the integrity of the simulated free–free boundary condition, as well as the integrity of the interface bond between the sensors and beam.

After establishing the integrity of the test set-up, the frequency, damping and the EMD_EDI analyses were performed on the vibration signals obtained from the healthy and damaged states of the beam. The results are respectively discussed in section 6.5.

6.5 EXPERIMENTAL RESULTS AND DISCUSSIONS

6.5.1 Frequency analysis

Figure 6-5 shows the frequency spectra obtained by applying FFT to one of the PZTs' signals obtained for different damage cases. Accordingly,

Table **6-4** presents the exact values of the obtained natural frequencies together with the maximum magnitude of the changes they experienced during each damage scenario. As

can be seen from Figure 6-5, the most noticeable shift in the frequency response occurs at the fourth frequency, which represents the highest mode in the selected frequency domain. The result of this part of the study (i.e. the changes in the natural frequencies reported in

Table **6-4**) reconfirms the fact that the frequency analysis could not be deemed as a sensitive means for detecting a fatigue crack, especially at the early stages of its propagation.

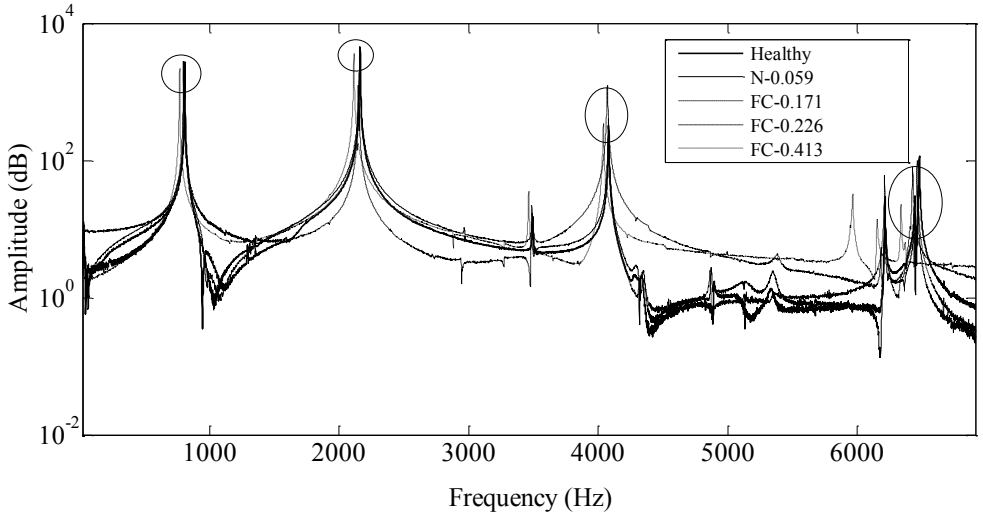

Figure 6-5: Frequency spectrum of the beam at the healthy and post-cracked states.

At this juncture, it is worth noting that investigation of damage using signals produced with higher sampling frequencies could even further improve the quality of the predicted EDIs. Our DAQ system, however, could only accommodate up to 100 kHz sampling rate (that is when only one channel is used; the rate is lowered when multi-channels are used). Even if higher sampling rates were possible, in order to excite the higher vibration modes, one would have to exert large impact energies to the structure by the impact hammer (not a practical task); this can be clearly noted by considering the logarithmic scale that can be extrapolated from the peak amplitude versus frequency curves illustrated in Figure 6-5. As the frequency increases, its amplitude (measured in dB) in the frequency spectrum (Figure 6-5) decreases, showing that the contributions of the higher modes to the vibration response become negligible.

Table 6-4: The bending natural frequencies of the beam. (Note: N: notched beam, FC: fatigue crack.)

Natural freq. (Hz)	**Healthy**	**Damage Scenarios- (a/H)**				**Maximum Change** (%)
		N-0.059	**FC-0.171**	**FC-0.266**	**FC-0.413**	
f_1	808	807	804	797	767	5.1
f_2	2161	2159	2159	2147	2113	2.2
f_3	4081	4079	4079	4070	4039	1.0
f_4	6481	6468	6462	6428	6337	2.2

6.5.2 Damping analysis

When the crack propagates in a structure, the crack surfaces could be fully closed, fully open or partially closed. The degree of the crack closure depends mainly on the stress intensity factor during the crack propagation [15]. The surfaces of a crack could contact continuously during a vibration event, provided that the dynamic load (or, alternatively, the vibration amplitude) exceeds a certain level required for the opening of the crack [15]. Therefore, the fatigue crack could impose a nonlinear amplitude-dependent behavior to the structure [16]. The partial discontinuity due to the crack closure together with the probable percussion of the crack surfaces during the vibration would cause the energy dissipation, which subsequently lead to damping the free vibration at a faster rate, hence increasing the damping characteristics of the structure. The damping measurements carried out in our investigation also further demonstrates the nonlinear response assessment capability of the damage index, which will be presented in the next section.

A MATLAB code was consequently developed for damping analysis of the test specimen using the logarithmic decrement technique. The vibration signal is fed to the code. With the aid of a digital filter, the first bending mode (among the other excited modes) of the beam is extracted. The code then applies the logarithmic decrement method on the filtered signal to estimate the damping ratio of the beam's first mode of vibration. Figure 6-6 depicts the change in the damping ratio of the beam, computed from the vibration signals of the two sensors, as it goes from the intact into the various damaged states. As was

expected, the damping ratios of the beam hosting different levels of damage are greater than that of the healthy one. An important observation is the nonlinear behavior of the damping ratio. This is believed to be due to the fact that the local damping caused by the crack would be affected by the crack size as well as the interaction of its surfaces during the vibration event. The latter factor, as was explained before, is controlled by the impact force, or alternatively the vibration amplitude, as well as the degree of the crack closure. Specifically, for the fatigue crack at the second stage (i.e. FC2-0.226 case), the damping ratio increases significantly (almost 1.5 times the damping of the intact beam), because of the noticeable beating phenomena which occurred due to the intense surface contact during the vibration.

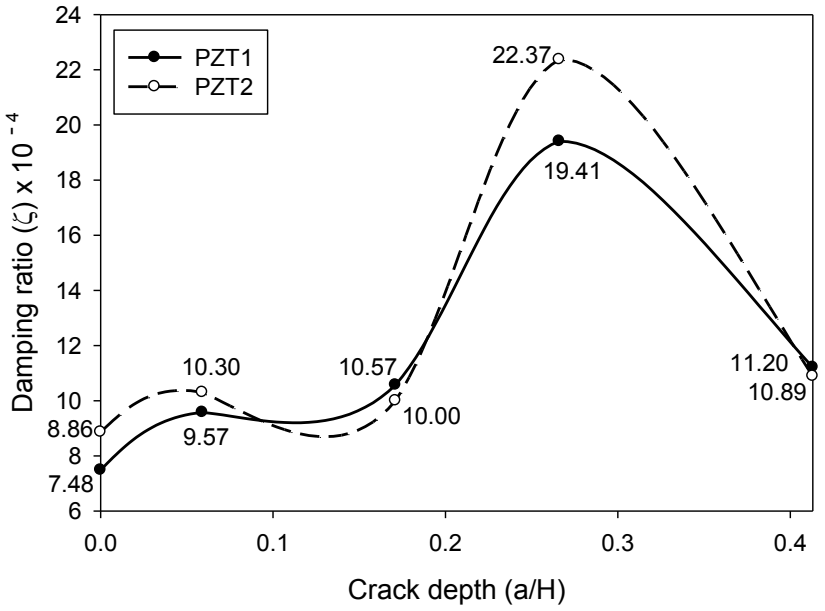

Figure 6-6: Experimentally computed damping ratio of the beam at the healthy and different damage states.

This can be observed through the examination of the vibration signals shown in Figure 6-7. Figure 6-7(c) shows that the beating phenomenon could also happen for other cases (i.e. FC3-0.413), provided that the impact load's amplitude is high enough to cause the interaction of the crack's surfaces. As can be seen, however, as a result of such high applied load amplitude, the induced voltage in the PZT exceeded the allowable voltage limit of the DAQ system (i.e. 10 V) at the initial stage, thus a portion of the digital signal was

automatically truncated and the signal could not be considered for further processing. Moreover, the computed damping ratios from the data of the second sensor are generally higher in value with respect to the ones derived from the data of the first sensor. This emphasizes that the closer sensor to the crack (i.e. PZT2 in Figure 6-2) triggers the locally induced damping in a more sensitive manner.

From the reported results, it can be concluded that the damping shows more sensitivity to the presence of the fatigue crack than the natural frequencies of the beam corroborating the same conclusion given in the aforementioned research on fatigue crack.

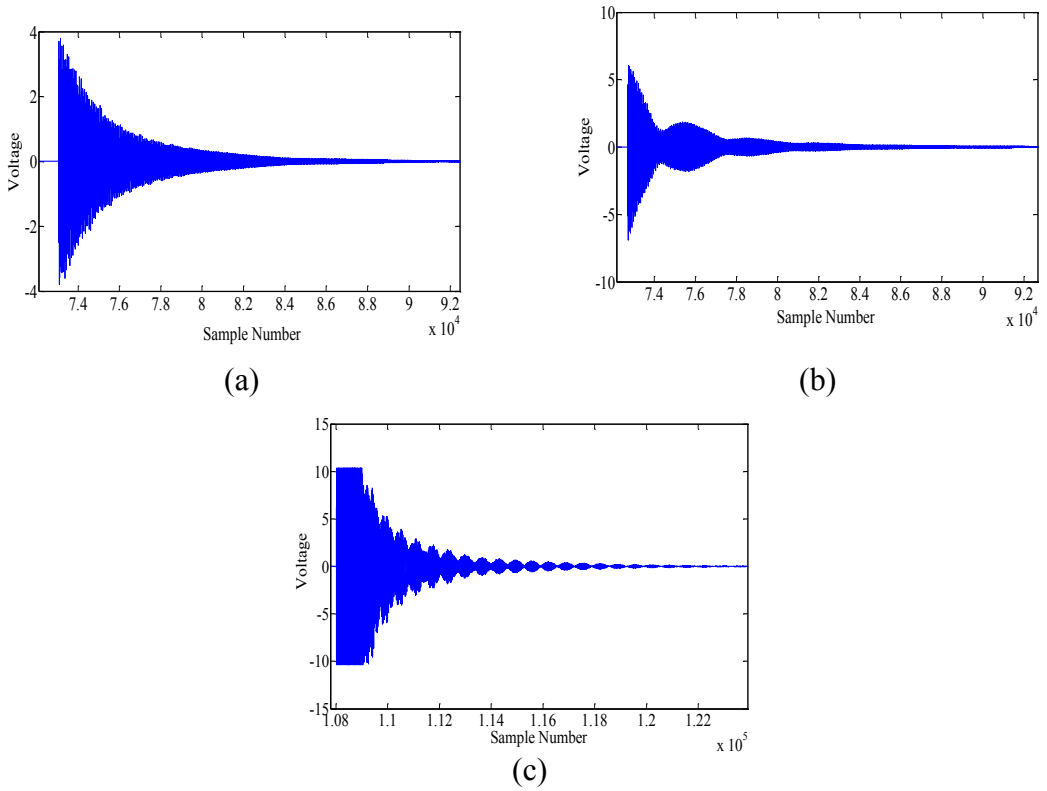

Figure 6-7: Free vibration of the beam corresponding to the (a) healthy and (b) damaged state (FC-0.266) and damaged state (FC-0.413).

6.5.3 EMD–EDI analysis

As was discussed earlier, the EMD–EDI exhibits a high level of sensitivity to very small-scale damages, rendering it as an effective candidate for detecting fatigue cracks. As a

result, the rest of the study details the application of the EMD–EDI analysis to the different damage scenarios outlined earlier and the establishment of the damage indices.

A MATLAB code was developed in-house to process the individual signals (obtained from the healthy and damaged states of the beam) to establish the damage indices following the procedure explained in section 6.3. Accordingly, a low-pass filter with the frequency range of 0-4 kHz was applied to the signals. The bandwidth of the filter was selected such that it would yield digital signals whose shapes are very close to that of the analog ones, and with the same frequency content (i.e. up to 4 kHz). Moreover, it would remove the portion of the signals that suffers from aliasing (i.e. in this case: (sampling frequency (F_s) = 20 kHz)/2 = 10 kHz). The program subsequently normalizes the sensors' signals with respect to the hammer signal in order to facilitate the comparison of consistent energies for each case. Finally, the program takes the normalized signals and processes them through the EMD as described earlier to extract the first (or second) IMF of the signals. The EMD energies of the first IMF of each normalized signal would then be reported in the output. It should be mentioned that the program is also tunable to calculate the energy term based on every individual IMFs (e.g. IMF2, IMF3, etc). Figure 6-8 illustrates a typical sensor's response and its first five IMFs after decomposition through the EMD sifting process, as discussed earlier.

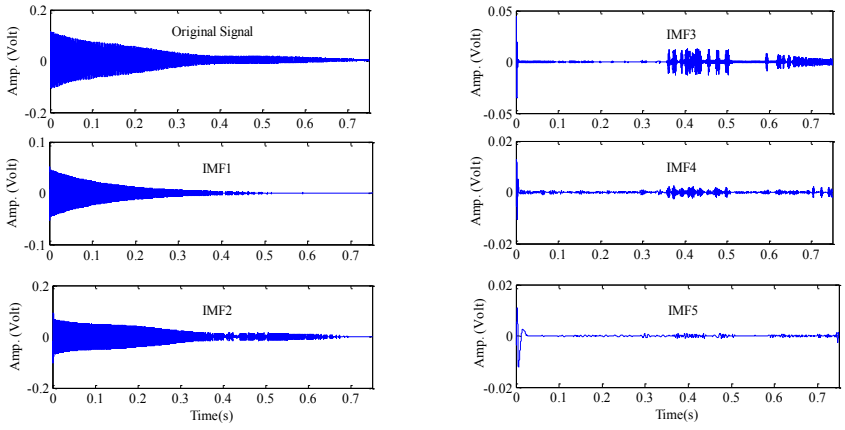

Figure 6-8: Typical PZT signal and its first five IMFs after decomposition.

In brief, the selection of IMF1 or IMF2 as the damage indicator is analogous to the selection of natural frequencies as used by other researchers for damage detection. The choice would

depend on the location of the damage (since the same damage can affect the natural frequencies in different ways when located in different locations along a structure). However, as stated earlier, in general the higher modes would serve as better indicators of damage. Moreover, referring to Figure 6-8, it can be visually inferred that the energies associated with the other IMFs (e.g. IMF3, IMF4, and IMF5) are negligible. In such cases, it is believed that the computed energies are highly affected by the inconsistent impacts and other anomalies, hence impeding the comparison of energies.

It is noteworthy to state that the beam was impacted ten times for each case. Then, seven out of ten signals resulted from the impacts were selected for processing. This was done in conjunction with the normalization procedure embedded in the program to minimize the discrepancy that would be inevitably caused using a manual hammer.

Table 6-5 reports the EMD energies for all of the damage cases computed from the signals of PZT1 based on Equation 6-2. The tabulated results highlight the ability of the method to produce reliable and repeatable energies for all the considered cases. It is also noteworthy that there is a considerable reduction in energy for the FC2-0.266 case, which again highlights the vivid beating phenomenon observed in the signals, thereby a severe nonlinearity of the beam's response in this case. Finally, the EMD–EDIs were established according to Equation 6-3, based on the averaged values of the EMD energies.

Loutridis [19] showed that the second IMF could also be regarded as an effective damage indicator. Therefore, the EMD–EDIs were also established based on the energy of the second IMF in an effort to assess the capability of IMF2 to identify the damage.

Table 6-5: Computed EMD energies.

Damage scenarios (a/H)	EMD energy (PZT1) # 1								
	Try 1	Try 2	Try 3	Try 4	Try 5	Try 6	Try 7	AVE.	Standard deviation
Healthy-0	0.271	0.274	0.281	0.282	0.297	0.304	0.305	0.288	0.0046
N- 0.059	0.218	0.219	0.221	0.230	0.230	0.240	0.246	0.229	0.0020
FC1- 0.171	0.168	0.168	0.170	0.175	0.192	0.194	0.207	0.182	0.0016
FC2- 0.266	0.045	0.045	0.045	0.046	0.047	0.052	0.052	0.047	0.0004
FC3- 0.413	0.133	0.134	0.134	0.145	0.152	0.154	0.158	0.144	0.0012

Figure 6-9 shows the EMD–EDIs is based on the energy of both IMF1 and IMF2 calculated from the recorded signals of the two sensors for different damage cases. The results reveal the following main observations.

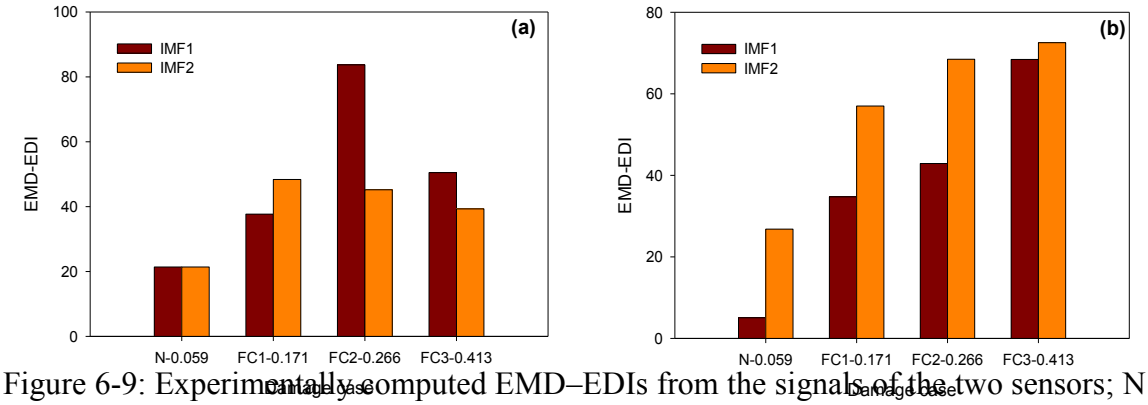

Figure 6-9: Experimentally computed EMD–EDIs from the signals of the two sensors; N: notched beam, FC: fatigue crack, (a) PZT1 and (b) PZT2.

Firstly, the EMD– EDI method can successfully detect the presence of a fatigue crack, since it yields distinct and high levels of damage indices compared to the percentages of changes in the natural frequencies. For instance, the damage index varies between 20–30% at the very early stages of the fatigue crack growth and exceeds 80% for the fatigue crack at its final level of propagation. Secondly, the method is also capable of quantifying the progression of the damage, since it generally produces relatively high damage indices as the crack propagates. Interestingly, IMF2 also shows a high level of sensitivity to the damage, even more notable than IMF1 in some cases (e.g. the ones obtained from the vibration signal of PZT2). As stated previously, the beating phenomenon results in a nonlinear variation in the calculated energies, thereby in the resulting EMD–EDIs. This trend is observed in the energies calculated based on the signals gathered through both sensors; however, its effect on the corresponding EMD–EDI of PZT2's signals is not as significant as that observed for PZT1's signals.

Moreover, the nonlinear variation in the indices reflects the nonlinear nature of the vibration as a result of the propagating crack.

6.6 FINITE ELEMENT ANALYSIS

6.6.1 Model description

A complete finite element model was established using the commercial FE code ABAQUS© [21] to simulate the vibration response of the aluminum beam whose basic geometric features and material properties were represented in Figure 6-2, and Table 6-1. The beam was modeled using three-dimensional eight-node reduced integration elements (C3D8R), while the two piezoelectric (PZT) sensors were modeled using three-dimensional linear eight-node piezoelectric elements (C3D8E). The sensors were modeled with the exact dimensions of the actual ones used in the experimental part of this study and placed at the exact specified locations as in the actual case. The material properties of aluminum are the same as listed in Table 6-1, while those of the PZT-5H sensors, as obtained from the manufacturer, are described using the following matrices:

$$S_E\left[\frac{m^2}{N}\right] = \left(10^{-12}\right)\begin{bmatrix} 16.5 & -4.78 & -8.45 & 0 & 0 & 0 \\ -4.78 & 16.5 & -8.45 & 0 & 0 & 0 \\ -8.45 & -8.45 & 20.7 & 0 & 0 & 0 \\ 0 & 0 & 0 & 43.5 & 0 & 0 \\ 0 & 0 & 0 & 0 & 43.5 & 0 \\ 0 & 0 & 0 & 0 & 0 & 42.6 \end{bmatrix}$$

$$d\left[\frac{C}{N}\right] = (10^{-12})\begin{bmatrix} 0 & 0 & 0 & 0 & 741 & 0 \\ 0 & 0 & 0 & 741 & 0 & 0 \\ -274 & -274 & 593 & 0 & 0 & 0 \end{bmatrix}$$

$$\varepsilon^S\left[F/m\right] = (10^{-9})\begin{bmatrix} 27.7 & 0 & 0 \\ 0 & 27.7 & 0 \\ 0 & 0 & 30.1 \end{bmatrix}$$

where S_E is the compliance matrix, d is the piezoelectric coupling matrix and ε^s is the permittivity of the piezoceramic. The density of PZT-5H was taken as ρ = 7500 kg/m^3. The 'extrude cut' (a special feature in ABAQUS-CAE©) was applied to the top surface of the beam to facilitate the modeling of the initial notch. The different crack lengths were

modeled using the 'crack' feature also provided in the ABAQUS-CAE© by assigning an appropriate 'seam' length.

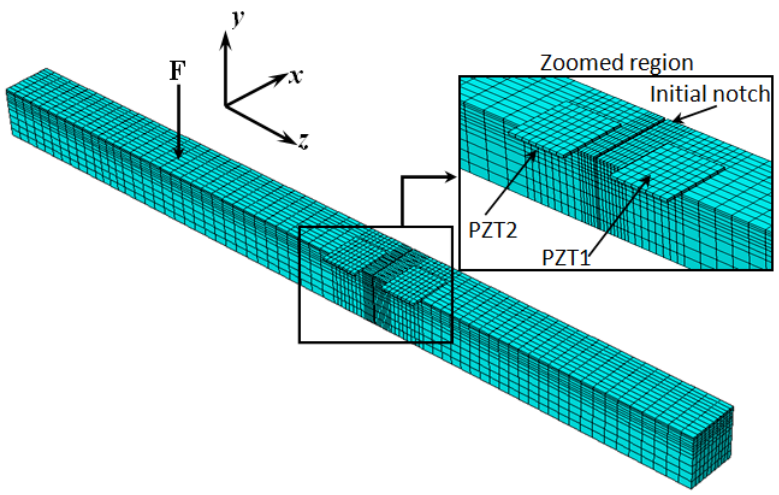

Figure 6-10: Finite element model and mesh details.

TIE multipoint constraints were used to connect the mating surface of the PZT sensors to the beam surface. The zero electric potential boundary condition was applied at the PZT's surface in contact with the beam. An impulse load with the same magnitude as that in the experiment was applied to the beam at the same location as that of the experiment to simulate the actual hammer's impact, thus exciting the beam. The dynamic response of the beam was obtained through a dynamic/implicit analysis step for a response period of 0.25 sec with 20 kHz sampling rate (i.e. 5000 increments were carried out to sample the first 0.25 sec output of the piezoelectric sensors' signal).

To simulate the free–free boundary condition, the solution was done in two successive analysis steps. In the first analysis step, the beam was assigned the appropriate boundary conditions at its left and right ends to prevent the rigid body motion while applying the impact force (i.e. at both ends, $u_x = u_y = 0$, see Figure 6-10), while in the second analysis step, the previously assigned boundary conditions were completely released, letting the beam vibrate freely. The first 0.25 sec of the signals for both sensors was acquired during the second analysis step.

Details of the FE model and the mesh for all components are shown in Figure 6-10. Both the healthy and damaged models had exactly the same mesh density with a refined mesh zone at the damaged region. This was done to eliminate any possibilities of differing response due to mesh variations in the two states, thus producing consistent evaluation of the EMD energy in both the healthy and damaged beams; therefore, the only difference between the two models was the introduction of the initial notch and the crack seam. The beam was modeled using 12 layers of elements through its thickness, while the PZT sensors were modeled by using only one layer of elements through its thickness. A mesh convergence study was performed to ensure that the calculated EMD energies were independent of the mesh density of the modeled components, thus optimizing the CPU runtime, without compromising the accuracy. This mesh convergence study was done by refining the mesh in the intact model, and then calculating the EMD energy by processing the PZT signals repeatedly until the relative difference between the energies calculated from the two successive runs was found to be less than 1%. The established mesh density was then used to model the intact beam and all the damaged cases. Each beam model consisted of approximately 14200 nodes connecting 11880 elements.

6.6.2 Finite element model verification and results

To verify that the signals obtained from the PZT sensors were indeed representative of the beam's vibration response, the first two natural frequencies were obtained by processing the signal obtained from the PZT1 sensor in the intact beam model using the fast Fourier transform (FFT) technique. The first and second bending natural frequencies were found to be 790 Hz and 2049 Hz, respectively. The absolute relative error was calculated to be 2.7% and 6.0%, respectively, for the first and second natural frequencies obtained analytically, while it was 2.2(%) and 5.2% when compared to the values obtained from the experiment (see Table 6-3 for the analytical and experimental values). Therefore, the integrity of the FE simulation in accurately replicating the vibration response of the actual beam under free–free boundary conditions was established.

As stated, the same damage scenarios described in the experimental part of this study were implemented in the FE model to further verify the integrity of the FEM simulation by comparing the computational results to the experimental ones. Figure 6-11 illustrates the

computational results of the calculated EMD–EDIs obtained for the four damage scenarios (the initial notch and the three fatigue crack states), as described in the experimental part of this study. As can be seen, in all cases the two sensors' results clearly identify the presence of the damage in the beam. Moreover, the increasing trend in the EMD–EDIs captures the progression of damage (fatigue crack).

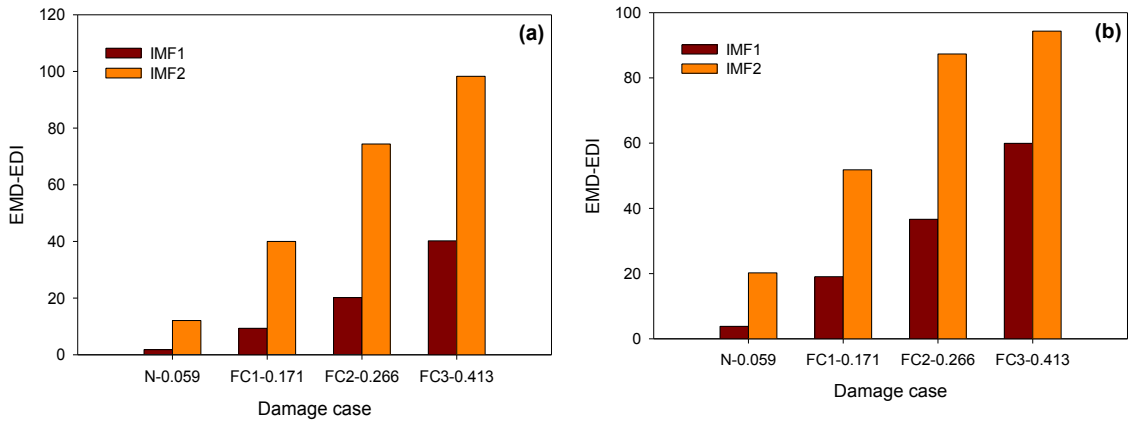

Figure 6-11: Computationally computed EMD–EDIs from the signals of the two sensors; N: notched beam, FC: fatigue crack, (a) PZT1 and (b) PZT2.

It should be noted that some differences are noted when comparing the experimental and computational results (Figure 6-9, and Figure 6-11, respectively), especially in relation to the nonlinear variation of the indices calculated based on IMF1 of the signals obtained experimentally (while the computational indices vary in a linear manner). This is due to the fact that the FEM analysis was done in a linear transient fashion, while the response is obviously nonlinear in reality. Moreover, the EMD–EDIs calculated using IMF2 of the signals are always greater than those calculated using IMF1 of the signals. This is believed to be due to the fact that IMF1 usually contains the higher vibration frequencies. Nevertheless, the preliminary results of the computational analysis reveal that FEM can be used as an effective tool for conducting parametric damage detection study.

6.7 CONCLUSIONS

The experimental and computational works presented in this paper examined the application of a novel vibration-based method, referred to as EMD–EDI, developed by

Cheraghi and Taheri [9], to the problem of fatigue crack identification. In the first part of the study, a sharp fatigue crack was introduced in an aluminum beam. Cyclic load was applied to the beam in order to initiate a sharp crack and propagate it by certain increments. The first four bending natural frequencies of the beam at three different fatigue crack lengths were recorded and compared with those obtained from the intact beam. The results reconfirmed the conclusions reported in previous studies regarding the insensitivity of the frequency-based methods in identifying the fatigue crack and its propagation.

Moreover, the damping analysis was performed on the test specimen. The results indicated that, in general, the damping ratio increased in the damage cases investigated compared to those evaluated for the beam in its healthy state. It was observed, however, that the trend is nonlinear, which was postulated to be related to the interaction of the crack surfaces during the vibration.

Furthermore, the recorded vibration signals were analyzed with the EMD–EDI method, which incorporates the energy of the intrinsic mode functions of the signal, extracted by applying the empirical modal decomposition. The damage index explained in this paper was demonstrated to be a sensitive and effective means for establishing the presence of damage. The method proved to be highly successful in both predicting the presence of a fatigue crack and its progression with a high level of sensitivity.

The entire experimental process was also simulated by the finite element method (FEM). The results demonstrated the ability of FEM as an effective tool for simulating such case studies. Thus it can be effectively used for future parametric studies.

It is therefore concluded that the EMD–EDI method exhibits a demonstrable advantage over the commonly used frequency-based damage detection methods from the perspective of the distinct identification of a crack and its sensitivity to progression of the crack. One of the aims of our future research on this method is to address the influence of consistency in applying the excitation force by using an automatic impact hammer. The use of an automated hammer is believed to produce consistent and repeatable impact forces (in terms of both magnitude and frequency domain), thus producing even more consistent results. The combination of the consistent excitation and the application of the EMD–EDI method in a real-time manner can present an effective and efficient opportunity for health monitoring of structures, as well as serving as an effective quality control tool.

6.8 ACKNOWLEDGMENTS

The financial support of the Petroleum Research Atlantic Canada (PRAC) and the Natural Sciences and Engineering Council of Canada (NSERC) in support of this work is gratefully acknowledged.

6.9 REFERENCES

1. Balageas, D.F., C. P.; G¨uemes, A., *Structural health monitoring*. 2006, Newport Beach, CA: ISTE.
2. Doebling, S.W., C.R. Farrar, and M.B. Prime, *A summary review of vibration-based damage identification methods.* Shock and vibration digest, 1998. **30**(2): p. 91-105.
3. Rizos, P.F., N. Aspragathos, and A.D. Dimarogonas, *Identification of crack location and magnitude in a cantilever beam from the vibration modes.* Journal of Sound and Vibration, 1990. **138**(3): p. 381-388.
4. Lele, S.P. and S.K. Maiti, *Modeling of transverse vibration of short beams for crack detection and measurement of crack extension.* Journal of Sound and Vibration, 2002. **257**(3): p. 559-583.
5. Kim, J.T. and N. Stubbs, *Crack detection in beam-type structures using frequency data.* Journal of Sound and Vibration, 2003. **259**(1): p. 145-160.
6. Nahvi, H. and M. Jabbari, *Crack detection in beams using experimental modal data and finite element model.* International Journal of Mechanical Sciences, 2005. **47**(10): p. 1477-1497.
7. Qian, G.L., S.N. Gu, and J.S. Jiang, *The dynamic behaviour and crack detection of a beam with a crack.* Journal of Sound and Vibration, 1990. **138**(2): p. 233-243.
8. Rezaei, D. and F. Taheri, *Damage identification in beams using empirical mode decomposition.* Structural Health Monitoring, 2011. **10**(3): p. 261-274.
9. Cheraghi, N. and F. Taheri, *A damage index for structural health monitoring based on the empirical mode decomposition.* Mechanics of Materials and Structures, 2007. **2**(1): p. 43-62.
10. Rezaei, D. and F. Taheri, *Health monitoring of pipeline girth weld using empirical mode decomposition.* Smart Materials and Structures, 2010. **19**(5): p. 055016.
11. Dimarogonas, A.D., *Vibration of cracked structures: A state of the art review.* Engineering Fracture Mechanics, 1996. **55**(5): p. 831-857.
12. Cawley, P. and R. Ray, *A comparison of the natural frequency changes produced by cracks and slots.* Vibration, Acoustics Stress and Reliability in Design, 1988. **110**(3): p. 366-370.
13. Modena, C., D. Sonda, and D. Zonta, *Damage localization in reinforced concrete structures by using damping measurements.* Key Engineering Materials, 1999. **167**: p. 132-141.
14. Andreaus, U. and P. Baragatti, *Fatigue crack growth, free vibrations, and breathing crack detection of aluminium alloy and steel beams.* The Journal of Strain Analysis for Engineering Design, 2009. **44**(7): p. 595-608.

15. Zhang, W. and R.B. Testa, *Closure effects on fatigue crack detection.* Engineering Mechanics, 1999. **125**(10): p. 1125-1132.
16. Rezaee, M. and R. Hassannejad, *Damped free vibration analysis of a beam with a fatigue crack using energy balance method.* Physical Science, 2010. **5**(6): p. 793-803.
17. Huang, N.E., et al., *The empirical mode decomposition and the Hilbert spectrum for nonlinear and non-stationary time series analysis.* Proceedings of the Royal Society of London. Series A: Mathematical, Physical and Engineering Sciences, 1998. **454**(1971): p. 903-995.
18. Cheraghi, N., M. Riley, and F. Taheri. *A novel approach for detection of damage in adhesively bonded joints in plastic pipes based on vibration method using piezoelectric sensors*. in *Systems, Man and Cybernetics, 2005 IEEE International Conference on*. 2005. IEEE.
19. Loutridis, S., *Damage detection in gear systems using empirical mode decomposition.* Engineering Structures, 2004. **26**(12): p. 1833-1841.
20. Tada, H., et al., *The stress analysis of cracks handbook*. Vol. 130. 2000: ASME press New York.
21. ABAQUS, *Dassault Systemes Americas Corp*. 2012.

CHAPTER 7 CONCLUSIONS AND RECOMMENDATIONS

7.1 CONCLUSIONS

This dissertation continued and improved the previous efforts, originated in our research group, in developing a reliable vibration-based health monitoring strategy. The adopted damage detection scheme applies the Empirical Mode Decomposition (EMD) to vibration signals gathered from structures through piezoelectric sensors in order to establish energy-based damage indices (EMD_EDIs). Interpretation of damage indices provides insight into locations and severity of damages within the structures. Experimental and numerical studies previously conducted in our research group had verified the integrity and robustness of the proposed energy-based damage index.

In the present work, some modifications were made to the application and instrumentation of the originally proposed strategy. The adjustments notably enhanced and improved the utility and consistency of the approach. In addition, the study examined the application of the method in health monitoring of submerged structures (specifically, in detecting fatigue cracks in pressurized pipelines' girth-welds).

This section outlines a summary of the achievements and conclusions made through the individual studies carried out within the present thesis.

1st Study: *Improvement of a vibration-based damage detection approach for health monitoring of bolted flange joints in pipelines.*

The study resolved a significant inconsistency reported in the previous efforts in detection of bolt loosening in bolted flanged joints. The inconsistency, which was routed in the reproducibility of the processed signals, caused large inaccuracies in predicting the advancement of damage. The main source of inconsistency was identified and attributed to the reconstruction of the vibration signals that were converted from analogue to digital. In addition, the sensory system was upgraded to a wireless system, thus it enhanced the utility of the method for remote applications. An experimental framework was therefore designated, incorporating the above-mentioned adjustments, for health monitoring of a full-scale pipeline's bolted flanged joint. Major improvements were observed in detection

of bolt loosening. The adjustments enabled a reasonably-accurate detection of the damage and tracking its advancement. The effect of variations in the boundary conditions on the accuracy of the damage detection was also examined through successive reductions of the clamped forces in the restraints. Interestingly, the methodology's performance was proved to be almost insensitive to the imposed variations in the fixity of the boundary. The study demonstrated that the detection of bolt loosening only required two sensors. The successful numerical verifications conducted afterwards suggested the developed numerical model as a robust means for future parametric studies.

2nd Study: *Some influential parameters in the vibration-based health monitoring of submerged pipelines.*

Thorough understanding of the dynamics of submerged pipelines is a prerequisite for a successful vibration-based structural health monitoring (VB-SHM). In particular, accurate representation of the associated fluid-structure interaction (FSI), and knowledge of the effect of external/internal pressures on the dynamics of such structures are of paramount importance in any VB-SHM strategy. As such, a comprehensive numerical study was performed to explore the effect of various influential parameters on the dynamic response, and in turn, on the VB-SHM of submerged pipes.

The associated FSI was modeled using two well-known approaches, namely the "added mass" and the "coupled acoustic-structural" approaches. It was demonstrated that application of the "added mass" approach may lead to erroneous results in certain cases. The reason was attributed to the assumptions used in formulating the "added mass" approach. Specifically, the issue is primarily due to the consideration of only the global bending modes of a vibrating pipe. As a result, the accuracy of the solutions would suffer in situations where the other modes (e.g., torsional, and longitudinal modes) contribute to the vibration response.

The effect of operational variability on the dynamics of submerged pipelines was also studies. Abrupt decreases/increases in the internal pressure of a pipe, and the potential variation in the external hydrostatic pressure that could be experienced by a submerged pipe were considered as the operational variability. It was observed that the variation in the external/internal pressures could variably affect the pipe's dynamic response, and therefore

could adversely affect the integrity and accuracy of the VB-SHM. The study concluded that the extent of change in the vibration response of submerged pipes (hence, the accuracy of VB-SHM conducted on those pipes) depends on pipe's stiffness and the extent of such operational variability. For instance, the vibration response of the submerged steel pipe considered in the study remained almost unaffected in the presence of the considered operational variability. Therefore, VB-SHM of the submerged steel pipe could be reliably accomplished with a high degree of accuracy in practice. On the other hand, dynamic response of less stiff pipes (i.e., the FRP composite pipes considered in this study) showed notable sensitivity to the same operational variability. Therefore, VB-SHM of FRP composite pipes should be conducted with great caution in practice.

3rd Study: *A vibration-based strategy for health monitoring of offshore pipelines' girth-welds.*

Our research group reported encouraging results on the application of EMD_EDI to health monitoring of an onshore pipeline's girth-weld against a propagating notch. It was the motivation for evaluation of the EMD_EDI's capability in identifying the same type of damage in offshore pipelines.

Some adjustments were made into the sensory network and the actuation units in order to accommodate the underwater measurements. Waterproofed piezoelectrics were bonded on either sides of an aluminum pipe's girth-weld. The pipe was submerged into a laboratory tank filled with water. A pneumatic hammer was fabricated and waterproofed to impart impulsive excitations to the pipe. A piezoelectric-based wave propagation scheme was also adopted as an alternative means of excitation for the first time in the EMD_EDI's applications. Encouraging results were observed in identification of an advancing notch in the girth-weld of the submerged pipe. The piezoelectric-based wave propagation technique was proved as an effective and reliable means in damage detection of the pipe. A chirp signal was propagated in the pipe, serving as the inspector wave. The experimental study concluded that the health monitoring of the girth-weld could be accomplished by only one piezoelectric sensor placed on each side of it.

Before conducting the experimental study, numerical simulations of the above practice were performed on the ABAQUS platform. The numerical model incorporated

piezoelectric elements serving as both sensors and actuators. The successful numerical modeling of the piezoelectric-based actuation unit introduced a major contribution towards enhancement of the EMD_EDI. The same structure hosting the damage scenarios of the experiments was modeled numerically and the performance was simulated; the damage could be successfully identified via the proposed approach. The outcome of the numerical study was in reasonably good agreement with the experimental results. The damage indices produced in the two studies showed a very close trend in identification and tracking of the damage.

4th Study: *Application of a robust vibration-based non-destructive method for detection of fatigue cracks in structures.*

The study examined the capability of the EMD_EDI in identification of real-life sharp cracks in an effort towards identification of fatigue cracks in the pipeline's girth-welds. It should be noted that in all the previous trials (by our research group as well as most others), the identification of a notch (as opposed to a sharp fatigue crack) was addressed.

To this end, a surface-breaking fatigue crack was initiated and was subsequently propagated in an aluminum beam. At various stages of the crack growth, the beam's vibrations were examined through the EMD_EDI. Noticeably high damage indices observed for the onset of the fatigue crack suggested the EMD_EDI as a robust tool for health monitoring of structures against real-life damages. The study was followed by the numerical simulations of the problem. The results from the numerical study were in good agreement with the experimental observations.

7.2 RECOMMENDATIONS

It is believed that future studies should be focused on the following recommendations in order to facilitate the application of EMD_EDI from the controlled laboratory environment to in-situ applications.

- The adopted piezoelectric-based wave propagation technique (i.e., chirping) yielded encouraging results in damage detection of a submerged pipeline. A chirp with a certain frequency range was propagated as the inspector wave. There are, however, other types of so-called inspector waves, such as the tone-

burst, which should be examined. It is therefore envisaged that tailoring the adopted inspector wave type along with the most efficient frequency range of excitation could enhance the method's capability, thus its reliability in identification of damage.

- Environmental conditions and the variation in boundary conditions are essentially the major concerns that could threaten the reproducibility of the collected vibration signal, which could affect the accuracy of any vibration-based damage detection strategy. The effect of variations in boundary conditions was studied to some extent in the present thesis. It is strongly suggested that the sensitivity of the adopted method be evaluated against variations in temperature, mass of structures, or environmentally-imposed dynamic loads such as low frequency ocean waves (in the case of submerged structures).
- Upon establishing the reliability of the strategy, a fully-remote application of the adopted methodology would significantly increase its utility. A wireless sensory network was tested and verified in the present dissertation. Wireless nodes could also communicate with piezoelectric actuator units, by receiving inspector wave signals from a remotely located satellite computer. In fact, programmable wireless nodes can practically replace the wire-based system and remove the necessity of some instrumentations (e.g., the required signal generator).

REFERENCES

Guidelines for the management of the integrity of bolted joints for pressurized systems. 2007, Energy Institue: London.

Na, W.-B. and T. Kundu, *Underwater pipeline inspection using guided waves*. Transactions-American Society of Mechanical Engineers Journal of Pressure Vessel Technology, 2002. 124(2): p. 196-200.

Application notes. 2012 [cited 2012 February]; Available from: http://www.olympus-ims.com/.

Balageas, D.F., C. P.; G¨uemes, A., *Structural health monitoring*. 2006, Newport Beach, CA: ISTE.

Razi, P., R.A. Esmaeel, and F. Taheri, *Application of a robust vibration-based non-destructive method for detection of fatigue cracks in structures*. Smart Materials and Structures, 2011. 20(11): p. 115017.

Afshari, M., T. Marquié, and D.J. Inman. *Automated structural health monitoring of bolted joints in railroad switches*. in Proceedings of ASME 2009 Rail Transportation Division Fall Conference. 2009.

Cheraghi, N. and F. Taheri, *A damage index for structural health monitoring based on the empirical mode decomposition*. Mechanics of Materials and Structures, 2007. 2(1): p. 43-

Rezaei, D. and F. Taheri*, Experimental validation of a novel structural damage detection method based on empirical mode decomposition*. Smart Materials and Structures, 2009. 18(4): p. 045004.

Rezaei, D. and F. Taheri, *Damage identification in beams using empirical mode decomposition*. Structural Health Monitoring, 2011. 10(3): p. 261-274.

Rezaei, D. and F. Taheri, *Health monitoring of pipeline girth weld using empirical mode decomposition*. Smart Materials and Structures, 2010. 19(5): p. 055016.

Esmaeel, R.A., J. Briand, and F. Taheri, *Computational simulation and experimental verification of a new vibration-based structural health monitoring approach using piezoelectric sensors*. Structural Health Monitoring, 2011. 11(2): p. 237-250.

Ewins, D.J., *Theoretical basis, modal testing: theory, practice and application*. 2nd ed. 2000, Philadelphia: PA: Research Studies Press Ltd.

Kim, J.T. and N. Stubbs, *Crack detection in beam-type structures using frequency data*. Journal of Sound and Vibration, 2003. 259(1): p. 145-160.

Farrar, C.R. and S.W. *Doebling, Damage detection II: field applications to large structures*, in Modal analysis and testing (NATO science series), J.M.M. Silva and N.M.M. Maia, Editors. 1999, Kluwer Academic Publishers: Dordrecht. p. 1-29.

Chandrashekhar, M. and R. Ganguli, *Structural damage detection using modal curvature and fuzzy logic*. Structural Health Monitoring, 2009. 8(4): p. 267-282.

Rezaee, M. and R. Hassannejad, *Damped free vibration analysis of a beam with a fatigue crack using energy balance method*. Physical Science, 2010. 5(6): p. 793-803.

Cheraghi, N., G.P. Zou, and F. Taheri, *Piezoelectric-based degradation assessment of a pipe using Fourier and Wavelet analyses*. Computer-Aided Civil and Infrastructure Engineering, 2005. 20(5): p. 369-382.

Peng, X.-L., H. Hao, and Z.-X. Li, *Application of wavelet packet transform in subsea pipeline bedding condition assessment*. Engineering Structures, 2012. 39: p. 50-65.

Melhem, H. and H. Kim, *Damage detection in concrete by Fourier and Wavelet analyses. Journal of Engineering Mechanics*, 2003. 129(5): p. 571-577.
Huang, N.E., et al., *The empirical mode decomposition and the Hilbert spectrum for nonlinear and non-stationary time series analysis*. Proceedings of the Royal Society of London. Series A: Mathematical, Physical and Engineering Sciences, 1998. 454(1971): p. 903-995.
Loutridis, S., *Damage detection in gear systems using empirical mode decomposition*. Engineering Structures, 2004. 26(12): p. 1833-1841.
Bao, C.X., H. Hao, and Z.X. Li, *Vibration-based damage detection of pipeline system by HHT method*. Applied Mechanics and Materials, 2011. 99: p. 1067-1072.
Doebling, S.W., C.R. Farrar, and M.B. Prime, *A summary review of vibration-based damage identification methods*. Shock and vibration digest, 1998. 30(2): p. 91-105.
He, K. and W.D. Zhu, *A vibration-based structural damage detection method and its applications to engineering structures*. International Journal of Smart and Nano Materials, 2011. 2(3): p. 194-218.
He, K. and W.D. Zhu, *Structural damage detection using changes in natural frequencies: theory and applications*. Journal of Physics: Conference Series, 2011. 305: p. 012054.
Milanese, A., et al., *Modeling and Detection of Joint Loosening using Output-Only Broad-Band Vibration Data*. Structural Health Monitoring, 2008. 7(4): p. 309-328.
Mickens, T., et al., *Structural health monitoring of an aircraft joint.* Mechanical Systems and Signal Processing, 2003. 17(2): p. 285-303.
Amerini, F. and M. Meo, *Structural health monitoring of bolted joints using linear and nonlinear acoustic/ultrasound methods.* Structural Health Monitoring, 2011. 10(6): p. 659-672.
Yang, J. and F.-K. Chang, *Detection of bolt loosening in C–C composite thermal protection panels: I. Diagnostic principle*. Smart Materials and Structures, 2006. 15(2): p. 581-590.
Yang, J. and F.-K. Chang, *Detection of bolt loosening in C–C composite thermal protection panels: II. Experimental verification*. Smart Materials and Structures, 2006. 15(2): p. 591-599.
Zou, G., N. Cheraghi, and F. Taheri, *Fluid-induced vibration of composite natural gas pipelines.* International journal of solids and structures, 2005. 42(3): p. 1253-1268.
Ross, C.T.F., et al., *Vibration of a thin-walled prolate dome under external water pressure*. Ocean Engineering, 2007. 34(3-4): p. 560-575.
Blevins, R.D., *Flow-Induced Vibration*. 2nd ed. 2001, Malabar: Krieger.
Zeinoddini, M., G.A.R. Parke, and S.M. Sadrossadat, *Free-spanning submarine pipeline response to severe ground excitations: water-pipeline interactions*. Journal of Pipeline Systems Engineering and Practice, 2012. 3(4): p. 135-149.
Zhu, X., H. Hao, and X. Peng, *Dynamic assessment of underwater pipeline systems using statistical model updating*. International Journal of Structural Stability and Dynamics, 2008. 8(02): p. 271-297.
Kramer, M.R., Z. Liu, and Y.L. Young, *Free vibration of cantilevered composite plates in air and in water*. Composite Structures, 2013. 95: p. 254-263.
Kwon, Y.W., et al., *Transient dynamic response and failure of sandwich composite structures under impact loading with fluid structure interaction*. Applied Composite Materials, 2012. 19(6): p. 921-940.

Li, H., S. Wang, and H. Yang. *Modal strain energy decomposition method for damage detection of an offshore structure using modal testing information*. in Third Chinese-German Joint Symposium on Coastal and Ocean Engineering. 2006.
Nichols, J.M., *Structural health monitoring of offshore structures using ambient excitation*. Applied Ocean Research, 2003. 25(3): p. 101-114.
Mangal, L., V. Idichandy, and C. Ganapathy, *Structural monitoring of offshore platforms using impulse and relaxation response*. Ocean Engineering, 2001. 28(6): p. 689-705.
Rizzo, P., J.-G. Han, and X.-L. Ni, *Structural health monitoring of immersed structures by means of guided ultrasonic waves*. Journal of Intelligent Material Systems and Structures, 2010. 21(14): p. 1397-1407.
Bao, C., H. Hao, and Z. Li, *Vibration-based structural health monitoring of offshore pipelines: numerical and experimental study*. Structural Control and Health Monitoring, 2012.
Chen, J., Z. Su, and L. Cheng, *Identification of corrosion damage in submerged structures using fundamental anti-symmetric Lamb waves*. Smart Materials and Structures, 2010. 19(1): p. 015004.
Dimarogonas, A.D., *Vibration of cracked structures: A state of the art review*. Engineering Fracture Mechanics, 1996. 55(5): p. 831-857.
Cawley, P. and R. Ray, *A comparison of the natural frequency changes produced by cracks and slots*. Vibration, Acoustics Stress and Reliability in Design, 1988. 110(3): p. 366-370.
Rizos, P.F., N. Aspragathos, and A.D. Dimarogonas, *Identification of crack location and magnitude in a cantilever beam from the vibration modes*. Journal of Sound and Vibration, 1990. 138(3): p. 381-388.
Lele, S.P. and S.K. Maiti, *Modeling of transverse vibration of short beams for crack detection and measurement of crack extension*. Journal of Sound and Vibration, 2002. 257(3): p. 559-583.
Montalvão E Silva, J.M. and A.J.M. Aráujo Gomes, *Experimental dynamic analysis of cracked free-free beams.* Experimental Mechanics, 1990. 30(1): p. 20-25.
Qian, G.L., S.N. Gu, and J.S. Jiang, *The dynamic behaviour and crack detection of a beam with a crack*. Journal of Sound and Vibration, 1990. 138(2): p. 233-243.
Nahvi, H. and M. Jabbari, *Crack detection in beams using experimental modal data and finite element model*. International Journal of Mechanical Sciences, 2005. 47(10): p. 1477-1497.
Modena, C., D. Sonda, and D. Zonta, *Damage localization in reinforced concrete structures by using damping measurements*. Key Engineering Materials, 1999. 167: p. 132-141.
Andreaus, U. and P. Baragatti, *Fatigue crack growth, free vibrations, and breathing crack detection of aluminium alloy and steel beams.* The Journal of Strain Analysis for Engineering Design, 2009. 44(7): p. 595-608.
Zhang, W. and R.B. Testa, *Closure effects on fatigue crack detection.* Engineering Mechanics, 1999. 125(10): p. 1125-1132.
Ritdumrongkul, S., et al., *Quantitative health monitoring of bolted joints using a piezoceramic actuator–sensor*. Smart Materials and Structures, 2004. 13(1): p. 20-29.
Carden, E.P. and P. Fanning, *Vibration based condition monitoring: a review.* Structural Health Monitoring, 2004. 3(4): p. 355-377.

Park, G., H.H. Cudney, and D.J. Inman, *Feasibility of using impedance-based damage assessment for pipeline structures*. Earthquake Engineering & Structural Dynamics, 2001. 30(10): p. 1463-1474.
Cheraghi, N., M. Riley, and F. Taheri. *A novel approach for detection of damage in adhesively bonded joints in plastic pipes based on vibration method using piezoelectric sensors.* in Systems, Man and Cybernetics, 2005 IEEE International Conference on. 2005. IEEE.
Kuo, W.-H., et al. *An intelligent positioning approach: RSSI-based indoor and outdoor localization scheme in Zigbee networks*. in Machine Learning and Cybernetics (ICMLC), 2010 International Conference on. 2010. IEEE.
Engelberg, S., *Signal reconstruction*, *in digital signal processing*: *an experimental approach*. 2008, Springer: London.
ABAQUS, Dassault Systemes Americas Corp. 2012.
Chambers, J.A., *Preloaded joint analysis methodology for space flight systems.* 1995, National Aeronautics and Space Administration (NASA), Lewis Research Center: Cleveland.
Recommended practice DNV-RP-F105 : free spanning pipelines. *2009, DNV* Det Norske Veritas (DNV): Oslo.
Peng, X.-L. and H. Hao, *A numerical study of damage detection of underwater pipeline using vibration-based method*. International Journal of Structural Stability and Dynamics, 2012. 12(03): p. 1250021.
Cengel, Y.A. and J.M. Cimbala, *Fluid Mechanics: Fundamentals and Applications*. 2006, New York: McGraw-Hill.
Zienkiewicz, O.C., R.L. Taylor, and J.Z. Zhu, *The Finite Element Method: Its Basis and Fundamentals*. 6th ed. 2005, Burlington: Butterworth-Heinemann.
Ohayon, R., *Symmetric variational formulation of harmonic vibrations problems by coupling primal and dual principles. Application to fluid-structure coupled systems.* La Recherche Aérospatiale, 1979. 3: p. 207-211.
Corporation, D.S.A. ABAQUS 2011 Version 6.10 User Manual. 2011 [cited 2011; Available from: www.abaqus.com.
Rao, S., S, *Mechancial Vibrations*. 2011, Upper Saddle River: Prentice Hall.
Kwon, Y.W., *Study of fluid effects on dynamics of composite structures*. Journal of Pressure Vessel Technology, 2011. 133(3): p. 031301.
Motley, M.R., M.R. Kramer, and Y.L. Young, *Free surface and solid boundary effects on the free vibration of cantilevered composite plates*. Composite Structures, 2013. 96: p. 365-375.
Hampson, P.R. and M. Moatamedi, *Fluid structure interaction of submerged metallic and composite plates subjected to low velocity impact loading*. International Journal of Crashworthiness, 2010. 15(1): p. 49-58.
Wiesshaar, T.A. and B.L. Foist, *Vibration Tailoring of Advanced Composite Lifting Surfaces*. Aircraft. 22(2): p. 141-147.
Razi, P., R.A. Esmaeel, and F. Taheri, *Improvement of a vibration-based damage detection approach for health monitoring of bolted flange joints in pipelines.* Structural Health Monitoring, 2013. 12(3): p. 207-224.
Tada, H., et al., *The stress analysis of cracks handbook*. Vol. 130. 2000: ASME press New York.

COPYRIGHT PERMISSIONS

A. 1 Copyright permission for Chapter 3

November 5th 2013

International Journal of Structural Health Monitoring

I am preparing my Ph.D. thesis for submission to the Faculty of Graduate Studies at Dalhousie University
, Halifax, Nova Scotia, Canada. I am seeking your permission to include a manuscript version of the following paper as a chapter in the thesis:
[Pejman Razi, Ramadan A Esmaeel and Farid Taheri, "*Improvement of a vibration-based damage detection approach for health monitoring of bolted flange joints in pipelines"*, Structural Health Monitoring. 2013, 12(3), 207-224.]

Canadian graduate theses are reproduced by the Library and Archives of Canada (formerly National Library of Canada) through a non-exclusive, world-wide license to reproduce, loan, distributor or sell these. I am also seeking your permission for the material described above to be reproduced and distributed by the LAX (NLC). Further details about the LAC (NLC) thesis program are available on the LAC (NLC) website (www.nlc-bnc.ca)
Full publication details and a copy of this permission letter will be included in the thesis.

Yours Sincerely,
Pejman Razi

Copyright Clearance Center RightsLink®

Home | Create Account | Help

SAGE

Title: Improvement of a vibration-based damage detection approach for health monitoring of bolted flange joints in pipelines:
Author: Pejman Razi, Ramadan A Esmaeel, Farid Taheri
Publication: Structural Health Monitoring
Publisher: SAGE Publications
Date: May 1, 2013
Copyright © 2013, SAGE Publications

User ID
Password
Enable Auto Login
LOGIN
Forgot Password/User ID?
If you're a copyright.com user, you can login to RightsLink using your copyright.com credentials. Already a RightsLink user or want to learn more?

Redirected Request

If you are an Author inquiring about the re-use of your journal article, please note that after publication of the journal article, Authors may re-use their content in any later work written or edited by the Author or for the Author's classroom use, without seeking permission from SAGE. For any other use of your work, please contact the publisher. For additional information see www.sagepub.com/repository/binaries/journals/permissions/author_use.doc.

BACK | CLOSE WINDOW

Copyright © 2013 Copyright Clearance Center, Inc. All Rights Reserved. Privacy statement.
Comments? We would like to hear from you. E-mail us at customercare@copyright.com

A. 2 Copyright permission for Chapter 6

November 5th 2013

International journal of Smart Materials and Structures

I am preparing my Ph.D. thesis for submission to the Faculty of Graduate Studies at Dalhousie University
, Halifax, Nova Scotia, Canada. I am seeking your permission to include a manuscript version of the following paper as a chapter in the thesis:
[Pejman Razi, Ramadan A Esmaeel and Farid Taheri, "*Application of a robust vibration-based non-destructive method for detection of fatigue cracks in structures"*, Smart Metr. Struct. 20 (2011), doi:10.1088/0964-1726/20/11/115017]

Canadian graduate theses are reproduced by the Library and Archives of Canada (formerly National Library of Canada) through a non-exclusive, world-wide license to reproduce, loan, distributor or sell these. I am also seeking your permission for the material described above to be reproduced and distributed by the LAX (NLC). Further details about the LAC (NLC) thesis program are available on the LAC (NLC) website (www.nlc-bnc.ca)
Full publication details and a copy of this permission letter will be included in the thesis.

Yours Sincerely,
Pejman Razi

Dear Pejman Razi

Thank you for your email.

When you assigned the copyright in your article to IOP, we granted back to you certain rights, including the right to include the article within any thesis or dissertation.

Therefore, please go ahead and make what use you wish of the content of the article.

Please let me know if you have any further questions.

Best Wishes

Sarah Ryder

Publishing Administrator
Email: permissions@iop.org